Diplomarbeit

Implementation of a WiMAX simulator in Simulink

Ausgeführt zum Zwecke der Erlangung des akademischen Grades eines
Diplom-Ingenieurs unter Leitung von

Univ.Prof. Dipl.-Ing. Dr.techn. Markus Rupp
Dipl.-Ing. Christian Mehlführer

E389
Institut für Nachrichtentechnik und Hochfrequenztechnik

eingereicht an der Technischen Universität Wien
Fakultät für Elektrotechnik und Informationstechnik

von

Amalia Roca
Matrikelnr.: 0526852
San Antonio 4, 12596 Torreblanca
Castellón - Spain

Vienna, February 2007 . . . . . .

I certify that the work presented in this diploma thesis was done by myself and the work of other authors is properly cited.

Amalia Roca
Vienna, February 2007

Acknowledgements

I would like to acknowledge many people who helped me during the course of this work, supporting it in one way or another. First and foremost, my appreciation and thanks go to my family. In particular, I can never thank my parents enough for their commitment, sacrifice, and overalls, their consistent encouragement and support.

I wish to express my gratitude to my supervisor, Christian Mehlführer, for his seasoned guidance. Without his helpful suggestions this thesis could not be done. I also want to thank the people I met during my stay in Vienna and my colleagues at UPV for their friendship, help, and cheerfulness. I could not possibly forget M.J, and C. and the rest of A.C. Thank you for your support when my confidence was down.

Last, but not least, I want to mention A.F., who would be very proud of me to see that, at the end, all the efforts have their recompense.

Abstract

In the last few years, the telecommunication industries' development has focused on an intensive use of broadband systems, which are characterized by high quality features. For this issue, new technologies with high transmission abilities have been designed. The broadband wireless access has become the best way to meet escalating business demand for rapid internet connection and integrated "triple play" services. In addition to not only topographic but also technological limitations, wireless solution alternatives have been found. That is the very base of the WiMAX concept: a wireless transmission infrastructure that allows a fast deployment as well as low maintenance costs. Based on the IEEE 802.16-2004 standard, WiMAX allows for an efficient use of bandwidth in a wide frequency range, and can be used as a last mile solution for broadband internet access.

The aim of this diploma thesis is to implement all compulsory features of the WiMAX OFDM physical layer specified in IEEE 802.16-2004 in Matlab Simulink. Optional space-time coding for more than one transmit antenna is implemented to allow performance investigations in various MIMO scenarios. Likewise, a maximum ratio combining diversity scheme is implemented in the receiver for the same purpose. In order to combat the temporal variations in quality on a multipath fading channel, an adaptive modulation and coding technique is used. This technique employs multiple modulation and coding schemes to instantaneously adapt to the variations in the channel SNR, thus maximizing the system throughput and improving BER performance.

The thesis gives an overview about the WiMAX standard and studies the performance of a WiMAX transmitter and receiver, also covering the performance gains of some optional features, such as the MIMO extension. The influence of these parts on the system performance is shown and analyzed in great detail in simulation results.

Contents

Chapter 1

Introduction

The experienced growth in the use of digital networks has led to the need for the design of new communication networks with higher capacity. The telecommunication industry is also changing, with a demand for a greater range of services, such as video conferences, or applications with multimedia contents. The increased reliance on computer networking and the Internet has resulted in a wider demand for connectivity to be provided "any where, any time", leading to a rise in the requirements for higher capacity and high reliability broadband wireless telecommunication systems.

Broadband availability brings high performance connectivity to over a billion users worldwide, thus developing new wireless broadband standards and technologies that will rapidly span wireless coverage. Wireless digital communications are an emerging field that has experienced an spectacular expansion during the last several years. Moreover, the huge uptake rate of mobile phone technology, WLAN (Wireless Local Area Network) and the exponential growth of Internet have resulted in an increased demand for new methods of obtaining high capacity wireless networks [1].

Worldwide Interoperability for Microwave Access, known as WiMAX, is a wireless networking standard which aims for addressing interoperability across IEEE[1] 802.16 standard-based products. WiMAX defines a WMAN[2], a kind of a huge hot-spot that provides interoperable broadband wireless connectivity to fixed, portable, and nomadic users. It allows communications which have no direct visibility, coming up as an alternative connection for cable, DSL[3], and T1/E1 systems, as well as a possible transport network for Wi-Fi[4] hot-spots, thus becoming a solution to develop broadband industry

[1] Institute of Electrical and Electronics Engineers
[2] Wireless Metropolitan Area Network
[3] Digital Subscriber Line
[4] Wireless-Fidelity, name given to WLAN IEEE 802.11b standard-based products.

platforms. Likewise, products based on WiMAX technology can be combined with other technologies to offer broadband access in many of the possible scenarios of utilization, as shown in Figure 1.0 - 1, where examples of the deployment of WiMAX systems are illustrated.

WiMAX will substitute other broadband technologies competing in the same segment and will become an excellent solution for the deployment of the well-known last mile infrastructures in places where it is very difficult to get with other technologies, such as cable or DSL, and where the costs of deployment and maintenance of such technologies would not be profitable. In this way, WiMAX will connect rural areas in developing countries as well as underserved metropolitan areas. It can even be used to deliver backhaul for carrier structures, enterprise campus, and Wi-Fi hot-spots. WiMAX offers a good solution for these challenges because it provides a cost-effective, rapidly deployable solution [2].

Additionally, WiMAX will represent a serious competitor to 3G (Third Generation) cellular systems as high speed mobile data applications will be achieved with the 802.16e specification.

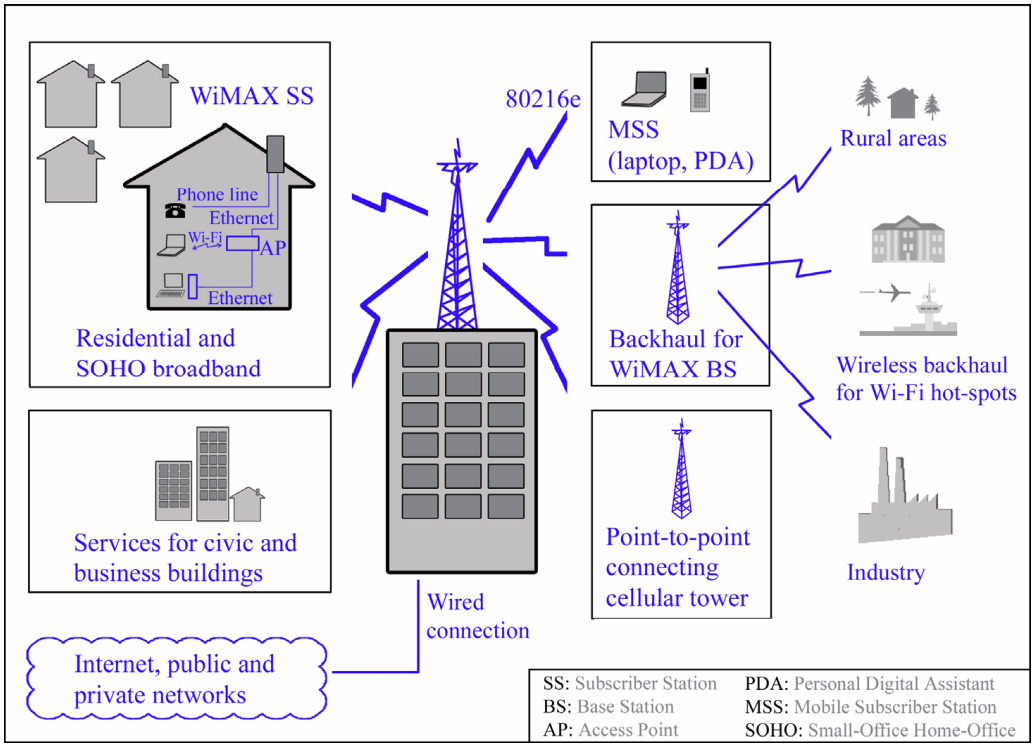

Figure 1.0 - 1: Possible scenarios for the deployment of WiMAX.

1.1 The WiMAX standard

The IEEE 802.16 standard was firstly designed to address communications with direct visibility in the frequency band from 10 to 66 GHz. Due to the fact that non-line-of-sight transmissions are difficult when communicating at high frequencies, the amendment 802.16a was specified for working in a lower frequency band, between 2 and 11 GHz. The IEEE 802.16d specification is a variation of the fixed standard (IEEE 802.16a) with the main advantage of optimizing the power consumption of the mobile devices. The last revision of this specification is better known as IEEE 802.16-2004 [3].

On the other hand, the IEEE 802.16e standard is an amendment to the 802.16-2004 base specification with the aim of targeting the mobile market by adding portability.

WiMAX standard-based products are designed to work not only with IEEE 802.16-2004 but also with the IEEE 802.16e specification. While the 802.16-2004 is primarily intended for stationary transmission, the 802.16e is oriented to both stationary and mobile deployments.

1.1.1 Technical overview

The WiMAX standard defines the air interface for the IEEE 802.16-2004 specification working in the frequency band 2-11 GHz. This air interface includes the definition of the medium access control (MAC) and the physical (PHY) layers.

Medium Access Control (MAC) layer

Some functions are associated with providing service to subscribers. They include transmitting data in frames and controlling the access to the shared wireless medium. The medium access control (MAC) layer, which is situated above the physical layer, groups the mentioned functions.

The original MAC is enhanced to accommodate multiple physical layer specifications and services, addressing the needs for different environments. It is generally designed to work with point-to-multipoint topology networks, with a base station controlling independent sectors simultaneously. Access and bandwidth allocation algorithms must be able to accommodate hundreds of terminals per channel, with terminals that may be shared by multiple end users. Therefore, the MAC protocol defines how and when a base station (BS) or a subscriber station (SS) may initiate the transmission on the channel. In the downstream direction there is only one transmitter, and the MAC

Feature	Benefit
TDM/TDMA scheduled uplink/downlink frames	• Efficient bandwidth usage.
Scalable from one to hundreds of subscribers	• Allows cost effective deployments by supporting enough subscribers to deliver a robust business case.
Connection-oriented	• Per connection QoS. • Faster packet routing and forwarding.
QoS support	• Low latency for delay sensitive services (TDM, Voice, VoIP). • Optimal transport for VBR[6]traffic (video). • Data priorization.
Automatic retransmission request (ARQ)	• Improves end-to-end performance by hiding RF layer induced errors from upper layer protocols.
Support for adaptive modulation	• Enables highest data rates allowed by channel conditions, exploiting system capacity.
Security and encryption (TripleDES)	• Protects user privacy.
Automatic power control	• Enables cellular deployments by minimizing self-interference.

Table 1.1 - 1: 802.16-2004 MAC features.

protocol is quite simple using TDM[5] to multiplex the data. However, in the upstream direction, where multiple SSs compete for accessing to the medium, the MAC protocol applies a time division multiple access (TDMA) technique, thus providing an efficient use of the bandwidth.

The services required by the multiple users are varied, including voice and data, Internet protocol (IP) connectivity, and voice over IP (VoIP). In order to support this variety of services, the MAC layer must accommodate both continuous and bursty traffic, adapting the data velocities and delays to the needs of each service. Additionally, mechanisms in the MAC provide for differentiated quality of service (QoS) supporting the needs of various applications.

Issues of transport efficiency are also addressed. Both modulation and coding schemes are specified in a burst profile that is adjusted adaptively for each burst to each subscriber station, making the use of bandwidth efficient, providing maximum data rates, and improving the capacity of the system. The request-grant mechanism is designed to be scalable, efficient, and self-

[5]Time Division Multiplexing
[6]Variable Bit Rate

correcting, allowing the system a scalability from one to hundreds of users. Another feature that improves the transmission performance is the automatic repeat request (ARQ) as well as the support for mesh topology rather than only point-to-multipoint network architectures. The possibility of working with mesh topologies allows direct communication between SSs, enhancing this way the scalability of the system. The standard also supports automatic power control, and security and encryption mechanisms. Further information about the MAC features can be found in [4] and [5].

Physical (PHY) layer

The IEEE 802.16-2004 standard defines three different PHYs that can be used in conjunction with the MAC layer to provide a reliable end-to-end link. These PHY specifications are:

- A single carrier (SC) modulated air interface.
- A 256-point FFT OFDM[7] multiplexing scheme.
- A 2048-point FFT OFDMA[8] scheme.

While the SC air interface is used for line-of-sight (LoS) transmissions, the two OFDM-based systems are more suitable for non line-of-sight (NLoS) operations due to the simplicity of the equalization process for multicarrier signals. The fixed WiMAX standard defines profiles using the 256-point FFT OFDM PHY layer specification. Furthermore, fixed WiMAX systems provide up to 5 km of service area allowing transmissions with a maximum data rate up to 70 Mbps in a 20 MHz channel bandwith, and offer the users a broadband connectivity without needing a direct line-of-sight to the base station.

The main features of the mentioned fixed WiMAX are detailed next:

- Use of an OFDM modulation scheme, which allows the transmission of multiple signals using different subcarriers simultaneously. Because the OFDM waveform is composed of multiple narrowband orthogonal carriers, selective fading is localized to a subset of carriers that are relatively easy to equalize.
- Design of an adaptive modulation and coding mechanism that depends on channel and interference conditions. It adjusts the modulation method almost instantaneously for optimum data transfer, thus making a most efficient use of the bandwidth.

[7] Orthogonal Frequency Division Multiplexing
[8] Orthogonal Frequency Division Multiple Access

- Support of both time and frequency division duplexing formats, FDD and TDD, allowing the system to be adapted to the regulations in different countries.

- Robust FEC[9] techniques, used to detect and correct errors in order to improve throughput. The FEC scheme is implemented with a Reed-Solomon encoder concatenated with a convolutional one, and followed by an interleaver. Optional support of block turbo coding (BTC) and convolutional turbo coding (CTC) can be implemented.

- Use of flexible channel bandwidths, comprised from 1.25 to 20 MHz, thus providing the necessary flexibility to operate in many different frequency bands with varying channel requirements around the world. This flexibility facilitates transmissions over longer ranges and from different types of subscriber platforms. In addition, it is also crucial for cell planning, especially in the licensed spectrum.

- Optional support of both transmit and receive diversity to enhance performance in fading environments through spatial diversity, allowing the system to increase capacity. The transmitter implements space-time coding (STC) to provide transmit source independence, reducing the fade margin requirement, and combating interference. The receiver, however, uses maximum ratio combining (MRC) techniques to improve the availability of the system.

- Design of a dynamic frequency selection (DFS) mechanism to minimize inteferences.

- Optional support of smart antennas, whose beams can steer their focus to a particular direction or directions always pointing at the receiver, and consequently, avoiding interference between adjacent channels, and increasing the spectral density and the SNR. There are two basic types of smart antennas, those with multiple beam (directional antennas), and those known as adaptive antenna systems (AAS). The first ones can use either a fixed number of beams choosing the most suitable for the transmission or an steering beam to the desired antenna. The second type works with multi-element antennas with a varying beam pattern. These smart antennas are becoming a good alternative for BWA[10] deployments.

[9] Forward Error Correction
[10] Broadband Wireless Access

Feature[11]	**Benefit**
256-point FFT OFDM waveform	• Simple equalization of multipath channels in outdoor LoS and NLoS environments.
Adaptive modulation and variable error correction encoding per radio frequency (RF) burst	• Ensures a robust RF link while maximizing the number of bits per second for each subscriber unit.
TDD and FDD duplexing support	• Addresses varying worldwide regulations when one or both may be allowed.
Flexible channel sizes (from 1.25 to 20 MHz)	• Provides the necessary flexibility to operate in many different frequency bands with varying requirements around the world.
DFS support	• Minimizes interference between adjacent channels.
Designed to support AAS	• Smart antennas are fast becoming more affordable, and as these costs come down, their ability to suppress interference and increase system gain is more important to BWA deployments.
TDM and FDM support	• Allows interoperability between cellular systems (TDM) and wireless systems (FDM).
Designed to support multiple-input multiple-output (MIMO) schemes	• Implemented in DL to increase diversity and capacity. • STC algorithms at the transmitter, MRC at the receiver.

Table 1.1 - 2: 802.16-2004 PHY features.

- Implementation of channel quality measurements which help in the selection and assignment of the adaptive burst profiles.
- Support of both time and frequency division multiplexing formats (TDM and FDM), to allow interoperability between cellular systems working with TDM, and wireless systems that use FDM.

The mobile WiMAX (IEEE 802.16e)[12] uses the 2048-point FFT OFDMA PHY specification. It provides a service area coverage from 1.6 to 5 km, allowing transmission rates of 5 Mbps in a 5 MHz channel bandwidth, and with a user maximum speed below 100 km/h. It presents the same features as those of the fixed WiMAX specification that have been already mentioned. However, other features such as handoffs and power-saving mechanisms are added to offer a reliable communication. Battery life and handoff are two critical issues for mobile applications. On one hand, maximizing battery life

[11] All these features are in great detail explained in [5].

[12] A complete description of the mobile WiMAX can be found in [6].

implies minimizing the mobile station (MS) power usage. On the other hand, handoff and handovers are necessary to enable the MS to switch from one BS to another at vehicular speeds without interrupting the connection.

The main features of the initial IEEE 802.16 standard, and those of the so-called fixed and mobile WiMAX, 802.16-2004 and 802.16e respectively, are summarized in the following chart:

	802.16	**802.16-2004**	**802.16e**
Spectrum	10-66 GHz	< 11 GHz	< 6 GHz
Maximum data rate	32-134 Mbps (28 MHz channel)	up to 70 Mbps (20 MHz channel)	up to 15 Mbps (5 MHz channel)
Alignment	LoS	LoS and NLoS	LoS and NLoS
Coverage range	2-5 km approx.	5-10 km approx. (maximum of 50 km)	2-5 km approx.
Channel bandwidth	20, 25 and 28 MHz	Flexible, from 1.25 up to 20 MHz	Equal to 802.16-2004
Modulation	2-PAM, 4-QAM, 16-QAM, and 64-QAM	OFDM with 256 subcarriers 2-PAM, 4-QAM, 16-QAM, and 64-QAM	OFDMA with 2048 subcarriers 2-PAM, 4-QAM, 16-QAM, and 64-QAM
Mobility	Fixed	Fixed and Pedestrian	Vehicular (20-100 km/h)

Table 1.1 - 3: IEEE 802.16, IEEE 802.16-2004, and IEEE 802.16e standards.

1.1.2 Relationship with other wireless technologies

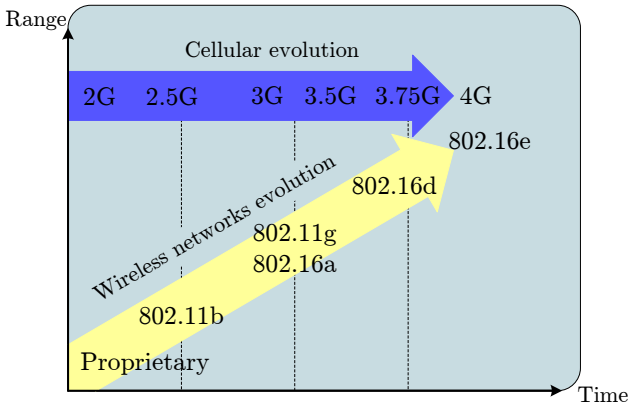

Figure 1.1 - 1: Convergence in wireless communications.

Wireless access to data networks is expected to be an area of rapid growth for mobile communication systems. The huge uptake rate of mobile phone technologies, WLANs and the exponential growth that is experiencing the use of the Internet have resulted in an increased demand for new methods to obtain high capacity wireless networks. WiMAX may be seen as the fourth generation (4G) of mobile systems as the convergence of cellular telephony, computing, Internet access, and potentially many multimedia applications become a real fact. The mentioned convergence between wireless and cellular networks is illustrated in Figure 1.1 - 1.

In any case, both WLAN and cellular mobile applications are being widely expanded to offer the demanded wireless access. However, they experience several difficulties for reaching a complete mobile broadband access, bounded by factors such as bandwidth, coverage area, and infrastructure costs. On one hand, Wi-Fi provides a high data rate, but only on a short range of distances and with a slow movement of the user. On the other hand, UMTS[13] offers larger ranges and vehicular mobility, but instead, it provides lower data rates, and requires high investments for its deployment. WiMAX tries to balance this situation . As shown in Figure 1.1 - 2, it fills the gap between Wi-Fi and UMTS, thus providing vehicular mobility (included in IEEE 802.16e), and high service areas and data rates.

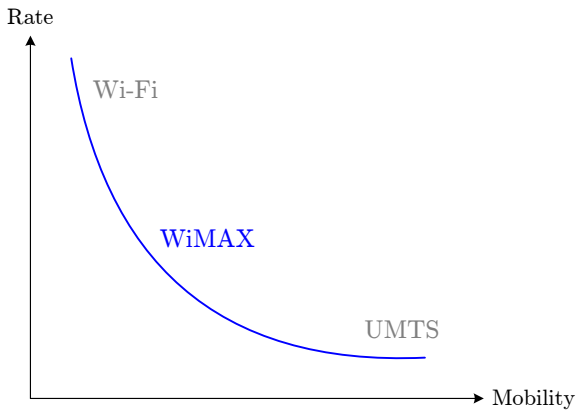

Figure 1.1 - 2: WiMAX fills the gap between Wi-Fi and UMTS.

Therefore, while WiMAX will complement Wi-Fi and UMTS in some of the possible scenarios where these systems are not sufficiently developed, i.e. they face several problems in the deployment and they do not offer enough capacity to serve all possible users, WiMAX will compete with Wi-Fi and

[13] Universal Mobile Telecommunications System

UMTS also in other possible scenarios, where, in general, the costs in the deployment, maintenance, or just the supply of the service would not be profitable.

Table 1.1 - 4 gives an overview on the comparison between the mentioned systems, WiMAX and its two closest competitors, Wi-Fi and UMTS. A deeper analysis of these three systems will be developed next.

	Wi-Fi	**WiMAX**		**UMTS HSDPA**
Standard	IEEE 802.11	IEEE 802.16		IMT2000[14]
Channel width	Fixed 20 MHz	Variable $\leq$ 20 MHz	Variable $\leq$ 28 MHz	Fixed 5 MHz
Spectrum	2.4/5.2 GHz	2-11 GHz	10-66 GHz	$\sim$2 GHz
Data rate	2/54 Mbps	70 Mbps	240 Mbps	1/14 Mbps
Range	100 m	1-7 km	12-15 km	50 km
Multiplexing	TDM	FDM/TDM	FDM/TDM	FDM
Transmission	SS[15]/OFDM	OFDM/OFDMA	SC	WCDMA
Mobility	Pedestrian	Vehicular (802.16e)	No	Vehicular
Advantages	Throughput and costs	Throughput and range		Mobility and range
Disadvantages	Short range	Interference issues?		Low rates and expensive

Table 1.1 - 4: Comparative table between Wi-Fi, WiMAX and UMTS.

WiMAX vs. Wi-Fi

Wi-Fi or WLAN is the name with which the IEEE 802.11 standard-based products are known. It includes the 802.11a specification, capable to offer data rates of 54 Mbps working in the frequency band of 5.2 GHz; and the 802.11b specification, in the 2.4 GHz frequency band, which provides users with data rates of 11 Mbps. This technology has generally a coverage area of 100 meters and fixed channel bandwidths of 20 MHz [7].

WiMAX appeared to fulfil the need for delivering wireless access to MANs. It was designed to offer BWA services to metropolitan areas providing users with larger coverage ranges and higher data rates. WiMAX systems are able to support users in ranges up to 50 km with a direct visibility to the base station and ranges from 1 to 7 km where no visibility is available. Rates from 70 to 240 Mbps are offered and can be achieved with this technology.

[15] International Mobile Communications
[15] Spread Spectrum

However, WiMAX does not create a conflict with the mentioned Wi-Fi, as they are complementary technologies. WiMAX provides a low cost way to backhaul Wi-Fi hot-spots and WLAN points in businesses and homes, offering a wireless last mile extension for cable and DSL infrastructures.

WiMAX vs. UMTS

UMTS is identified with the so-called third generation of cellular networks standardized by the 3GPP[16]. The frequency bands that are assigned to this technology are the licensed frequencies from 1885 to 2025 MHz, and from 2110 to 2200 MHz. It uses wideband code division mutiple access (WCDMA) as the carrier modulation scheme, and it has been specified as an integrated solution for mobile voice and data with wide coverage area, offering data rates that may decrease while the velocity of the user increases. This system provides for theoretical bit rates of up to 384 kbps in high mobility situations, which rise as high as 2 Mbps in stationary user environments, employing a 5 MHz channel width. Moreover, HSDPA[17] technology further increases the throughput speeds, providing theoretical data rates as high as 14 Mbps [8].

WiMAX is becoming a serious threat for 3G cellular networks because of its broadband and distance capabilities, as well as its ability to effectively support voice with full QoS. WiMAX is also able to offer higher data rates than UMTS, but it does not allow the same grade of mobility. However, it is expected to be set up as an alternative to cellular networks, as the investments the operators need to carry out for its deployment are not so high.

1.2 Outline of the thesis

This thesis examines the implementation of a WiMAX simulator built with Matlab Simulink. This simulator is targeted to the 256-point FFT OFDM PHY layer. The thesis is organized in eight chapters, in which a detailed overview of every element of the system is given taking into account both the standard specifications and the corresponding theoretical aspects, which are necessary to understand all the different methods and processes that have been used.

An overview of the WiMAX system has already been exposed in the present chapter, where the main features of the standard are summarized. In order to understand the objectives and the applications of this system, a

[16] 3rd Generation Partnership Project

[17] High Speed Downlink Packet Access

comparison between WiMAX and other wireless systems is also included in the chapter.

The remaining seven chapters discuss the implementation of the WiMAX simulator.

As any other communication system, WiMAX has three basic elements, a transmitter, a receiver, and a channel over which the information is sent. The main components of a WiMAX communication system are shown in Figure 1.2 - 1.

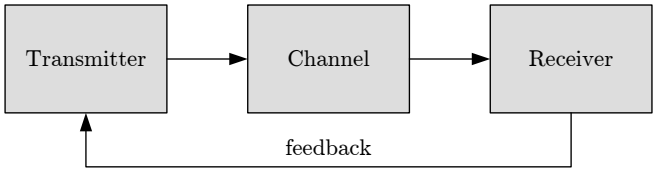

Figure 1.2 - 1: Basic communication system.

The transmitter, presented in Chapter 2, is the one who generates the signal to be sent over the channel. Before sending it, the signal has to be adapted to the channel conditions using a specific adaptive modulation and coding scheme. As data is transmitted using the OFDM transmission technique, it also needs to be conformed into an OFDM symbol by performing the corresponding operations, which include a frequency-time transformation and the addition of a guard period. Then, the signal is sent over the channel, discussed in the next chapter.

Chapter 3 examines the communication channel. For the WiMAX system, it is a wireless channel. The performance of any wireless communication system is highly dependent on the propagation channel, and so, a detailed knowledge of radio propagation effects, such as path loss, frequency-selective fading, Doppler spread, and multipath delay spread have to be considered for the optimization of the communication link. This way, this chapter gives a theoretical explanation about time-variant channels, to afterwards outline two fading channel models, flat and frequency-selective fading channels. The channel implementation of our simulator is also discussed in this chapter, which offers in its end an overview of the well-known I-METRA[18] used to model fading channels.

The receiver is examined in Chapter 4. It observes the signal after the channel and performs the necessary operations to obtain the transmitted information. These operations include a channel estimation as well as an equalization process to solve the degrading effects of the signal caused by

[18] Intelligent Multi-Element Transmit and Receive Antennas

multipath propagation. Furthermore, a method that accomplishes the proper decoding of soft or hard demodulator outputs to reproduce, as accurately as possible, the data that was transmitted is also implemented.

Chapter 5 introduces MIMO systems. The use of multiple antennas at the transmitter and/or at the receiver in a communication link opens a new dimension in reliable wireless communications, improving the performance of the system substantially. The core idea in the MIMO transmitter is STC in which signal processing in time is completed with signal processing in the spatial dimension by using multiple spatially distributed antennas at both link ends. The MRC diversity scheme, by which multiple replicas of the same information signal received over different diversity branches are combined so as to maximize the instantaneous signal-to-noise ratio (SNR) at the combiner output, is used in the MIMO receiver.

Additionally, a feedback mechanism that allows to transfer information about the channel state back to the transmitter is described. Using this information, an adaptive modulation and coding (AMC) mechanism can be implemented. Chapter 6 is devoted to the analysis of the mentioned AMC process. Based on the current channel characteristics, it adaptively changes the coding and the carrier modulation scheme allowing the data rate to be maximized.

Chapter 7 analyzes the obtained results. Firstly, simulation results using an AWGN[19] channel are discussed. Next, simulations with MIMO channels show not only the improvement in BER[20] performance but also the increase in data rate that can be achieved without any bandwidth expansion when using these systems. Lastly, several results show the enhancement in throughput obtained with the performance of the AMC mechanism.

Finally, the concluding remarks are summed up in Chapter 8.

Additionally, this work also includes five appendices that complete the thesis already outlined. Appendix A is intended to give an overview of OFDM systems. Appendix B presents a detailed analysis on the derivation of some formulas explained in the thesis. In Appendix C, a set of values for the parameters of the simulator is listed. A comparison between parameters used in a previously implemented WLAN and those of the newly built WiMAX simulator is also given in this appendix. Appendix D gives a general view of the WiMAX simulator through the whole Simulink block diagram. Finally, Appendix E includes two lists, the first contains the acronyms used in the thesis, written in their full length, and the second includes the notations that have been employed through this work.

[19] Additive White Gaussian Noise
[20] Bit Error Rate

Chapter 2

Transmitter

This chapter describes the different steps the transmitter performs before transmitting the data. The functional blocks that compose the transmitter of the WiMAX simulator are depicted in Figure 2.0 - 1.

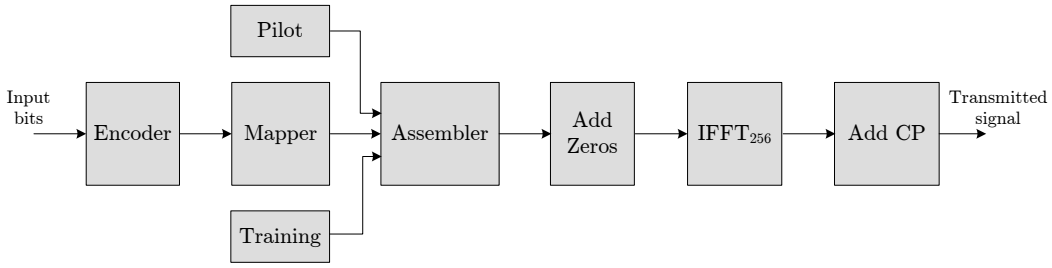

Figure 2.0 - 1: Transmitter of the WiMAX system.

First of all, the data from the source is randomized and afterwards, coded and mapped into QAM[1] symbols. As previously explained in Chapter 1, the simulator implemented in the thesis works for the WirelessMAN-OFDM physical (PHY) layer of WiMAX. This PHY layer uses orthogonal frequency division multiplexing (OFDM) with 256 subcarriers.

Each OFDM[2] symbol is composed of 192 data subcarriers, 1 zero DC subcarrier, 8 pilot subcarriers, and 55 guard carriers. Therefore, a process of assembling the zero DC subcarrier, data, and pilots is needed to built the symbols. Furthermore, preambles consisting of training sequences are appended at the beginning of each burst. These training sequences are used for performing an estimation of the channel coefficients at the receiver.

[1] Quadrature Amplitude Modulation

[2] A detailed analysis of the OFDM theory is given in Appendix A.

After the assembling process, a zero padding is performed. The signal is converted to the time domain by means of the inverse fast Fourier transform (IFFT) algorithm, and finally, a cyclic prefix (CP) with the aim of preventing inter-symbol interference is added.

2.1 Source

As described in the standard [4], the information bits must be randomized before the transmission. The randomization process is used to minimize the possibility of transmissions of non-modulated subcarriers. The process of randomization is performed on each burst of data on the downlink and uplink, and on each allocation of a data block (subchannels on the frequency domain and OFDM symbols on the time domain).

In our case, instead of performing a randomization process, a binary source that produces random sequences of bits is used. The number of bits that are generated is specified to be frame-based and is calculated from the packet size required in each situation. The packet size depends on the number of transmitted OFDM symbols and the overall coding rate of the system, as well as the modulation alphabet.

Equation 2.1 - 1 calculates the number of transmitted OFDM symbols in one frame. It depends on the total number of transmitted symbols, N_{Tsym}, which also includes the symbols used for the preamble, specified by N_{train}:

$$N_{\text{OFDM}} = N_{\text{Tsym}} - N_{\text{train}}. \tag{2.1 - 1}$$

Furthermore, the total number of transmitted symbols is defined as

$$N_{\text{Tsym}} = \frac{T_{\text{frame}}}{T_{\text{sym}}}. \tag{2.1 - 2}$$

In the formula, T_{sym} is the OFDM symbol time, and T_{frame} denotes the frame duration. The expression that defines T_{sym} as well as the possible values specified for the frame duration can be found in Section C.1.1.

Once the number of OFDM symbols is known, the number of bits to be sent by the source is calculated:

$$S_{\text{packet}} = N_{\text{OFDM}} R N_{\text{data}} M_{\text{a}}. \tag{2.1 - 3}$$

Here, R represents the overall coding rate, N_{data} is the number of used data subcarriers, and M_{a} defines the modulation alphabet, which is specified by the number of transmitted bits per symbol.

2.2 Encoder

As shown in Figure 2.2 - 1, the encoding process consists of a concatenation of an outer Reed-Solomon (RS) code and an inner convolutional code (CC) as a FEC scheme. That means that first data passes in block format through the RS encoder, and then, it goes across the convolutional encoder. It is a flexible coding process due to the puncturing of the signal, and allows different coding rates. The last part of the encoder is a process of interleaving to avoid long error bursts.

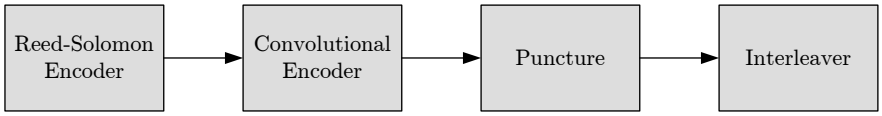

Figure 2.2 - 1: The coding process in WiMAX.

A variable-rate coding scheme that depends on the channel conditions is designed to offer optimal error protection levels to the users. The FEC options are paired with several modulation schemes to form burst profiles of varying robustness and efficiency. Table 2.2 - 1 gives the block sizes and code rates used for the different modulations.

AMC	**Modulation**	**RS code**	**CC code rate**	**Overall code rate**
1	2-PAM[3]	(12,12,0)	1/2	1/2
2	4-QAM	(32,24,4)	2/3	1/2
3	4-QAM	(40,36,2)	5/6	3/4
4	16-QAM	(64,48,4)	2/3	1/2
5	16-QAM	(80,72,4)	5/6	3/4
6	64-QAM	(108,96,6)	3/4	2/3
7	64-QAM	(120,108,6)	5/6	3/4

Table 2.2 - 1: WiMAX modulation and coding schemes.

The users report the current channel condition to the base station (BS) and, based on this report, a specific coding rate is selected for the downlink data transmissions. Thus, users who experience a "bad" channel condition, i.e. low SNR, at a given time, will be provided with better error correction

[3] Pulse Amplitude Modulation

than those users experiencing "good" channel conditions at the same time. This process is called adaptive modulation and coding (AMC)[4].

In the next sections, each one of the different encoder blocks will be explained in detail. It will be given a thorough description of how they work and are implemented in the simulator.

2.2.1 Reed-Solomon encoder

The properties of Reed-Solomon codes make them suitable to applications where errors occur in bursts. Reed-Solomon error correction is a coding scheme which works by first constructing a polynomial from the data symbols to be transmitted, and then sending an oversampled version of the polynomial instead of the original symbols themselves.

A Reed-Solomon code is specified as RS(n, k, t) with l-bit symbols. This means that the encoder takes k data symbols of l bits each and adds $2t$ parity symbols to construct an n-symbol codeword. Thus, n, k and t can be defined as:

- n: number of bytes after encoding,
- k: number of data bytes before encoding,
- t: number of data bytes that can be corrected.

The error correction ability of any RS code is determined by $(n - k)$, the measure of redundancy in the block. If the location of the erroneous symbols is not known in advance, then a Reed-Solomon code can correct up to t symbols, where t can be expressed as $t = (n - k)/2$.

As specified in the standard, the Reed-Solomon encoding shall be derived from a systematic RS($n = 255$, $k = 239$, $t = 8$) code using a Galois field specified as GF(2^8). The primitive and generator polynomials used for the systematic code are expressed as follows:

Primitive Polynomial:

$$p(x) = x^8 + x^4 + x^3 + x^2 + 1 \tag{2.2-1}$$

Generator Polynomial:

$$g(x) = (x + \lambda^0)(x + \lambda^1)(x + \lambda^2)...(x + \lambda^{2t-1}) \tag{2.2-2}$$

[4]Further information of the AMC mechanism can be found in Chapter 6.

The primitive polynomial is the one used to construct the symbol field and it can also be named as field generator polynomial. The code generator polynomial is used to calculate parity symbols and has the form specified as before, where λ is the primitive element of the Galois field over which the input message is defined. See [9] and [10] for more information about Reed-Solomon codes.

To make the RS code flexible, i.e. to allow for variable block sizes and variable correction capabilities, it is shortened and punctured. When a block is shortened to k bytes, $239 - k$ zero bytes are added as a prefix, and, after the encoding process, the $239 - k$ encoded zero bytes are discarded. Once the process of shortening has been done, the number of symbols going in and out of the RS encoder change, and also the number of symbols that can be corrected, t. With the puncturing, only the first $2t$ of the total 16 parity bytes[5] shall be employed. Figure 2.2 - 2 shows the RS encoding, shortening, and puncturing process.

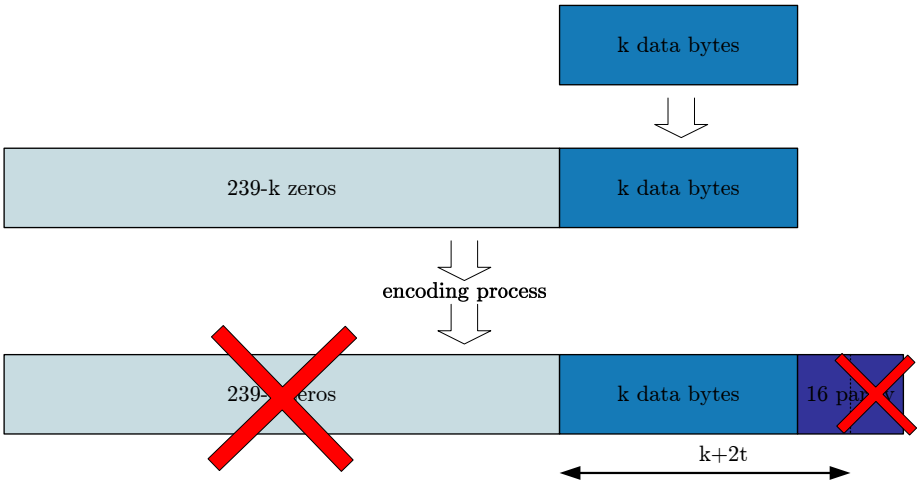

Figure 2.2 - 2: Process of shortening and puncturing of the RS code.

The input of the RS encoder block defined by Simulink is specified to be a vector whose length is an integer multiple of lk, being l the length of the binary sequences corresponding to elements of the Galois field GF(2^l), and the output, a vector whose length is the same integer multiple of ln. Therefore, the first step to implement is to divide the data vector in a number of blocks whose length fits the requirement quoted above. At the same time, it has to be taken into account that the number of data bytes before encoding,

[5]The parity bytes are calculated from the systematic RS(255, 239, 8) code, as $2t = n-k$.

k, the number of overall bytes after encoding, n, and the number of data bytes that can be corrected, t, are the ones specified in Table 2.2 - 1, and they change for every modulation scheme. Thus, the number of blocks used in the Reed-Solomon encoder is calculated as

$$N_{\mathrm{RS}} = \frac{S_{\mathrm{packet}}}{8k}. \tag{2.2 - 3}$$

A block diagram of the Reed-Solomon encoder implemented in Matlab Simulink is depicted in Figure 2.2 - 3.

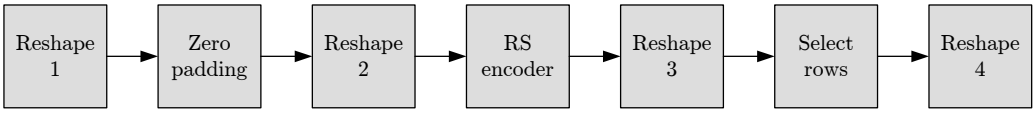

Figure 2.2 - 3: Block diagram of the Reed-Solomon encoder of WiMAX.

"Reshape 1" arranges the input data of the RS encoder in a matrix form, where the corresponding number of rows is calculated from the length of the blocks before encoding, k, and the number of calculated Reed-Solomon blocks, as specified in Equation 2.2 - 3, determines the number of columns. Zero padding along columns at the beginning is performed to achieve a length of 239 bytes for each block. "Reshape 2" shapes out the matrix structure into a vector[6]. Once data has passed through the encoder, the block "Reshape 3" distributes the output vector of the encoder in a matrix with size $255 \times N_{\mathrm{RS}}$. The "Select rows"-block deals with selecting the correct amount of bytes after the encoding process. Thus, the zero prefix is discarded, and data is punctured by taking only the first $2t$ bytes of the total parity bytes, as previously explained. To end, "Reshape 4" rearranges the matrix data in a column vector, ready for the convolutional coding.

2.2.2 Convolutional encoder

After the RS encoding process, the data bits are further encoded by a binary convolutional encoder, which has a native rate of $1/2$ and a constraint length of 7. The generator polynomials used to derive its two output code bits, denoted X and Y, are specified in the following expressions:

$$G_1 = 171_{OCT} \quad \text{for} \quad X, \tag{2.2 - 4}$$

$$G_2 = 133_{OCT} \quad \text{for} \quad Y. \tag{2.2 - 5}$$

[6]The RS encoder block of Simulink only works with vector structures.

A convolutional encoder accepts messages of length k_0 bits and generates codewords of n_0 bits. Generally, it is made up of a shift register of L segments, where L denotes the constraint length.

The binary convolutional encoder that implements the described code is shown in Figure 2.2 - 4. A connection line from the shift register feeding into the adder means a "one" in the octal representation of the polynomials, and no connection is represented by a "zero".

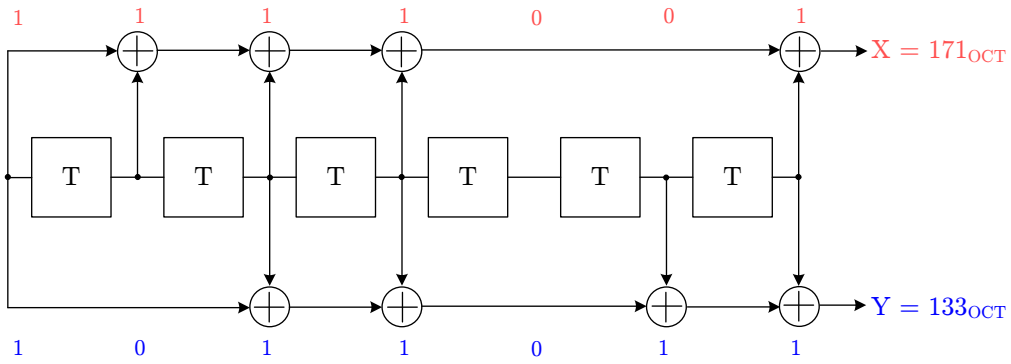

Figure 2.2 - 4: Convolutional encoder of binary rate 1/2.

2.2.3 Puncturing process

Puncturing is the process of systematically deleting bits from the output stream of a low-rate encoder in order to reduce the amount of data to be transmitted, thus forming a high-rate code. The bits are deleted according to a perforation matrix, where a "zero" means a discarded bit.

The process of puncturing is used to create the variable coding rates needed to provide various error protection levels to the users of the system. The different rates that can be used are rate 1/2, rate 2/3, rate 3/4, and rate 5/6. The puncturing vectors for these rates are given in Table 2.2 - 2.

Rate	**Puncture vector**
1/2	[1]
2/3	[1 1 1 0]
3/4	[1 1 0 1 1 0]
5/6	[1 1 0 1 1 0 0 1 1 0]

Table 2.2 - 2: Puncture vectors for different convolutional coding rates.

The convolutional coding and puncturing is directly supported by Simulink in a single block. This block was used for the implementation.

2.2.4 Interleaver

Data interleaving is generally used to scatter error bursts and thus, reduce the error concentration to be corrected with the purpose of increasing the efficiency of FEC by spreading burst errors introduced by the transmission channel over a longer time. Interleaving is normally implemented by using a two-dimensional array buffer, such that the data enters the buffer in rows, which specify the number of interleaving levels, and then, it is read out in columns. The result is that a burst of errors in the channel after interleaving becomes in few scarcely spaced single symbol errors, which are more easily correctable.

WiMAX uses an interleaver that combines data using 12 interleaving levels. The effect of this process can be understood as a spreading of the bits of the different symbols, which are combined to get new symbols, with the same size but with rearranged bits.

The interleaver of the simulator has been implemented in two steps. First, data passes through a matrix interleaver which performs block interleaving by filling a matrix with the input symbols row by row, and then sending this matrix content column by column. The parameters used for this block are the number of rows and columns that compose the matrix:

$$N_{\text{rows}} = 12, \qquad N_{\text{columns}} = \frac{N_{\text{tcb}}}{N_{\text{rows}}}.$$

The second step consists of a block interleaver. It rearranges the elements of its input according to an index vector. This vector is defined as

$$I = \sum_{i=0}^{N_{\text{tcb}}-1} \left(s \left\lfloor \frac{i}{s} \right\rfloor + \text{mod} \left(i + N_{\text{tcb}} - \left\lfloor \frac{i N_{\text{rows}}}{N_{\text{tcb}}} \right\rfloor, s \right) + 1 \right), \qquad (2.2\text{-}6)$$

where:

- N_{tcb} is the total number of coded bits,

$$N_{\text{tcb}} = N_{\text{cpc}} N_{\text{tx-data}}$$

- N_{cpc} is the number of coded bits per subcarrier, being the same as specified with the modulation alphabet, M_{a},

- $N_{\text{tx-data}}$ is the total number of transmitted data symbols, and

$$N_{\text{tx-data}} = N_{\text{data}} N_{\text{OFDM}}$$

- $s = \left\lceil \frac{N_{\text{cpc}}}{2} \right\rceil$.

2.3 Modulation mapper

Once the signal has been coded, it enters the modulation block. All wireless communication systems use a modulation scheme to map coded bits to a form that can be effectively transmitted over the communication channel. Thus, the bits are mapped to a subcarrier amplitude and phase, which is represented by a complex in-phase and quadrature-phase (IQ) vector. The IQ plot for a modulation scheme shows the transmitted vector for all data word combinations. Gray coding is a method for this allocation so that adjacent points in the constellation only differ by a single bit. This coding helps to minimize the overall bit error rate as it reduces the chance of multiple bit errors ocurring from a single symbol error.

2-PAM, 4-QAM, 16-QAM, and 64-QAM modulations are supported by the system. The support of the last one, the 64-QAM modulation, is optional for license-exempt bands. The constellation maps for 2-PAM, 4-QAM, and 16-QAM modulations are shown in Figure 2.3 - 1.

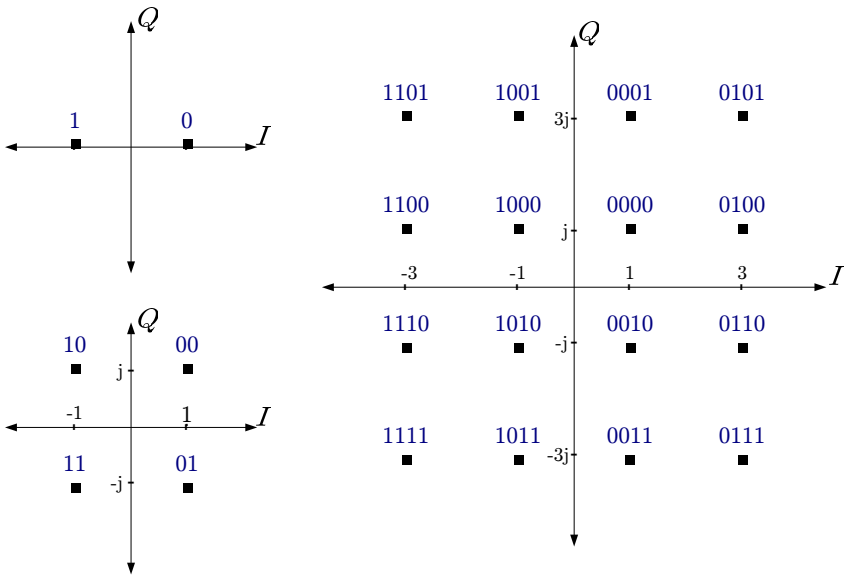

Figure 2.3 - 1: 2-PAM, 4-QAM and 16-QAM constellation maps.

To achieve equal average symbol power, the constellations described above are normalized by multiplying all of its points by an appropriate factor C_{m}. Values for this factor C_{m} are given in Table 2.3 - 1.

The modulation mapping is built in the simulator by a Simulink block implemented as a Matlab m-file. The symbol alphabet, A_{s}, represents the coordinate points in the constellation map and is defined in Table 2.3 - 2.

Modulation scheme	**Normalization constant for unit average power**
2-PAM	$C_{\mathrm{m}} = 1$
4-QAM	$C_{\mathrm{m}} = 1/\sqrt{2}$
16-QAM	$C_{\mathrm{m}} = 1/\sqrt{10}$
64-QAM	$C_{\mathrm{m}} = 1/\sqrt{42}$

Table 2.3 - 1: Normalization factors.

Modulation scheme	**Symbol alphabet**
2-PAM	$A_{\mathrm{s}} = (1, -1)$
4-QAM	$A_{\mathrm{s}} = (1+j, 1-j, -1+j, -1-j)$
16-QAM	$A = (j, 3j, -j, -3j)$ $A_{\mathrm{s}} = (A+1, A+3, A-1, A-3)$
64-QAM	$A = (j, 3j, 5j, 7j-j, -3j, -5j, -7j)$ $A_{\mathrm{s}} = (A+1, A+3, A+5, A+7, A-1, A-3, A-5, A-7)$

Table 2.3 - 2: Modulation alphabet for the constellation map.

Furthermore, an adaptive modulation and coding mechanism is supported in the downlink with the purpose of allowing the number of transmitted bits per symbol to be varied depending on the channel conditions. A more detailed explanation of adaptive modulation as well as a description of how it is implemented in the simulator is given in Chapter 6.

2.4 Pilot symbols

Pilot symbols can be used to perform a frequency offset compensation at the receiver. Additionally, as recent results showed [11], they can be used for channel estimation in fast time-varying channels. Pilot symbols allocate specific subcarriers in all OFDM data symbols. These pilots are obtained by a pseudo-random binary sequence (PRBS) generator that is based on the polynomial $x^{11} + x^9 + 1$. They are, moreover, 2-PAM modulated. This kind of mapping is given by the operations $1 - 2w_{\mathrm{k}}$ and $1 - 2\overline{w_{\mathrm{k}}}$, where w_{k} is the sequence produced by the PRBS generator, and $\overline{w_{\mathrm{k}}}$ denotes the binary inversion. The indices represent the subcarrier numbers where the pilots are going to be inserted:

$$p_{\text{-}88} = p_{\text{-}38} = p_{63} = p_{88} = 1 - 2w_{\mathrm{k}},$$

$$p_{\text{-}63} = p_{\text{-}13} = p_{13} = p_{38} = 1 - 2\overline{w_{\mathrm{k}}}.$$

The initialization sequences for the PRBS generator vary depending on the direction of transmission, i.e. the downlink or the uplink. A sequence of all "ones" is used in the downlink while a sequence of alternated "ones" and "zeros", being the first bit equal to "one", is used in the uplink.

2.5 Training sequences

In WiMAX systems, preambles, both in DL[7] and in UL[8], are composed using training sequences. Although three types of training sequences are specified, they are derived from the same sequence in the frequency domain. This sequence, that has a length of 201 subcarriers, is called P_{ALL}. A deeper definition of it can be found in [4].

For DL transmissions, the first preamble as well as the initial ranging preamble consists of two consecutive OFDM symbols. The first symbol is a short training sequence, P_{SHORT}, used for synchronization. It is a sequence which uses only the subcarriers of P_{ALL} whose indices are a multiple of 4, filling the other subcarriers with "zeros". Thus, in the time domain it is composed of four repetitions of a 64-sample fragment. The frequency domain sequence for this first DL preamble is defined in Equation 2.5 - 1.

The second OFDM symbol uses a long training sequence, necessary in the receiver for channel estimation. As it occurs with the first OFDM symbol of the preamble, the long training sequence is constructed also using a subset of the subcarriers of P_{ALL}. In this case, the long training sequence utilizes only even subcarriers. Therefore, it is called P_{EVEN} and its time domain waveform consists of two repetitions of a 128-sample fragment. Equation 2.5 - 2 defines the frequency domain sequence for this long training.

$$P_{\text{SHORT}}(k) = \begin{cases} \sqrt{2}\sqrt{2}\text{conj}(P_{\text{ALL}}(k)) & k \mod 4 = 0 \\ 0 & k \mod 4 \neq 0 \end{cases} \tag{2.5 - 1}$$

$$P_{\text{EVEN}}(k) = \begin{cases} \sqrt{2}\text{conj}(P_{\text{ALL}}(k)) & k \mod 2 = 0 \\ 0 & k \mod 2 \neq 0 \end{cases} \tag{2.5 - 2}$$

In both, Equation 2.5 - 1 and Equation 2.5 - 2, a factor of $\sqrt{2}$ representing a boost of 3 dB appears. Furthermore, there is an additional factor of $\sqrt{2}$ in P_{SHORT} which has the aim of equating the root-mean-square (RMS) power with the power of the data symbols.

[7] DownLink
[8] UpLink

Another training sequence shall be used when transmitting space-time coded (STC) downlink bursts. Because the STC scheme achieves diversity by transmitting with two antennas, a preamble has to be transmitted from both transmit antennas simultaneously. Thus, the first antenna transmits a preamble using P_{EVEN} and the preamble transmitted from the second antenna is set according to the sequence P_{ODD}. Again, like P_{EVEN}, it is derived from the sequence P_{ALL}, but using, in this case, a subset of odd subcarriers.

$$P_{\text{ODD}}(k) = \begin{cases} 0 & k \mod 2 = 0 \\ \sqrt{2}\text{conj}(P_{\text{ALL}}(k)) & k \mod 2 \neq 0 \end{cases} \quad (2.5\text{-}3)$$

The time domain structure of the described preamble, referred to as the long preamble, is shown in the next figure.

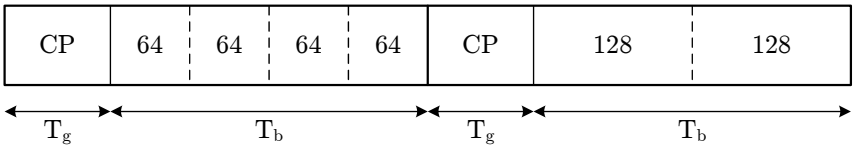

Figure 2.5 - 1: Long preamble structure, used for DL transmissions.

Furthermore, the long preamble is followed by the FCH[9], which contains decoded information for the subscriber station, i.e. information about the modulation type and the FEC code length for each burst profile as well as the DL and UL maps. In the WiMAX simulator the FCH is filled with dummy data, i.e. it is assumed that the receiver knows all FCH information perfectly. User data follows the FCH and contains several OFDM symbols of payload data.

2.6 Assembler

WiMAX specifications for the 256-point FFT OFDM PHY layer define three types of subcarriers; data, pilot and null, as shown in Figure 2.6 - 1. 200 of the total 256 subcarriers are used for data and pilot subcarriers, eight of which are pilots permanently spaced throughout the OFDM spectrum. The remaining 192 active carriers take up the data subcarriers. The rest of the potential carriers are nulled and set aside for guard bands and removal of the center frequency subcarrier.

[9] Frame Control Header

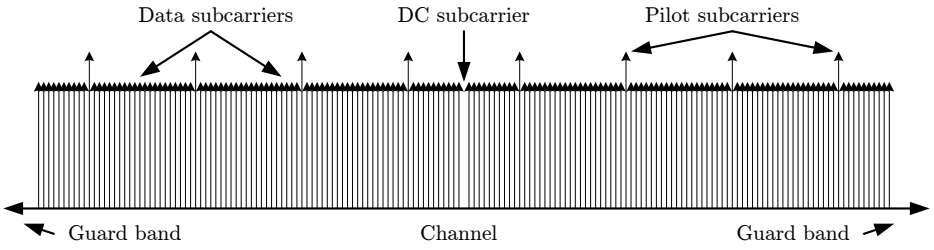

Figure 2.6 - 1: OFDM frequency description.

In order to construct an OFDM symbol, a process to rearrange these carriers is needed. With this purpose, the assembler block is inserted in the simulator. It performs this operation in two steps by first inserting the pilot tones and the zero DC subcarrier between data with a process of vertical concatenation, and then appending the training symbols at the beginning of each burst in an horizontal way, as shown in Figure 2.6 - 2. It is shown that while the first step performs a concatenation in the frequency domain, the second step does it in the time domain.

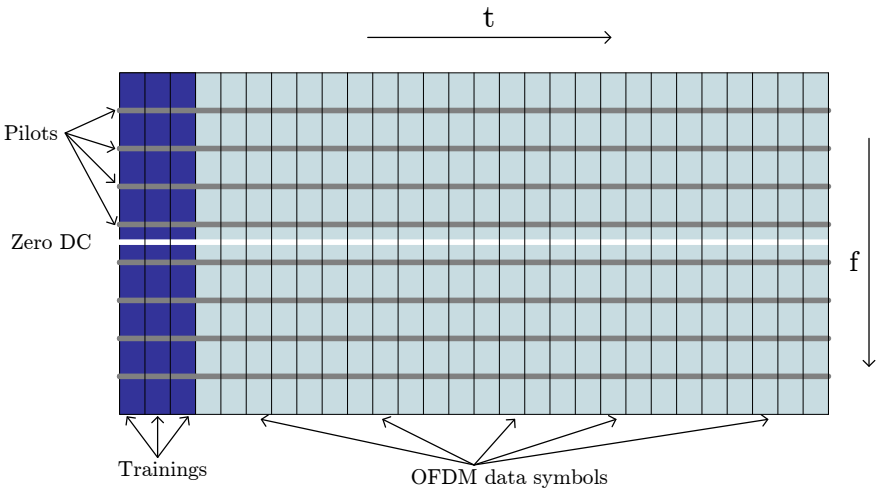

Figure 2.6 - 2: OFDM burst structure obtained after assembling.

The process of assembling the total number of 201 subcarriers is explained next. Frequency indices are defined in the standard from index -127 to index 128. However, Matlab allows only positive indices, and so, a shift on these index values is needed in the simulator. Therefore, pilot subcarriers are inserted in frequency offset indices of 13, 38, 63, 88, 114, 139, 164, and 189.

The same action occurs with the zero DC, situated in the centered subcarrier, which is, in this case, the one with index 101.

After this first concatenation, the training symbols are appended at the beginning of each burst.

2.7 The guard bands

The OFDM physical layer of the IEEE 802.16-2004 standard specifies that transmission must be performed using 256 frequency subcarriers. The total amount of subcarriers to be used is determined by the number of points needed to perform the IFFT.

After the assembling process described in Section 2.6, only 201 of the total 256 subcarriers are used. The remaining 55 carriers, that are zero subcarriers appended at the end of the cited structure, act as guard bands with the purpose to enable the naturally decay of the signal. These guard bands are used to decrease emissions in adjacent frequency channels.

Figure 2.7 - 1 and Figure 2.7 - 2 show the structure of the subcarriers before and after appending the guard bands.

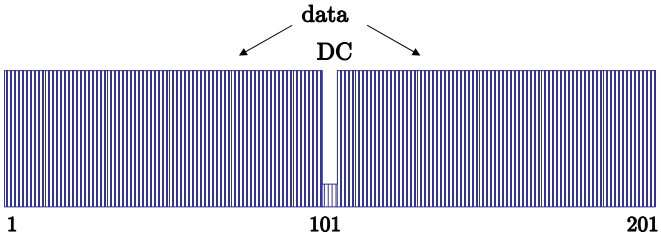

Figure 2.7 - 1: Structure composed with data, pilots and zero DC subcarriers.

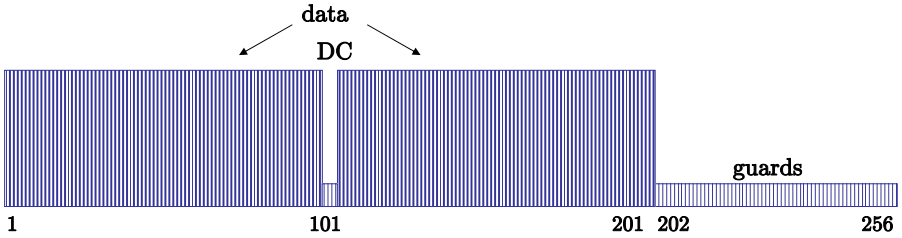

Figure 2.7 - 2: Structure after appending the guard bands.

2.8 Inverse Fast Fourier Transform algorithm

The IFFT is used to produce a time domain signal, as the symbols obtained after modulation can be considered the amplitudes of a certain range of sinusoids. This means that each of the discrete samples before applying the IFFT algorithm corresponds to an individual subcarrier. Besides ensuring the orthogonality of the OFDM subcarriers, the IFFT represents also a rapid way for modulating these subcarriers in parallel, and thus, the use of multiple modulators and demodulators, which spend a lot of time and resources to perform this operation, is avoided.

Before doing the IFFT operation in the simulator, the subcarriers are rearranged. Figure 2.8 - 1 shows the subcarrier structure that enters the IFFT block after performing the cited rearrangement. As seen in the following figure, zero subcarriers are kept in the center of the structure.

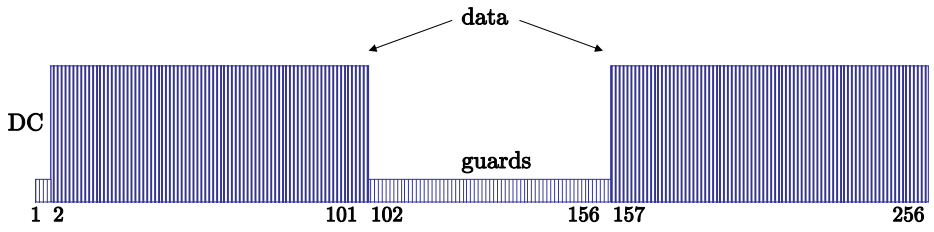

Figure 2.8 - 1: Rearrangement performed before realizing the IFFT operation.

Furthermore, the FFT (or IFFT) should be of length 2^r (where r is an integer number) to facilitate the realization of the algorithm. For this reason, the FFT length is given by

$$N_{\text{FFT}} = 2^{\lceil \log_2(N_{\text{data}}) \rceil}. \tag{2.8 - 1}$$

2.9 The cyclic prefix

The robustness of any OFDM transmission against multipath delay spread is achieved by having a long symbol period with the purpose of minimizing the inter-symbol interference. Figure 2.9 - 1 depicts one way to perform the cited long symbol period, creating a cyclically extended guard interval where each OFDM symbol is preceded by a periodic extension of the signal itself. This guard interval, that is actually a copy of the last portion of the data symbol, is known as the cyclic prefix (CP).

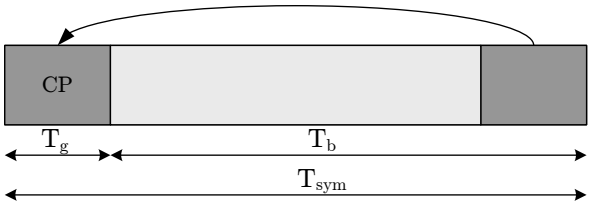

Figure 2.9 - 1: OFDM symbol with the cyclic prefix.

Copying the end of a symbol and appending it to the start results in a longer symbol time. Thus, the total length of the symbol is

$$T_{\text{sym}} = T_{\text{b}} + T_{\text{g}}, \tag{2.9 - 1}$$

where:

- T_{sym} is the OFDM symbol time,
- T_{b} is the useful symbol time, and
- T_{g} represents the CP time.

The parameter G defines the ratio of the CP length to the useful symbol time. When eliminating ISI[10], it has to be taken into account that the CP must be longer than the dispersion of the channel. Moreover, it should be as small as possible since it costs energy to the transmitter. For these reasons, G[11] is usually less than 1/4:

$$G = \frac{T_{\text{g}}}{T_{\text{b}}}. \tag{2.9 - 2}$$

[10] Inter-Symbol Interference

[11] Values for this parameter are specified in Appendix C.

Chapter 3

Channel

When communicating over a wireless radio channel the received signal cannot be simply modeled as a copy of the transmitted signal corrupted by additive Gaussian noise. Instead, signal fading, while caused by the time-varying characteristics of the propagation environment, appears. In this way, short-term fluctuations caused by signal scattering of objects in the propagation environment lead to a phenomenon known as multipath propagation. The time dispersion in a multipath environment causes the signal to undergo either flat or frequency-selective fading. Furthermore, the time dispersion is manifested by the spreading in time of the modulated symbols leading to inter-symbol interference (ISI). In order to avoid ISI in OFDM systems, the cyclic prefix time has to be chosen larger than the maximum delay spread of the channel. In addition, root-raised cosine (RRC) filters, usually used for band-limiting the transmitted signal, are utilized as interpolation filters in the simulator.

This chapter deals with the modeling, analysis, and simulation of the channel. It provides a description of the mentioned RRC filters as well as a brief explanation about the fading characteristics.

As the simulation results depend strongly on the radio channel, it is very important to use accurate and realistic channel models in the simulation to enable realistic and reliable results. Thus, the well-known I-METRA channel model is introduced.

3.1 Filters

Data transmission over band limited channels requires a technique of pulse shaping at the transmitter. Since the pulse shaping filter does not cause inter-symbol interference (ISI), this implies the fundamental shapes of the

pulses to be such that they do not interfere each other. A criteria that ensures non-interference specifies the shape of the pulses to be such that its amplitude decays rapidly outside the pulse interval. A widely used filter for this purpose is the well known raised cosine filter, which satisfies Nyquist's first criterion[1]. However, in practical applications the overall magnitude response of the raised cosine spectrum is equally split between the transmitter and the receiver, thus obtaining square-root raised cosine filters, also known as root-raised cosine (RRC) filters. The advantage of such subsystems is that if the transmit side filter is stimulated by an impulse, then the receive one is forced to filter an input pulse with a shape that is identical to its own impulse response, therefore setting up a matched filter and maximizing the SNR while at the same time minimizing ISI [12].

The RRC filter is generally used in series pairs so that the total filtering effect is that of a raised cosine filter. Since the frequency response of the transmit and receive filters is multiplied at the receiver, the receiver sees a signal that has been filtered by a raised cosine filter overall:

$$H_{\mathrm{T}}(f)H_{\mathrm{R}}(f) = H_{\mathrm{rc}}(f), \tag{3.1-1}$$

$$|H_{\mathrm{T}}(f)| = |H_{\mathrm{R}}(f)| = H_{\mathrm{rrc}}(f). \tag{3.1-2}$$

$H_{\mathrm{rrc}}(f)$ defines the root-raised cosine filter frequency response, while $H_{\mathrm{rc(f)}}$ is used for defining the raised cosine filter.

The ideal root-raised cosine filter frequency response is simply the square root of the frequency response of a raised cosine filter. The RRC frequency response is specified in Equation 3.1-3, and it consists of a unity gain at low frequencies, the square root of a raised cosine function in the middle, and a total attenuation at high frequencies.

$$H_{\mathrm{rrc}}(f) = \begin{cases} 1 & |f| \leq f_{\mathrm{N}}(1-\alpha) \\ \sqrt{\cos\left(\frac{\pi T_{\mathrm{sym}}}{2\alpha}\left(|f| - \frac{1-\alpha}{2T_{\mathrm{sym}}}\right)\right)} & f_{\mathrm{N}}(1-\alpha) \leq |f| \leq f_{\mathrm{N}}(1+\alpha) \\ 0 & |f| > f_{\mathrm{N}}(1+\alpha) \end{cases} \tag{3.1-3}$$

[1]Nyquist's first criterion establishes the conditions the transmission pulse $p(t)$ must accomplish to avoid ISI. It specifies $p(t)$ to be one for the sampling interval of the desired symbol, and zero for the another symbols:

$$p(iT_{\mathrm{s}} - kT_{\mathrm{s}}) = \begin{cases} 1 & i = k \\ 0 & i \neq k \end{cases}$$

f_{N} is the Nyquist frequency defined as

$$f_{\mathrm{N}} = \frac{1}{2T_{\mathrm{sym}}} = \frac{R_{\mathrm{sym}}}{2},$$

where T_{sym} is the modulation symbol duration, and R_{sym} is the symbol rate.

The width of the central frequencies is defined by the roll-off factor, α, which determines the sharpness of the frequency response and can take values comprised between 0 and 1. Specifically, α governs the bandwidth occupied by the pulse and the rate at which the tails of the pulse decay. Figure 3.1 - 1 shows that when $\alpha = 0$ the frequency response has a form of a rectangle offering the narrowest bandwidth but the slowest rate of decay in the time domain. However, when $\alpha = 1$ the frequency response is completely round but the impulse response presents the added benefit of rapidly decaying time domain tails. Therefore, it can be deduced that the smaller the roll-off factor, the more efficient is the scheme since it gives the narrowest bandwidth.

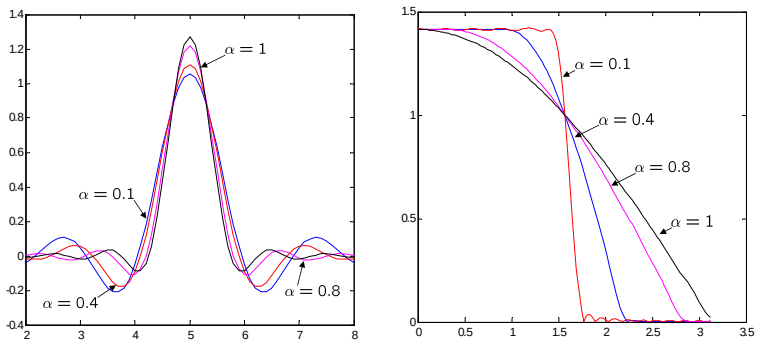

(a) Impulse response $h_{\mathrm{rrc}}(t)$. (b) Frequency response $H_{\mathrm{rrc}}(f)$.

Figure 3.1 - 1: Spectral shape and inverse Fourier transform of the RRC pulse.

The most commonly used design methodology for this kind of filters is the *frequency sampling design*, where the frequency response of the filter is sampled at constant intervals and an inverse fourier transform (IFFT) is applied to the frequency samples to obtain the filter coefficients. The more the number of frequency samples, the more will the actual response match the desired response. That means that if more filter taps are used, a more accurate response is obtained, and therefore, better rejection is given.

3.2 Fading channel models

3.2.1 Description of the fading channel

In a realistic wireless radio environment, a single received signal is composed of a number of scattered waves, caused by the reflection and diffraction of the original transmitted signal by objects in the surrounding geographical area. These multipath waves are combined at the receiver to give a resultant signal that can widely vary in amplitude and phase. Physical factors influencing the characteristics of the fading experienced by the transmitter are multipath propagation, mobility of the reflecting objects and scatterers, and the relative motion between the transmitter and the receiver.

The presence of reflecting objects and scatterers in the wireless channel causes a constant change in the propagation environment. This changing environment alters the signal energy in amplitude, phase, and time, and as a result, multipath propagation occurs causing signal fading. The transmitted signal arrives at the receiver via multiple propagation paths, each of which has an associated time delay. Because the received signal is spread in time due to the multipath scatterers at different delays, the channel is said to be time dispersive. The difference between the largest and the smallest among these delays defines the maximum delay spread.

On the other hand, when the receiver and the transmitter are in relative motion, the received signal is subject to a constant frequency shift, called the Doppler shift (see Equation 3.2 - 1). Therefore, as it occurs in the time domain, the Doppler spread is defined as the difference between the largest and the smallest among these frequency shifts,

$$f_{\mathrm{d}} = f_{\mathrm{M}} \cos \varphi, \tag{3.2 - 1}$$

where:

- $f_{\mathrm{M}} = f_{\mathrm{c}} v/c$ is the maximum Doppler shift,
- v is the vehicle speed,
- f_{c} is the carrier frequency,
- c is the speed of light, and
- φ is the arrival angle of the received signal component.

Furthermore, a time-varying Doppler shift is induced on each multipath component if the reflecting objects and scatterers in the propagation channel are in motion, causing frequency dispersion.

As a result of such time variations, the response of the channel to any signal transmitted through it will change with time. Hence, physical channels with time-varying transmission characteristics may be characterized as time-varying linear filters. Such linear filters are described by a time-varying impulse response, $h(t,\tau)$, which represents the response of the channel at time t due to an impulse applied at time $t-\tau$. Thus, the variable t specifies the time dependance in the variations of the impulse response due to motion, whereas τ represents the channel multipath delay for a fixed value of t.

Assuming that the pass-band input signal to a multipath fading channel is $s(t)$, and ignoring the effects of AWGN, the pass-band output signal is given by

$$r(t) = s(t) \otimes h(t,\tau), \tag{3.2-2}$$

where $\otimes$ represents the continuous-time convolution.

The pass-band channel impulse response can also be written as

$$h(t,\tau) = \mathrm{Re}\{h_{\mathrm{b}}(t,\tau)\exp(j2\pi f_{\mathrm{c}}t)\}, \tag{3.2-3}$$

where $h_{\mathrm{b}}(t,\tau)$ is the baseband equivalent impulse response of the channel, and f_{c} is the carrier frequency of the pass-band input signal.

When L discrete multipath components exist in the multipath fading channel, this baseband channel impulse response is written as

$$h_{\mathrm{b}}(t,\tau) = \sum_{i=1}^{L} \alpha_i(t,\tau)\delta(\tau-\tau_i(t))\exp(j(2\pi f_{\mathrm{c}}\tau_i(t)+\theta_i(t,\tau))). \tag{3.2-4}$$

$\alpha_i(t,\tau)$ and $\tau_i(t,\tau)$ are the delay dependent instantaneous amplitude and the time delay associated with the i-th multipath component, respectively. The instantaneous phase shift encountered by the i-th multipath component due to its delay is represented by the factor $2\pi f_{\mathrm{c}}\tau_i(t)$, whereas any other phase alteration experienced by this multipath component is incorporated in $\theta_i(t,\tau)$. To simplify Equation 3.2-4, the phase delays are lumped together and represented by

$$\phi_i(t,\tau) = 2\pi f_{\mathrm{c}}\tau_i(t) + \theta_i(t,\tau).$$

Tapped delay line channel model

A general model for a time-variant multipath channel consists of a tapped delay line with uniformly spaced taps, as the one depicted in Figure 3.2-1. The spacing between adjacent taps is $K/(MW)$, where W is the bandwidth of the signal that is being transmitted through the channel. Hence, $K/(MW)$

defines the time resolution of the channel model implementation, where an interpolation factor of M/K is being used. Moreover, the tap coefficients, denoted as $c_i(t) = \alpha_i(t)\exp(j\phi_i(t))$, are usually modeled as complex-valued Gaussian random processes which are mutually uncorrelated. The length of the delay line corresponds to the amount of time dispersion in the multipath channel, usually called the multipath spread, $T_m = L/W$, where L represents the maximum number of possible multipath signal components.

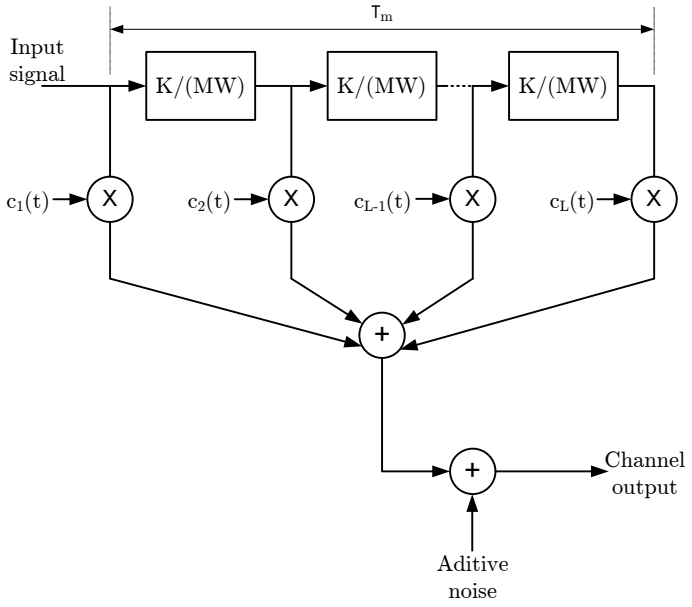

Figure 3.2 - 1: Model for a time-variant multipath channel based on a tapped delay line.

Delay spread and Doppler spread

As previously explained, two manifestations of the channel time variations are the delay spread and the Doppler spread. Depending on their values, the signal transmitted through the channel will undergo flat or frequency-selective fading. On one hand, the delay spread is a measure of the spread in time over which the multipath signals arrive. It is a measure of the time dispersion of a channel, and is very important in determining how fast the symbol rate can be in digital communications. One of the most widely used measurement for characterizing the delay spread of a multipath channel is the rms delay spread, σ_τ. Furthermore, the inverse of the delay spread defines the coherence bandwidth, B_{coh}. It is the frequency separation at which two

frequency components of the signal undergo independent attenuations and a measure of the range of frequencies over which the multipath fading channel frequency response can be considered to be flat or not.

On the other hand, the Doppler spread, B_{d}, is a measure of the spectral broadening caused by the time rate of change of the multipath components due to the relative motion between transmitter and receiver. Depending on how rapidly the multipath components change, the channel may be classified either as a fast or a slow fading channel. Inversely proportional to one another are the Doppler spread and the coherence time. The coherence time, T_{coh}, is the time domain dual of Doppler spread and is used to characterize the time-varying nature of the frequency dispersiveness of the channel in the time domain. It is a statistical measure of the time duration over which the channel impulse response is essentially invariant quantifying the similarity of the channel response at different times [13]. In 802.16-2004, the coherence time of the channel is assumed to be longer than the frame duration, leading to quasi-static scenarios.

Rayleigh and Ricean fading models

Wireless channels can be characterized with tap coefficients that are complex-valued Gaussian random variables. A channel model where there are only non line-of-sight communications is characterized by a Rayleigh distribution. On the contrary, if dominating paths are present, the channel coefficients are modeled by a Ricean distribution.

As already mentioned, a Rayleigh distribution is normally used to model NLoS communications. It is statistically characterized by a fading amplitude, $\alpha(t)$, modeled with a Rayleigh probability distribution, which has zero-mean Gaussian components. Furthermore, the phase, $\phi(t)$, is uniformly distributed over the interval $(0, 2\pi)$. The fading amplitude is described by the probability density function (pdf):

$$f_{\mathrm{Ray}}(a) = \begin{cases} \frac{a}{\sigma^2} \exp(-\frac{a^2}{2\sigma^2}) & \text{if} \quad a \geq 0 \\ 0 & \text{if} \quad a < 0. \end{cases} \tag{3.2-5}$$

On the other hand, when the components of $\alpha(t)$ are Gaussian with non-zero mean values and the phase is also non-zero mean, the amplitude is characterized statistically by the Rice probability distribution. In this case, the channel presents multipath propagation with some dominating paths, i.e. representing a major part of the channel energy. The pdf of the Ricean fading amplitude is given by

$$f_{\mathrm{Rice}}(a) = \begin{cases} \frac{a}{\sigma^2} \exp(-\frac{a^2+\rho^2}{2\sigma^2}) I_0\left(\frac{a\rho}{\sigma^2}\right) & \text{if} \quad a \geq 0 \\ 0 & \text{if} \quad a < 0, \end{cases} \tag{3.2-6}$$

where the parameter ρ^2 represents the power of the received non-fading signal component, and I_0 is the modified Bessel function of first kind and order zero.

The Ricean distribution is usually expressed with the K-factor defined as the ratio of the power of the deterministic signal to the variance of the multipath component:

$$K = \frac{\rho^2}{2\sigma^2}. \tag{3.2-7}$$

If K approaches zero, then the Rice distribution degenerates in a Rayleigh distribution. Thus, when ρ has values near to 0, K is prone to $-\infty$ dB, and since the dominant path decreases in amplitude, the Rice distribution becomes a Rayleigh distribution. Furthermore, if K approaches infinity, one path will contain the whole channel energy, corresponding to a LoS scenario.

3.2.2 Flat fading

When considering the transmission of a specific signal, the properties of that signal play a role in determining whether the effects caused by the channel on it are invariant in any given domain. This relationship existing between the coherence of the channel and the properties of the signal is captured by the notion of selectivity. If the channel is selective, then the region of support[2] of the transmitted signal is larger than the coherence interval. Therefore, the channel is not flat with respect to the signal in that domain.

However, when the channel has a constant gain and linear phase response over a bandwidth that is greater than the bandwidth of the transmitted signal, the received signal undergoes flat fading. For this kind of fading, the spectral characteristics of the transmitted signal are preserved when it propagates through the channel, and only the received signal power fluctuates due to the multipath effects. For this reason, flat fading channels are also known as amplitude varying channels. Moreover, they are sometimes referred to as narrowband channels since the bandwidth of the applied signal is narrow as compared with the fading bandwidth.

To summarize, a signal undergoes flat fading if

$$W < B_{\text{coh}} \tag{3.2-8}$$

and

$$T_{\text{sym}} > \sigma_\tau. \tag{3.2-9}$$

[2]The region of support of a function $f(x)$ is defined as the set $\chi = x|f(x) \neq 0$. The size of such region is defined to be $max_{x\in\chi}(x) - min_{x\in\chi}(x)$.

3.2.3 Frequency-selective fading

The frequency-selective behaviour of the wireless propagation channel can be obtained easily from the correlation between two signals (which have different frequencies) in the receiver. The existence of different delay spread for the different propagation paths cause the statistical properties of two carriers to be independent if they are sufficiently frequency spaced. The maximum frequency difference for which a high correlation level between the signals are kept is known as the coherence bandwidth of the channel. That means that for frequency-selective fading the spectrum of the transmitted signal has a bandwidth which is greater than the coherence bandwidth of the channel. Under such conditions the channel impulse response has a multipath delay spread that exceeds the symbol period of the transmitted symbol. When this occurs, the received signal includes multiple versions of the transmitted waveform that are attenuated and delayed in time, and hence, the received signal is distorted. Frequency-selective fading is due to time dispersion of the transmitted symbols within the channel, thus inducing to inter-symbol interference (ISI).

To summarize, a signal undergoes frequency-selective fading if

$$W > B_{\text{coh}} \tag{3.2 - 10}$$

and

$$T_{\text{sym}} < \sigma_\tau. \tag{3.2 - 11}$$

However, when communicating with OFDM techniques, the effects of frequency-selective channel conditions can be decreased. Since the signal is split into many narrowband subchannels, the channel can be considered as constant (flat) over each OFDM subchannel, provided that the respective conditions for flat fading channels are accomplished.

3.2.4 Channel model implementation

The goal of this section is to describe the different steps that have been performed to implement the channel in our simulator. The signal is firstly oversampled and filtered using an RRC interpolation filter at the transmitter. The resulting signal is resampled to 100 MHz, that is the channel simulator sampling frequency. After resampling, the signal is sent through the channel itself, characterized by the channel model. This channel model distinguishes three kinds of channels: a block fading channel, a time-variant channel, and a time-variant block fading channel. At the receiver, some noise is added, and the signal is decimated from the channel simulator sampling frequency. Finally, it is filtered and downsampled.

Block fading channel

The block fading channel [14] is used for simulating slowly-varying fading channels. That means that the fading varies slowly in time and the channel coefficient, h_i, do not change during the transmission of one OFDM frame, as it is shown in Figure 3.2 - 2.

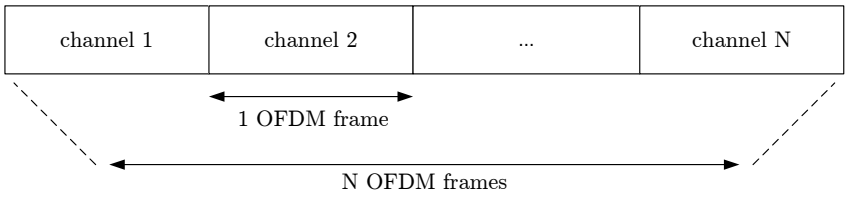

Figure 3.2 - 2: Block fading channel model.

Here, the channel realizations for consecutive frames are independent, which allows for fast BER simulations but not for simulations incorporating adaptive modulation and coding (AMC).

Time-variant channel

As previously explained, the variation in time of the wireless channel is caused by user mobility and multipath propagation. The impulse response of time-varying channels is characterized as a time-variant linear filter, $h(t, \tau)$, and a frequency shift appears in the received signal, f_d, when users are in relative motion.

The time-variant filtering is implemented in the function "*tvfilter*", which convolutes every sample of the transmitted signal with the instantaneous impulse response. Since such a filtering operation is of very high complexity, the "time-variant block fading" model was implemented.

To generate the time-varying characteristic of the fading channel [15], the function "*jakes*" is used. It utilizes a so-called sum of sinusoids to perform this operation.

The assumptions of this model are [16]:

- The transmitter is fixed and employs an omnidirectional antenna, that has been vertically polarized.
- The field incident on the receiver consists of N azimuthal plane waves.

- Each of the N azimuthal plane waves has an arbitrary carrier phase and an arbitrary angle of arrival. The phase angles are assumed to be uniformly distributed.
- The N azimuthal plane waves have equal average amplitudes, implying the absence of a LoS path.

The model assumes that N equal-strength rays arrive at a moving receiver with uniformly distributed arrival angles, φ_n, such that ray n experiences a Doppler shift given by

$$\omega_n = \omega_M \cos(\varphi_n). \tag{3.2 - 12}$$

As a result, the k-th fading waveform, $T_k(t)$, from a system that has M independent fading waveforms, each of which is composed of N sinusoids, can be expressed as in Equation 3.2 - 13:

$$T_k(t) = \sum_{n=0}^{N-1} C_{nk} \exp j(\omega_{nk} t + \phi_{nk}), \qquad k = 0, 1, 2, ..., M-1, \tag{3.2 - 13}$$

where C_{nk}, ω_{nk}, and ϕ_{nk} represent the amplitude, frequency, and uniformly random phase of the n-th complex sinusoid in the k-th fader.

For this situation, $\omega_{nk} = \omega_M \cos \varphi_{nk}$, where $n = 0, 1, 2, 3, ..., N-1$, and $k = 0, 1, 2, 3, ..., M-1$. Note that φ_{nk}, that denotes the n-th arrival angle in the k-th fader, depends on both, the fading waveform and the sinusoid.

The parameter C_{nk} can be reduced to a constant value by assuming a uniform antenna gain pattern and uniformly distributed incident power [15]:

$$C = \frac{1}{\sqrt{N}}. \tag{3.2 - 14}$$

Furthermore, different spectrum shapes are obtained depending on the values the parameters ϕ_{nk} and φ_{nk} take. Hence, a flat spectrum, a Jake's spectrum, and a Clarke's spectrum are defined.

- Flat spectrum

The parameter φ_{nk} takes the values $\pm\pi/2$ thus making null the operation $\cos \varphi_{nk}$.

Therefore, the exponential describing the fading waveform follows the next expression:

$$X_t = \exp(j(2\pi f_{\mathrm{d}} t + \phi_{nk})). \tag{3.2 - 15}$$

- Clarke's spectrum

For this kind of spectrum, however, the phase of the sinusoid, ϕ_{nk}, is zero. Therefore, the formula for the fading waveform is

$$X_t = \exp(j(2\pi f_{\mathrm{d}} \cos \varphi_{nk})). \tag{3.2-16}$$

-Jake's spectrum

Finally, the Jakes spectrum takes into account all the parameters that have been previously described[3]:

$$X_t = \exp(j(2\pi f_{\mathrm{d}} t \cos \varphi_{nk} + \phi_{nk})). \tag{3.2-17}$$

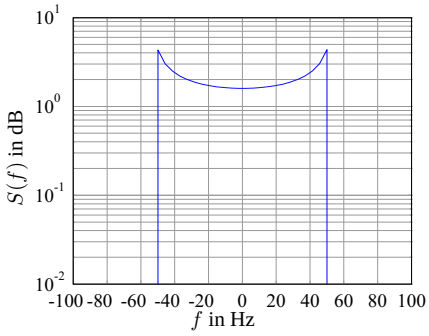

Figure 3.2-3: Jake's Doppler spectrum.

The values of the parameters for the three kinds of spectrum already defined are summarized in Table 3.2-1.

Spectrum	$\varphi_{\mathbf{nk}}$	$\phi_{\mathbf{nk}}$
Flat	$\pm\pi/2$	$\neq 0$
Clarke	$\neq \pm\pi/2$	0
Jake	$\neq \pm\pi/2$	$\neq 0$

Table 3.2-1: Spectrum shapes for time-variant channels.

[3]Simulation results have been performed using this spectrum.

Time-variant block fading channel

This kind of channels are a combination of block fading channels and time-variant channels. The channel filtering operation is the same as in the block fading channel, i.e. a constant channel is assumed during one OFDM frame. The generated channel impulse responses in successive frames are changing in a time-varying manner, i.e. the channel changes steadily. The steading changing channel allows for AMC simulations when the channel changes slowly compared to the OFDM frame duration.

3.3 The I-METRA channel model

The power delay profiles (PDP) specifying the energy distribution for several propagation scenarios are defined according to I-METRA. These scenarios are derived from measurements in typical indoor and outdoor environments, and specify the power delay profile of each scenario from the relative delays and the average power for each delay.

The I-METRA channel model specifies the channel taps at a sample rate of 100 MHz, i.e. it assumes that the 20 MHz bandwidth signal is oversampled by a factor of five. Moreover, it is assumed that the channel supports a maximum number of eight paths [17].

Table 3.3 - 1 shows all different scenarios supported by the channel model. The scenarios A to F are from I-METRA, U is a simple uncorrelated flat fading channel, and AWGN represents a channel that is only affected by an additive white Gaussian noise, which also have uncorrelated flat fading. The values for scenarios D, E, and F have been obtained from Medbo models A, B and C, respectively.

Model	**Environment**	**Scattering situation**	**K (dB)**[4]	**RMS delay spread (ns)**
U	Uncorrelated flat fading	LoS/NLoS	$-\infty$	0
A	Flat fading	LoS/NLoS	$-\infty$	0
B	Residential	LoS/NLoS	10	15
C	Residential/Small office	LoS/NLoS	3	30
D (A)	Typical office	NLoS	$-\infty$	50
E (B)	Large office	NLoS	$-\infty$	100
F (C)	Wide space (in- and outdoor)	NLoS	$-\infty$	150

Table 3.3 - 1: Channel model scenarios.

[4]The Rician factor, K, utilized when LoS transmissions are being performed, is only applied for the first tap.

Chapter 4

Receiver

As illustrated in Figure 4.0 - 1, the receiver basically performs the reverse operation as the transmitter as well as a channel estimation necessary to reveal the unknown channel coefficients. This section explains the different steps performed by the receiver to reconstruct the transmitted bits.

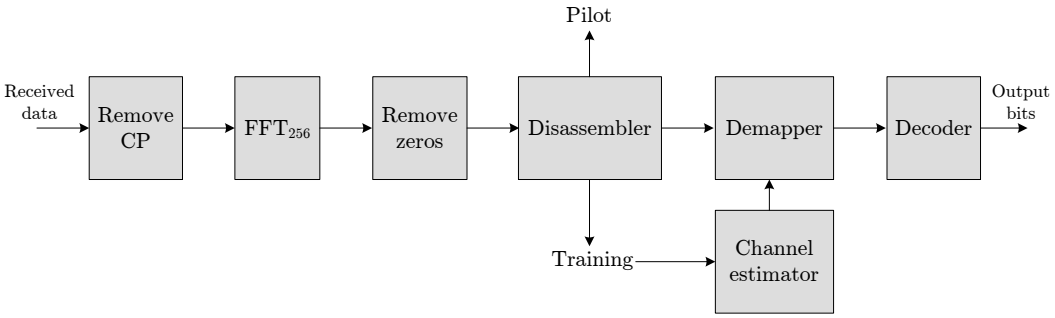

Figure 4.0 - 1: Receiver of the WiMAX system.

Firstly, the CP is removed and the received signal is converted to the frequency domain using, in this case, the FFT algorithm. As it has been previously explained in Section 2.6, an OFDM symbol is composed by data, pilots, a zero DC subcarrier, and some guard bands. Thus, a process to separate all these subcarriers is needed. First, the guard bands are removed, and then, a disassembling is performed to obtain pilots, data, and trainings. The training is used in the channel estimator, which calculates the channel coefficients. The estimated channel coefficients can be used in the demapper to perform an equalization of the data, and so, compensate the frequency-selective fading of the multipath propagation channel. Once the data has been demapped, it enters the decoder block.

4.1 Fast Fourier Transform algorithm

As explained in Section 2.8, the IFFT algorithm represents a rapid way for modulating a group of subcarriers in parallel. Either the FFT or the IFFT are a linear pair of processes, therefore the FFT is necessary to convert the signal again to the frequency domain[1]. The number of points used to perform the FFT is also described in Section 2.8.

4.2 Removing the guard bands

When removing the subcarriers that correspond to the guard bands, the frequency structure has to be taken into account. Although zero padding acting as guard band is appended at the end of the subcarrier structure at the transmitter, a rearrangement of this subcarriers is performed when doing the IFFT operation, as shown in Figure 2.8 - 1. Thus, the guard bands are removed from the center of the OFDM symbol, that is where they are allocated after the arranging process.

4.3 Disassembler

The disassembler deals with the task of separating the signal, either in time or in frequency domain, to get data, training, and pilots. These three different symbol streams form the output of the disassembler.

4.4 Channel estimator

The message sent by the transmitter is modified when it passes through the channel, as some noise is added to the transmitted signal. Furthermore, if the channel is a wireless channel, the received signal is additionally affected by the multiple reflections due to multipath transmission. Thus, the receiver must determine, from the received signal, which of all possible messages was the transmitted one. On the other hand, detection algorithms at the receiver require knowledge of the channel impulse response (CIR). This knowledge can be provided by performing channel estimation.

Usually, channel estimation is based on known sequences of bits, which are unique at the transmitter and repeated in every transmission burst. This way, the channel estimator is able to estimate CIR for each burst separately

[1]Remember that the data symbols, originally in frequency domain, were converted to the time domain in the transmitter using the IFFT.

by exploiting the known transmitted bits and the corresponding received samples. In our case, channel estimation is based on the technique of least-squares (LS) and is performed using one training symbol per carrier.

The received signal on the k-th subcarrier y_k can be expressed as follows:

$$y_k = p_k h_k + n_k, \tag{4.4-1}$$

where h_k is the channel coefficient for the k-th subcarrier, p_k is the training symbol, and n_k is a noise symbol.

The LS channel estimates can be obtained by finding the minimum squared error, as expressed in Equation 4.4-2:

$$\widehat{h}_k = \arg\min_{h_k} |y_k - p_k h_k|. \tag{4.4-2}$$

If white Gaussian noise is assumed, Equation 4.4-2 results in

$$\widehat{h}_{k,\mathrm{LS}} = (p_k^* p_k)^{-1} p_k^* y_k, \tag{4.4-3}$$

where the expressions $(\cdot)^*$ and $(\cdot)^{-1}$ denote conjugation and inverse operation, respectively. This estimator is implemented for all subcarriers where a pilot symbol unequal to zero is transmitted.

In the simulator, channel estimation is implemented using either the short, the long or both training symbols. The use of one or another training sequence depends on the values of the averaging parameters.

The long training used for channel estimation is P_{EVEN}, and as described in Equation 2.5-2, it has null values for the odd indices. If only the long training sequence is used for channel estimation, Equation 4.4-3 results in

$$\widehat{h}_{k,\mathrm{LS}} = 0.25 p_k^* y_k. \tag{4.4-4}$$

The short training has values different than zero only for the indices that are multiple of 4, as defined in Equation 2.5-1. Here, Equation 4.4-3 reduces to the expression

$$\widehat{h}_{k,\mathrm{LS}} = 0.125 p_k^* y_k. \tag{4.4-5}$$

A better channel estimate can be achieved if averaging in the frequency domain is performed. This way, the averaging parameter defines how many subcarriers are taken into account when performing the cited averaging. While small averaging factors improve the performance in strongly frequency-selective channels, large averaging factors improve the performance in flat fading channels.

The two parameters defining the described averaging factors are called *LongAveraging* and *ShortAveraging*, and can be zero or positive. A value

of "zero" means that no averaging over the corresponding training sequence is performed, and so, the corresponding training symbol is not used while performing the channel estimation. In this way, it can also be determined if only the short or long training sequence, or both training sequences are used for channel estimation.

4.5 Demapper

At the receiving end of the communication link the demapper provides the interface between the transmission channel and the functions that compute and deliver estimates of the transmitted data bits to the user. Furthermore, the demapper operates on the waveform that is received in each separate transmission symbol interval and produces a number or a set of numbers that represent an estimate of a transmitted binary or M-ary symbol. Thus, the demapping methods are used for decision metrics with the aim of making a decision about which bit, "zero" or "one", was transmitted. This decision metric can be as simple as hard decision, or more sophisticated, being then a soft decision.

Hard demapping methods output a hard decision as a function of the input, and this form of output is application-dependent. However, the soft demapping outputs a real number, in the form of a log-likelihood ratio. This is the logarithm of the ratio between the likelihood that the target produced the speech input and the likelihood that a non-target produced the input. In contrast, this form of output is application-independent in the sense that this likelihood ratio output can theoretically be used to make optimal decisions for any given target prior.

4.5.1 Hard Demapping

Hard demapping is based on the minimum Euclidean distances between the received symbol and all allowed points in the constellation map. This method involves calculating all cited distances and selecting as the received symbol the point in the constellation map with the smallest Euclidean distance.

Equation 4.5 - 1 gives the formula to calculate the Euclidean distance from which the decision metric is obtained. As it can be seen, the knowledge of the channel coefficients, or its estimates, is needed to implement hard demapping:

$$d_{\mathrm{E}} = |y - hs|. \tag{4.5 - 1}$$

d_{E} is the Euclidean distance, y denotes the received symbol, h represents the channel coefficients, and s is used to denote the transmitted symbols.

Thus, the decision metric is calculated as follows:

$$\widehat{s} = \mathrm{argmin}_s \, d_{\mathrm{E}} = \mathrm{argmin}_s \, |y - hs|. \tag{4.5-2}$$

4.5.2 Soft demapping

Soft demapping uses log-likelihood ratios [18] to propose a decision metric. This log-likelihood ratios are calculated for every bit of the symbol. The method gives probabilities of well receiving a bit or not. These probabilities can be further used to improve the performance of the succeeding Viterbi decoder. In the simulator, the so-called max-log-MAP was implemented.

The log-likelihood ratio (LLR) of decision $\hat{b}_{\mathrm{k}}$ is defined in Equation 4.5-3:

$$\mathrm{LLR}(b_{\mathrm{k}}) = \ln \frac{\sum_{s|b_{\mathrm{k}}=1} p(y|s)}{\sum_{s|b_{\mathrm{k}}=0} p(y|s)}. \tag{4.5-3}$$

The conditional pdf[2] of the received bit, which is complex Gaussian, is defined as follows:

$$p(y|s) = \frac{1}{\sqrt{2\pi}\sigma_v} \exp\left\{-\frac{1}{2}\frac{|hs-y|^2}{\sigma_v^2}\right\},$$

where σ_v^2 is the noise variance of the signal, and σ_v the standard deviation. Thus, Equation 4.5-3 yields

$$\mathrm{LLR}(b_{\mathrm{k}}) = \ln \frac{\sum_{s|b_{\mathrm{k}}=1} \exp\left\{-\frac{1}{2}\frac{|hs-y|^2}{\sigma_v^2}\right\}}{\sum_{s|b_{\mathrm{k}}=0} \exp\left\{-\frac{1}{2}\frac{|hs-y|^2}{\sigma_v^2}\right\}}. \tag{4.5-4}$$

Since the calculation of Equation 4.5-4 is of very high complexity a log-sum approximation is used. This approximation is good as long as the sum in the left-hand side is dominated by the largest term: $\ln \sum_{\mathrm{j}} z_{\mathrm{j}} \approx \max_{\mathrm{j}} \ln z_{\mathrm{j}}$. Thus, the computational complexity is reduced, and the LLR is calculated as in Equation 4.5-5:

$$\mathrm{LLR}(b_{\mathrm{k}}) \approx \ln \frac{\max_{s|b_{\mathrm{k}}=1} \exp\left\{-\frac{1}{2}\frac{|hs-y|^2}{\sigma_v^2}\right\}}{\max_{s|b_{\mathrm{k}}=0} \exp\left\{-\frac{1}{2}\frac{|hs-y|^2}{\sigma_v^2}\right\}}. \tag{4.5-5}$$

[2] Probability Density Function

At the end, the algorithm consists on calculating the minimum distance between the received symbol and all symbols in the constellation map where the bit b_k is equal to "one", the minimum distance between the received symbol and the constellation points where the bit b_k is equal to "zero" in this position, and then, taking the difference between both distances:

$$\mathrm{LLR}(b_k) = \min_{s|b_k=1} |hs - y|^2 - \min_{s|b_k=0} |hs - y|^2. \qquad (4.5\text{-}6)$$

A positive LLR corresponds to a "zero", and a negative LLR corresponds to a "one". Therefore, the larger the LLR is in absolute term the higher is the probability that a "zero" or a "one" was transmitted.

An example of how the LLR calculation works is going to be shown next. The example uses a 4-QAM constellation map, and the received symbol has been represented with an "x". Moreover, channel coefficients equal to "one" have been assumed to make the example easier to explain.

The example begins with the calculation of the LLR for the bit b_0, situated on the right side, as shown in Figure 4.5-1.

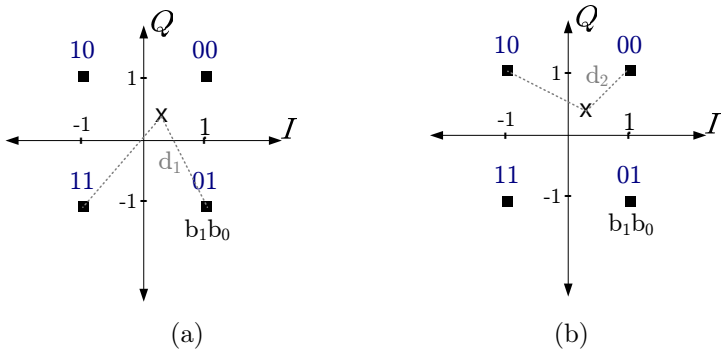

Figure 4.5-1: Example of calculating the LLR for the bit b_0. In subfigure (a), the minimum distance between the received bit and $b_0 = 1$ is calculated. Subfigure (b) makes the same calculation for $b_0 = 0$.

d_1 is the minimum distance between the received bit and the points in the constellation map that have a bit equal to "one" in the position of the bit b_0. The same operation is performed for the bit b_0 equal to "zero", obtaining the distance d_2. The numerical values for these distances are $d_1 = 1.56$ and $d_2 = 0.92$. The LLR can be calculated as the difference between both distances: $LLR = d_1 - d_2$. Replacing the numerical values, it has been obtained a result of 0.64 for $LLR(b_0)$.

The same steps must be followed to get the LLR value for the bit b_1. This process is depicted in Figure 4.5 - 2. In this case, $d_1 = 1.43$, $d_2 = 0.92$, and $LLR(b_1) = 0.51$.

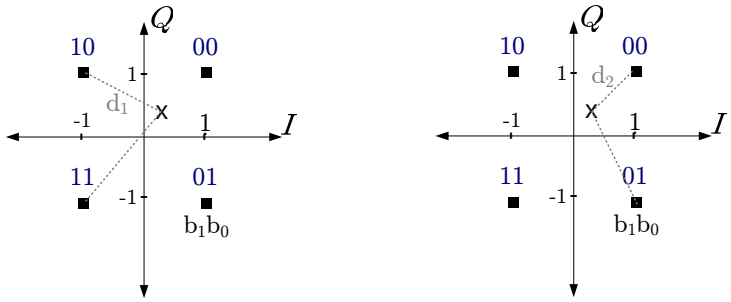

(a) Calculation of d_1. (b) Calculation of d_2.

Figure 4.5 - 2: Example of calculating the LLR for the bit b_1.

Both $LLR(b_0)$ and $LLR(b_1)$ have positive values. Therefore, it can be concluded that the symbol "00" is the one that have been transmitted with the highest probability.

4.6 Decoder

The final stage of receive processing is the decoder. A block diagram of the decoder is depicted in Figure 4.6 - 1.

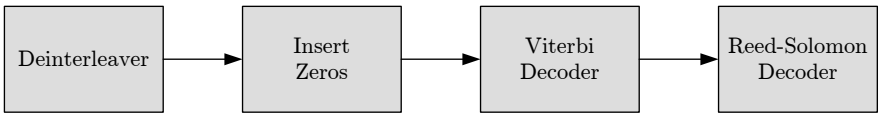

Figure 4.6 - 1: Block diagram of the decoding process.

The decoder accepts the sequence of bits or LLRs from the demapper and, in accordance with the encoding method that was used, attempts to reproduce the information originally generated by the source. Like in the encoder block, the decoder is also composed of four steps, which perform diverse operations with the aim of reversing the process done by the encoder.

4.6.1 Deinterleaving

The deinterleaver rearranges the bits from each burst in the correct way by ordering them consecutively as before the interleaving process. It consists of two blocks, a general block deinterleaver and a matrix deinterleaver.

These blocks work similarly as the ones used in the interleaver. The general block deinterleaver rearranges the elements of its input according to an index vector. The matrix deinterleaver performs block deinterleaving by filling a matrix with the input symbols column by column, and then, sending its contents to the output row by row. The parameters used in both blocks are the same as those ones used in the interleaving process[3].

4.6.2 Inserting zeros

The block named "Insert Zeros" deals with the task of reversing the process performed by the "Puncture" block. As previously explained in Section 2.2.3, the puncturing process consists of deleting bits from a stream. The receiver does not know the value of the deleted bits but it can know their position from the puncturing vectors. Thus, zeros are used to fill the corresponding hollows of the stream in order to get the same code rate as before performing the puncturing process.

The inserted zeros can also be seen as erasures from the channel. They have no influence on the metric calculation of the succeeding Viterbi decoder described in the following section.

4.6.3 Viterbi decoder

The Viterbi algorithm reduces the computational load by taking advantage of the special structure of the trellis code. Another advantage is its complexity, which is not a function of the number of symbols that compose the codeword sequence. The Viterbi algorithm performs approximate maximum likelihood decoding. It involves calculating a *measure of similarity* or *distance* between the received signal at time t_{i}, and all the trellis paths entering each state at the same time.

The algorithm works by removing those trellis paths from consideration that could not possibly be candidates for the maximum likelihood choice. When two paths enter the same state, the one that has the best metric is chosen as the "surviving" path. The selection of the different "surviving" paths is performed for all the states. The decoder continues in this way

[3]See Section 2.2.4 for the equations that describe the parameters of both, the interleaver and the deinterleaver.

to advance deeper into the trellis making decisions by eliminating the least likely paths. The early rejection of unlikely paths is the fact that reduces the complexity. The goal of selecting the optimum path can be expressed equivalently as choosing the codeword with the maximum likelihood metric, or as choosing the codeword with the minimum distance metric.

Furthermore, the delay introduced in the decoding process has to be taken into account. The rejection of possible paths does not really begin until the third step in the representation in the trellis diagram. This is due to the fact that until this time two branches can not have converged in one state, and thus, no decision can be done. This delay effect is considered in a parameter called *traceback depth*, which specifies how many symbols may preceed the beginning of the algorithm. For code rates of 1/2, a typical value for the *traceback depth* is about five times the constraint length of the code.

Another parameters of the Viterbi decoder block of Simulink are the *trellis structure* used in the convolutional encoder, the *decision type* of decoding, and the *operation mode*. They are defined as follows:

- The type of signals that can support the Viterbi decoder block are based on the *decision type* parameter. This parameter can have three values: unquantized, hard-decision, or soft-decision.

  As the decision process has been implemented in the demapper, the last kind of *decision type*, that is the "unquantized", is the one used in our simulator. It accepts real numbers as inputs for the decoder block. The positive numbers are interpreted as a logical zero, and the negative ones, as a logical one. However, when this parameter is set to "soft-decision", the entries of this block are integers between 0 (most confident decision for logical zero) and 2^b (most confident decision for logical one), being b the number of soft-decision bits.

- The *operation mode* parameter controls which method the block uses for transitioning between successive frames.

  The "truncated" mode, in which each frame is treated independently and the *traceback depth* parameter starts at the state with the best metric and ends in the all-zeros state, is the *operation mode* used in the simulator.

  Other values for this parameter are the "continuous" and "terminated" modes.

For more details about these parameters consult the documentation help of Matlab, or see [19].

4.6.4 Reed-Solomon decoder

The last part of the decoding process is the Reed-Solomon decoding. It performs the necessary operations to decode the signal, and get, at the end, the original message sent by the source. As in all the receiver blocks, the RS decoder reverses the different steps performed by its corresponding encoding block, explained in Section 2.2.1. Thus, the RS decoder takes codewords of length n, and, after decoding the signal, it returns messages of length k, being $n = 255$ and $k = 239$, the same as the ones described in the RS encoder. Furthermore, the implementation for the RS decoder block has been performed with a Matlab S-function using a C-file[4].

The block diagram of the RS decoder is depicted in Figure 4.6 - 2.

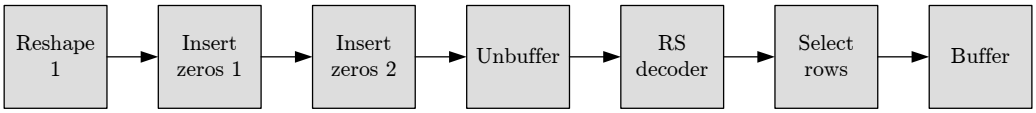

Figure 4.6 - 2: Block diagram of the Reed-Solomon decoder.

The input of the RS decoder block of Simulink accepts vectors, with a length that are integer multiples of ln. Its output is, in this case, a vector with a length that is the same integer multiple of lk. Hence, a process to get the correct amount of bytes that enter the RS decoder block, and afterwards, rearranges these bytes, needs to be performed firstly.

After the encoding process, a data block with size $(k + 2t) \times N_{\text{RS}}$ is obtained, as it can be appreciated in Figure 2.2 - 2. Nonetheless, the structure that will enter the decoder block has to be the same as the one that outputs the encoder block, before discarding the corresponding added bytes from the shortening and puncturing process. "Reshape 1" deals with the task of rearranging the data in a matrix form, with the specified size $(k+2t) \times N_{\text{RS}}$, being k and t the parameters listed in Table 2.2 - 1. The block "Insert zeros 1" adds $239 - k$ zero-bytes at the beginning of the structure with the aim of constructing the zero prefix. The $16 - 2k$ parity bytes are obtained from "Insert zeros 2". "Unbuffer" arranges the data from the matrix structure in a row vector. It has to be taken into account that this block introduces a delay equal to one frame in the system. Finally, "Select rows" has the task of selecting only the k original data bytes, and the "Buffer"-block redistributes its input samples in a new frame size, kN_{RS}.

[4]The sourcecode used to generate a Matlab S-funcion is available from *http://rscode.sourceforge.net* and has been published under the Lesser General Public License (LGPL).

Chapter 5

MIMO transmission

Applying multiple antennas at both ends of a communication system can not only greatly improve the capacity and the throughput of a wireless link in flat-fading but also in frequency-selective fading channels, specially when the environment provides rich scattering.

Multiple-input multiple-output systems, also known as MIMO, have MEA[1] arrays at both transmit and receive sides. High data rates are achieved when implementing such structures without increasing neither the bandwidth nor the total transmission power. Additionally, the use of multiple antennas at both transmitter and receiver provides a diversity advantage, that means a significant increase in capacity, i.e. improvement in SNR and hence in BER at the receiver [20] [21].

This chapter presents the theoretical background of the MIMO channel. Space-time coding (STC) as well as the maximum ratio combining (MRC) technique are presented as the solutions implemented to perform the MIMO transmission and reception, respectively. Finally, a detailed description of the MIMO implementation in the simulator is included.

5.1 MIMO communications theory

When communicating through a wireless channel, transmitted signals suffer from attenuation and fading due to multipath in the channel, thus making it difficult for the receiver to determine these signals. Diversity techniques take advantage of the multipath propagation characteristics to improve receiver sensitivity. MIMO systems utilize antenna diversity to obtain the mentioned improvement and hence combat fading.

[1] Multi-Element Antenna

A MIMO system characterizes itself by using multiple antennas at both transmitter and receiver. However, if only multiple antennas are deployed at one end of the communication system, or both ends use a single antenna, the MIMO system changes into a SIMO, MISO or SISO system [22]. In this way, when only multiple antennas are deployed at the receiver, the MIMO system reduces to a single-input multiple-output (SIMO) system. Similarly, when the system has only one receive antenna but multiple antennas at the transmitter side, the MIMO system reduces to a multiple-input single-output (MISO). When both, transmitter and receiver, use a single antenna, the MIMO system simplifies to a single-input single-output(SISO).

The main advantages of MIMO channels over traditional SISO channels are the array gain, the diversity gain, and the multiplexing gain. Array gain and diversity gain are not exclusive of MIMO channels and also exist in SIMO and MISO channels. Multiplexing gain, however, is a unique characteristic of MIMO channels [23]. Array gain is the improvement in SINR[2] obtained by coherently combining the signals on multiple transmit or multiple receive dimensions and is easily characterized as a shift of the BER curve due to the gain in SINR. Diversity gain is the improvement in link reliability obtained by receiving replicas of the information signal through independently fading links, branches, or dimensions. It is characterized by an steepen slope of the BER curve in the low BER region.

The three major forms of diversity exploited in wireless communication systems are temporal, frequency, and spatial diversity. Transmit diversity is more difficult to exploit than receive diversity since special modulation and coding schemes are required, i.e. space-time coding, whereas receive diversity simply needs the multiple receive dimensions to fade independently without requiring any specific modulation or coding scheme.

5.1.1 The MIMO channel model

The signal model for a MIMO channel composed by N_T transmit and N_R receive dimensions is

$$\mathbf{y} = \mathbf{H}\mathbf{s} + \mathbf{n}, \tag{5.1-1}$$

where $\mathbf{s} \in \mathbb{C}^{N_T \times 1}$ is the transmitted vector, $\mathbf{H} \in \mathbb{C}^{N_R \times N_T}$ is the channel matrix, $\mathbf{y} \in \mathbb{C}^{N_R \times 1}$ is the received vector, and $\mathbf{n} \in \mathbb{C}^{N_R \times 1}$ is the noise vector. This signal model represents a single transmission. For a communication with multiple transmissions the signals are indexed with a time-discrete index as $\mathbf{y}(t) = \mathbf{H}\mathbf{s}(t) + \mathbf{n}(t)$. The channel can even be considered time-varying, where it may be denoted as $\mathbf{H}(t)$.

[2] Signal to Interference-plus-Noise Ratio

Figure 5.1 - 1 depicts a MIMO scenario with N_T transmit antennas and N_R receive antennas. The signals at the transmit antenna array are denoted by vector $\mathbf{s}(t) = [s_1(t), s_2(t), ..., s_{N_T}(t)]^T$, and similarly, the signals at the receiver are $\mathbf{y}(t) = [y_1(t), y_2(t), ..., y_{N_R}(t)]^T$, where $(\cdot)^T$ denotes transposition, and $s_m(t)$ and $y_m(t)$ are the signals at the m-th transmit antenna port and at the m-th receive antenna port, respectively.

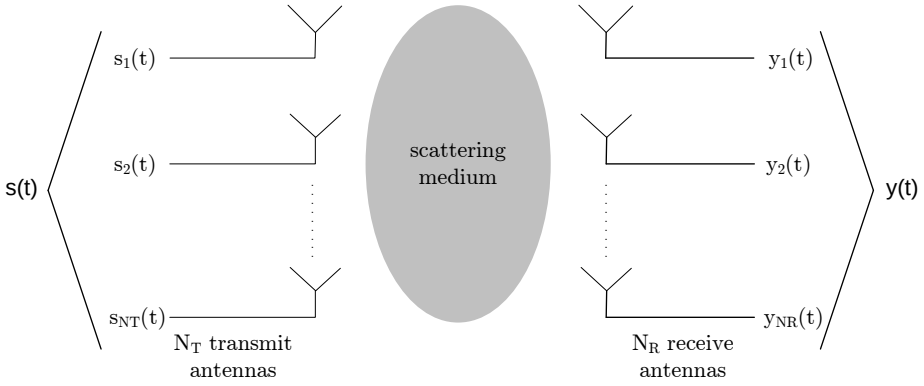

Figure 5.1 - 1: A MIMO channel model in a scattering environment.

The MIMO radio channel describing the connection between transmitter and receiver can be expressed as

$$\mathbf{H} = \begin{pmatrix} \alpha_{11} & \alpha_{12} & \cdots & \alpha_{1N_T} \\ \alpha_{21} & \alpha_{22} & \cdots & \alpha_{2N_T} \\ \vdots & \vdots & \ddots & \vdots \\ \alpha_{N_R1} & \alpha_{N_R2} & \cdots & \alpha_{N_RN_T} \end{pmatrix}, \qquad (5.1\text{-}2)$$

where α_{nm} is the complex transmission coefficient from antenna m at the transmitter to antenna n at the receiver. Moreover, the path gains, $\{\alpha_{ij}\}$, are correlated depending on the propagation environment, the polarization of the antenna elements, and the spacing between them.

The relation between the vectors $\mathbf{s}(t)$ and $\mathbf{y}(t)$ can be expressed as

$$\mathbf{y}(t) = \mathbf{H}(t)\mathbf{s}(t). \qquad (5.1\text{-}3)$$

In order to take the channel correlation into account, which has a strong impact on the achievable performance of the system, two different spatial channel models are considered.

Spatially uncorrelated channel

In spatially uncorrelated channels, the antenna elements are located far away from each other. Thus, the entries of the channel matrix $\mathbf{H}$ can be modeled as independent identically distributed (i.i.d.), circularly symmetric, complex Gaussian random variables, with zero mean and unit variance:

$$\mathbf{H} \sim \mathcal{N}_{\mathcal{C}}^{\mathrm{N_T} \times \mathrm{N_R}}(0, 1). \tag{5.1-4}$$

Spatially correlated channel

For spatially correlated channels, the widely known Kronecker model is used [24]. In order to model this kind of channel, a transmit correlation matrix $\mathbf{R}_{\mathrm{T}}$, a receive correlation matrix $\mathbf{R}_{\mathrm{R}}$, and an i.i.d. complex Gaussian matrix $\mathbf{G} \in \mathcal{N}_{\mathcal{C}}^{\mathrm{N_T} \times \mathrm{N_R}}$ are used:

$$\mathbf{H} = \mathbf{R}_{\mathrm{R}}^{1/2} \mathbf{G} (\mathbf{R}_{\mathrm{T}}^{1/2})^{\mathrm{T}}. \tag{5.1-5}$$

The correlation matrices $\mathbf{R}_{\mathrm{R}}$ and $\mathbf{R}_{\mathrm{T}}$ are taken from the I-METRA model explained in Section 3.3. These matrices are calculated as $\mathbf{R}_{\mathrm{R}} = E\{\mathbf{H}\mathbf{H}^{\mathrm{H}}\}$ and $\mathbf{R}_{\mathrm{T}} = E\{\mathbf{H}^{\mathrm{H}}\mathbf{H}\}$. Furthermore, they are normalized in such a way that $E\{\mathrm{tr}(\mathbf{H}^{\mathrm{H}}\mathbf{H})\} = \mathrm{N_R N_T}$, as in the i.i.d. case[3].

5.1.2 Space-Time Coding

Space-time coding (STC) is an efficient approach to exploit the enormous diversity offered by the MIMO. It is used to obtain gains due to spatial diversity via multiple transmit and receive antennas. Moreover, a diversity gain proportional to the number of antennas at both transmit and receive sides can be achieved. One popular representation of these codes is the Alamouti scheme [25] for two transmit antennas.

STC techniques are used to improve the performance of MIMO systems. Their central issue is the exploitation of multipath effects in order to achieve very high spectral efficiencies. With this purpose, the principal aim of the space-time coding lies in the design of two-dimensional signal matrices to be transmitted during a specified time period on a number of antennas. Thus, it introduces redundancy in space through the addition of multiple antennas, and redundancy in time through channel coding, enabling us to exploit diversity in the spatial dimension, as well as a obtaining a coding gain. Therefore, the transmit diversity plays an integral role in the STC design.

[3] A complete definition of the correlation matrices is held in Section B.1.

The Alamouti concept

Alamouti [25] [26] introduced a very simple scheme of space-time block coding (STBC) allowing transmissions from two antennas with the same data rate as on a single antenna, but increasing the diversity at the receiver from one to two in a flat fading channel. As shown in Figure 5.1 - 2, the Alamouti algorithm uses the space and the time domain to encode data, increasing the performance of the system by coding the signals over the different transmitter branches. Thus, the Alamouti code achieves diversity two with full data rate as it transmits two symbols in two time intervals.

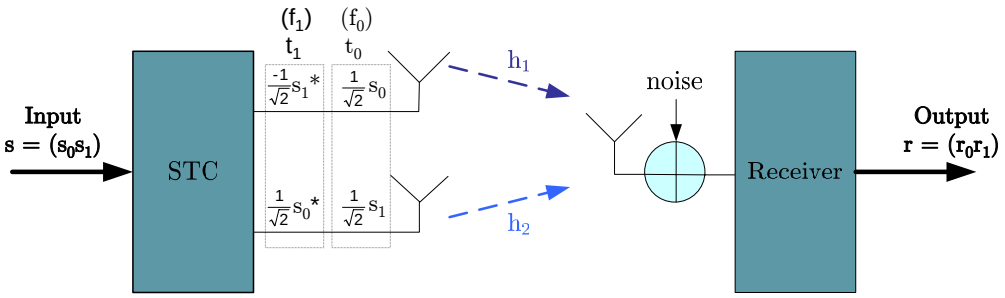

Figure 5.1 - 2: 2×1 Alamouti scheme.

In the first time slot, transmit antennas Tx1 and Tx2 are sending symbols s_0 and s_1, respectively. In the next time slot, symbols $-s_1^*$ and s_0^* are sent, where $(\cdot)^*$ denotes complex conjugation. Each symbol is multiplied by a factor of a squared root of two in order to achieve a transmitted average power of one in each time step. Furthermore, it is supposed that the channel, which has transmission coefficients h_1 and h_2, remains constant and frequency flat over the two consecutive time steps.

The received vector, $\mathbf{r}$, is formed by stacking two consecutive received data samples in time, resulting in

$$\mathbf{r} = \frac{1}{\sqrt{2}}\mathbf{S}\mathbf{h} + \mathbf{n}, \tag{5.1-6}$$

where $\mathbf{r} = [r_0, r_1]^{\mathrm{T}}$ represents the received vector, $\mathbf{h} = [h_1, h_2]^{\mathrm{T}}$ is the complex channel vector, $\mathbf{n} = [n_0, n_1]^{\mathrm{T}}$ is the noise at the receiver, and $\mathbf{S}$ defines the STC:

$$\mathbf{S} = \begin{pmatrix} s_0 & s_1 \\ s_1^* & -s_0^* \end{pmatrix}.$$

The vector equation in Equation 5.1 - 6 can be read explicitly as

$$r_0 = \frac{1}{\sqrt{2}} s_0 h_1 + \frac{1}{\sqrt{2}} s_1 h_2 + n_0, \tag{5.1 - 7}$$

$$r_1 = \frac{-1}{\sqrt{2}} s_1^* h_1 + \frac{1}{\sqrt{2}} s_0^* h_2 + n_1. \tag{5.1 - 8}$$

At the receiver, the vector $\mathbf{y}$ of the received signal is formed according to $\mathbf{y} = [r_0, r_1^*]^{\mathrm{T}}$, which is equivalent to

$$r_0 = \frac{1}{\sqrt{2}} s_0 h_1 + \frac{1}{\sqrt{2}} s_1 h_2 + n_0, \tag{5.1 - 9}$$

$$r_1^* = \frac{1}{\sqrt{2}} s_0 h_2^* - \frac{1}{\sqrt{2}} s_1 h_1^* + n_1^*. \tag{5.1 - 10}$$

These both equations can be rewritten in a matrix system as specified in Equation 5.1 - 11:

$$\begin{pmatrix} r_0 \\ r_1^* \end{pmatrix} = \frac{1}{\sqrt{2}} \begin{pmatrix} h_1 & h_2 \\ h_2^* & -h_1^* \end{pmatrix} \begin{pmatrix} s_0 \\ s_1 \end{pmatrix} + \begin{pmatrix} n_0 \\ n_1^* \end{pmatrix}. \tag{5.1 - 11}$$

The short notation for this system is the following:

$$\mathbf{y} = \frac{1}{\sqrt{2}} \mathbf{H}_\nu \mathbf{s} + \widetilde{\mathbf{n}}, \tag{5.1 - 12}$$

where $\widetilde{\mathbf{n}}$ represents the new noise vector obtained after the conjugation of the second equation, $\widetilde{\mathbf{n}} = [n_0, n_1^*]^{\mathrm{T}}$.

The resulting virtual (2×2) channel matrix, $\mathbf{H}_\nu$, is orthogonal, i.e.

$$\mathbf{H}_\nu{}^{\mathrm{H}} \mathbf{H}_\nu = \mathbf{H}_\nu \mathbf{H}_\nu{}^{\mathrm{H}} = h^2 \mathbf{I}_2,$$

where $(\cdot)^H$ represents the hermitian operation, $\mathbf{I}_2$ is the 2×2 identity matrix, and h^2 is the power gain of the channel, with $h^2 = |h_1|^2 + |h_2|^2$. Due to this orthogonality, the Alamouti scheme decouples the MISO channel into two virtually independent channels with channel gain h^2 and diversity $d = 2$.

The mentioned channel gain is deduced from Equation 5.1 - 13, which specifies that transmitted symbols can be estimated at the receiver as the result of multiplying the received signals by the hermitian of the virtual channel matrix. After performing the corresponding operations it results in a signal with a gain of h^2 plus some modified noise[4]:

$$\widehat{\mathbf{s}} = \mathbf{H}_\nu{}^{\mathrm{H}} \mathbf{y} = \frac{1}{\sqrt{2}} h^2 \mathbf{s} + \mathbf{H}_\nu^{\mathrm{H}} \widetilde{\mathbf{n}}. \tag{5.1 - 13}$$

[4]The whole derivation of Equation 5.1 - 13 can be found in Section B.2.1.

Alamouti scheme with arbitrary number of receive antennas

A system with two transmit antennas and an arbitrary number of receive antennas [27], as the one depicted in Figure 5.1 - 3, is analyzed next. The already explained steps are applied to each of the receive antennas, denoting the received signal in the first and second time slot as $\mathbf{r}_0$ and $\mathbf{r}_1$, respectively.

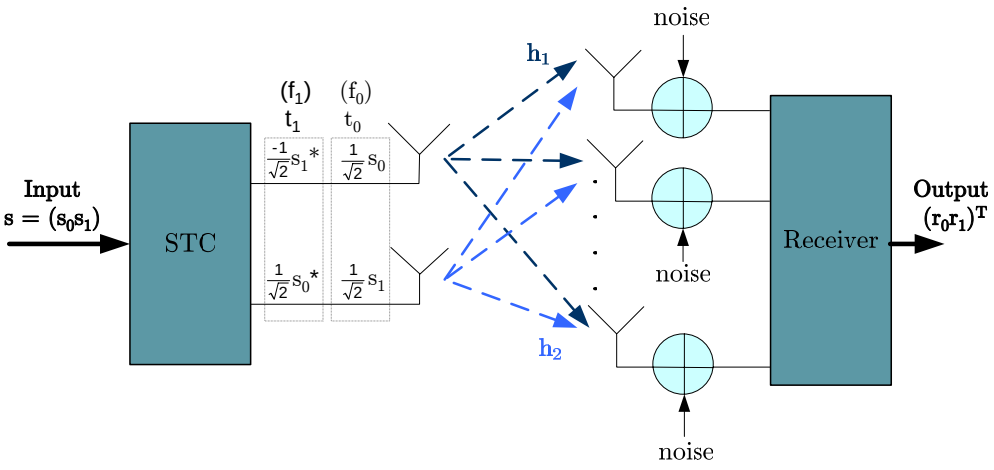

Figure 5.1 - 3: $2\times N_R$ Alamouti scheme.

Vectors $\mathbf{h}_1 = [h_{11}, h_{12}, ..., h_{1N_R}]^T$ and $\mathbf{h}_2 = [h_{21}, h_{22}, ..., h_{2N_R}]^T$ contain the channel coefficients corresponding to the transmission from antenna Tx1 and antenna Tx2 to every receive antenna, respectively.

As in the previous section, the received vector is

$$\begin{pmatrix} \mathbf{y}_0 \\ \mathbf{y}_1 \end{pmatrix} = \begin{pmatrix} \mathbf{r}_0 \\ \mathbf{r}_1^* \end{pmatrix} = \frac{1}{\sqrt{2}} \begin{pmatrix} \mathbf{h}_1 & \mathbf{h}_2 \\ \mathbf{h}_2^* & -\mathbf{h}_1^* \end{pmatrix} \begin{pmatrix} s_0 \\ s_1 \end{pmatrix} + \begin{pmatrix} \mathbf{n}_0 \\ \mathbf{n}_1^* \end{pmatrix}, \qquad (5.1\text{-}14)$$

where $\mathbf{n}_0$ and $\mathbf{n}_1$ are noise vectors, corresponding to the noise added in each receive branch.

Following the same steps as in the 2×1 Alamouti scheme, the estimation of the transmitted symbols at the receiver is performed in Equation 5.1 - 15. Since the power gain of the channel is, in this case, $h^2 = \|\mathbf{h}_1\|^2 + \|\mathbf{h}_2\|^2$, it is possible to achieve a diversity order of $2N_R$. The whole description of this formula for a 2×2 Alamouti scheme is further explained in section Section B.2.2.

$$\widehat{\mathbf{s}} = \mathbf{H}_\nu{}^H \mathbf{y} = \frac{1}{\sqrt{2}} h^2 \mathbf{s} + \mathbf{H}_\nu^H \widetilde{\mathbf{n}} \qquad (5.1\text{-}15)$$

For a system with two receive antennas, Rx1 and Rx2, and according to the above equations, the received signals would be $\mathbf{r}_0 = [\mathbf{r}_0(1)\mathbf{r}_0(2)]^{\mathrm{T}}$ and $\mathbf{r}_1 = [\mathbf{r}_1(1)\mathbf{r}_1(2)]^{\mathrm{T}}$, where $\mathbf{r}_0(1)$ is the symbol received in antenna Rx1 at time slot t_0, and $\mathbf{r}_1(1)$, the symbol received at time slot t_1. In the same way, $\mathbf{r}_0(2)$ and $\mathbf{r}_1(2)$ are the symbols received in antenna Rx2 during the two time slots. Therefore, the signal that is received at the end is $\mathbf{y} = [\mathbf{r}_0\mathbf{r}_1^*]^{\mathrm{T}}$:

$$\begin{pmatrix} \mathbf{r}_0 \\ \mathbf{r}_1^* \end{pmatrix} = \begin{pmatrix} \mathbf{r}_0(1) \\ \mathbf{r}_0(2) \\ \mathbf{r}_1^*(1) \\ \mathbf{r}_1^*(2) \end{pmatrix} = \frac{1}{\sqrt{2}} \begin{pmatrix} h_{11} & h_{21} \\ h_{12} & h_{22} \\ h_{21}^* & -h_{11}^* \\ h_{22}^* & -h_{12} \end{pmatrix} \begin{pmatrix} s_0 \\ s_1 \end{pmatrix} + \begin{pmatrix} n_0(1) \\ n_0(2) \\ n_1^*(1) \\ n_1^*(2) \end{pmatrix}. \tag{5.1-16}$$

In this case the power gain of the channel is $h^2 = \|\mathbf{h}_1\|_2^2 + \|\mathbf{h}_2\|_2^2$ and a diversity order of 4 is achieved.

5.1.3 Maximum Ratio Combining

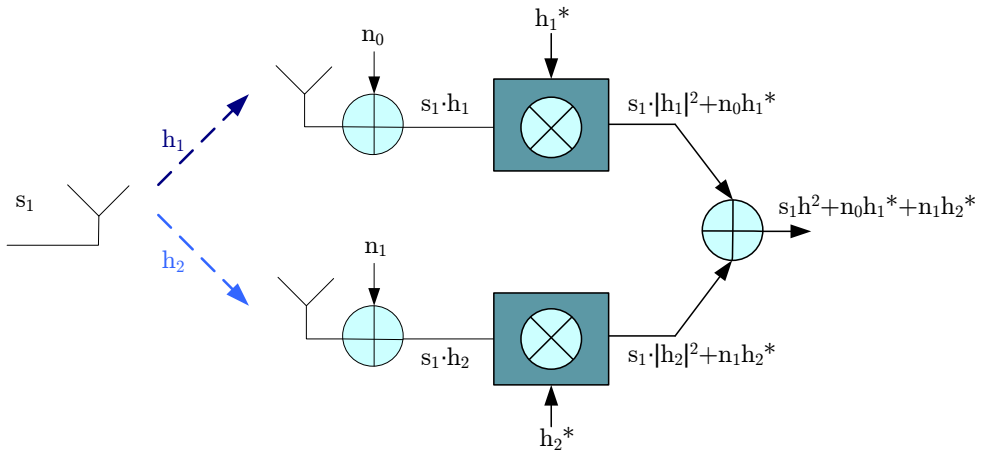

Figure 5.1-4: A system using two antennas in reception.

Maximum ratio combining (MRC) [26] is a special form of diversity where multiple replicas of the same signal, received over different diversity branches, are combined in order to maximize the instantaneous SNR at the combiner output. Before summing the signals of every receive branch the symbols on all receive antennas are weighted. The weight factor corresponds with the complex conjugated channel coefficient of each receive branch.

The signal received on each antenna is given by

$$y_i = h_i s + n_i, \qquad i = 1, 2, \cdots, \mathrm{N_R}, \tag{5.1-17}$$

where h_i and n_i are the channel coefficients and the noise experienced by antenna i, respectively, s is the transmitted signal, and $\mathrm{N_R}$ is the number of receive antennas. Moreover, it is considered that the antennas are sufficiently spaced from each other and the channel coefficients, affected by fading, can be assumed to be independent.

The weighted combination for the input antennas to be taken into account is expressed as follows:

$$y = \sum_{i=1}^{\mathrm{N_R}} \beta_i y_i = s \sum_{i=1}^{\mathrm{N_R}} \beta_i h_i + \sum_{i=1}^{\mathrm{N_R}} \beta_i n_i. \tag{5.1-18}$$

From this combination, the SNR of the channel is given by

$$\mathrm{SNR}(h_1, h_2, \cdots, h_{\mathrm{N_R}}) = \frac{E|s\sum_{i=1}^{\mathrm{N_R}} \beta_i h_i|^2}{E|\sum_{i=1}^{\mathrm{N_R}} \beta_i n_i|^2} = \frac{|\sum_{i=1}^{\mathrm{N_R}} \beta_i h_i|^2}{\sum_{i=1}^{\mathrm{N_R}} |\beta_i|^2}. \tag{5.1-19}$$

Applying the Cauchy-Schwartz inequality, it is straightforward to verify that $\beta_i = h_i^*$ maximizes the SNR. Replacing this value in Equation 5.1-19, the maximal SNR yields

$$\mathrm{SNR}(h_1, \cdots, h_{\mathrm{N_R}}) = \mathrm{SNR} \sum_{i=1}^{\mathrm{N_R}} |h_i|^2. \tag{5.1-20}$$

The process described above is shown in Figure 5.1-4, where an example of a receiver with dual antenna diversity is depicted. The signal is sent over a channel with transmission coefficients h_1 and h_2, and reaches both receive antennas with some added noise. Then, the process consists of multiplying the signal in each receive branch by the corresponding conjugated channel coefficient, and at the end, the signals from both branches are summed.

It can be appreciated that the received signal is very similar to the one obtained with the Alamouti scheme in Equation 5.1-13, as the same gain in the signal is achieved, as well as some modified noise. However, better performance is obtained with this scheme as only one symbol is transmitted in one time interval and the unity average transmit power is already achieved in each interval. Therefore, the resultant signal is not multiplied by the factor $1/\sqrt{2}$ as in the Alamouti scheme, and consequently, a gain of 3 dB in power is obtained.

5.2 MIMO implementation

This section describes the implementation of the mentioned MIMO in the simulator, thus explaining in detail the respective changes to be performed in both transmitter and receiver.

5.2.1 Transmitter

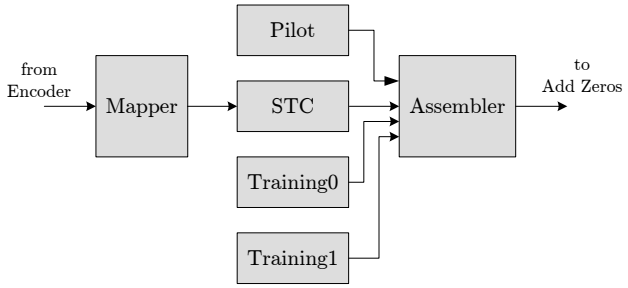

Figure 5.2 - 1: MIMO transmitter in the WiMAX system.

The main aspects to be taken into account when implementing the MIMO transmitter are focused on applying the STC algorithms in both OFDM symbols and pilot subcarriers, as well as in the assembling process, as two long training sequences are used now.

STC block

This block performs the Alamouti algorithm described in Equation 5.1 - 11. As explained, the basic Alamouti scheme transmits two complex symbols, s_0 and s_1, using the multiple-input single-output channel twice with channel vector values h_1 and h_2. During the first channel use antenna Tx1 transmits s_0, and antenna Tx2, s_1. In the following channel use, symbols $-s_1^*$ and s_0^* are transmitted from Tx1 and Tx2 respectively.

Pilot symbols

On a given pilot subcarrier, the same pilot symbol is used for the STC block. The pilot symbol for pilot subcarrier "s" obtained after it has been 2-PAM modulated is p_s, and the OFDM symbols that enter into the STC block are symbols "k" and "k+1". The standard [4] specifies that the modulation on pilot subcarrier "s" during the transmission of symbol "k" shall be p_s on both transmit antennas. Nevertheless, during symbol "k+1", the modulation on the pilot subcarrier shall be $-p_s$ for antenna 1, and p_s for antenna 2.

	Antenna 1	**Antenna2**
symbol k	pilot p_s	pilot p_s
symbol $k+1$	pilot $-p_s$	pilot p_s

Preambles

Two long training sequences are needed when using the MIMO transmission. As explained in Section 2.5, preambles for DL transmissions are composed of three consecutive OFDM symbols. The first one, set according to the short training P_{SHORT}, is used for synchronization. The second symbol uses a long training sequence, necessary in the receiver for channel estimation. The first antenna transmits the sequence P_{EVEN} as long training sequence, and the second antenna transmits the sequence P_{ODD}. As in the SISO case, the last symbol of the preamble is the FCH.

The following expressions describe the idea already explained:

$$\text{Antenna 1} = P_{\text{SHORT}} + P_{\text{EVEN}} + \text{FCH},$$

$$\text{Antenna 2} = P_{\text{SHORT}} + P_{\text{ODD}} + \text{FCH}.$$

Assembler

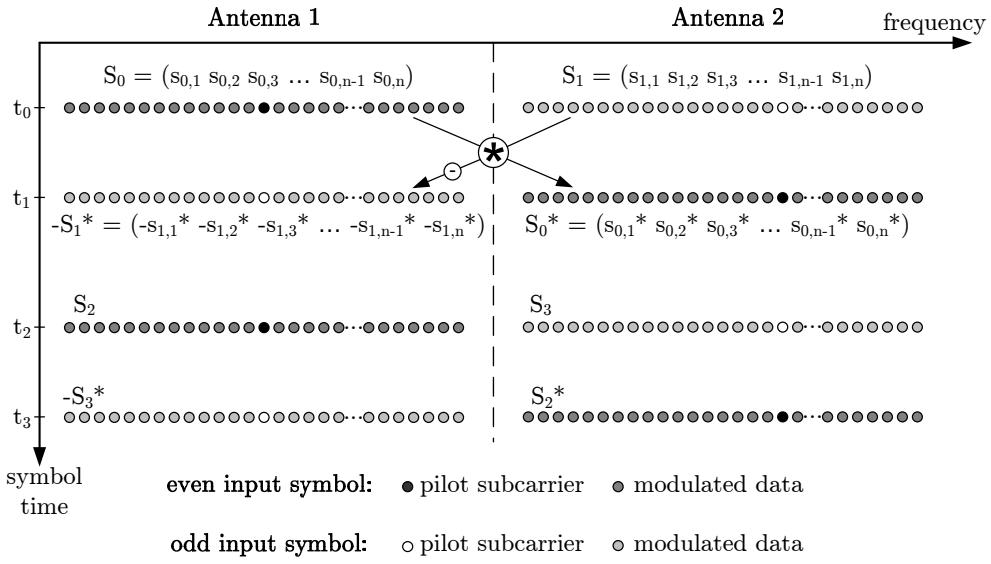

Figure 5.2 - 2: STC usage with OFDM.

The assembling process for the MIMO system is very similar to the SISO transmission explained in Section 2.6.

For a better understanding, the STC usage with the OFDM symbols is illustrated in Figure 5.2 - 2. During the first time step, symbols S_0 and S_1 are sent simultaneously from antenna 1 and antenna 2, respectively. Following

the Alamouti algorithm, the OFDM symbols $-S_1^*$ and S_0^* are sent in the next time step. The same operations are performed for the next time intervals, thus the symbol pair (S_2, S_3) is sent during the time steps t_2 and t_3, and so on.

On the other hand, the pilot symbols are inserted between the OFDM symbols as previously explained. Antenna 1 transmits p_s and $-p_s$ in time steps t_0 and t_1, respectively. However, only p_s is transmitted from antenna 2 during both time intervals.

5.2.2 Receiver

At the receiver only the blocks described in the following have to be changed to allow detection of Alamouti coded signals.

Disassembler

When implementing the MIMO disassembler it has to be taken into account that, although from different antennas, two OFDM symbols are transmitted in each time interval. Each OFDM symbol is processed as a matrix, where each row represents a subcarrier. In this way, 3D-matrices would be needed in order to also specify, in this case, the antenna from where the OFDM is being transmitted in each time step. However, Simulink does not support 3D-matrices, and therefore, these OFDM symbols of different antennas are processed consecutively.

The mentioned disassembling process separates first the two transmitted OFDM symbols, and next, performs the separation of training sequences, pilot subcarriers, and DC subcarrier from the original data subcarriers, as explained in Section 4.3.

Channel estimator

The estimated channel coefficients are calculated for each receive antenna as explained in Section 4.4. Moreover, two long training sequences, P_{EVEN} and P_{ODD}, are used when applying MIMO transmissions, and so, both have to be considered for the channel estimation. If only one transmit antenna exists, the channel estimation is performed using the sequence P_{EVEN}. However, when the two transmit antennas are being used, the second antenna will estimate its channel coefficients with P_{ODD}. This is possible because P_{EVEN}

uses only even subcarriers and P_{ODD} only odd subcarriers, making the OFDM symbols P_{EVEN} and P_{ODD} orthogonal.

Demapper

The aim of the demapper is determining the symbol that was transmitted. With this purpose, decision metric algorithms are developed. Both hard demapping and soft demapping are implemented as described in Section 4.5. However, the estimate of the received signal has to be calculated first, and depending on the diversity scheme, this calculation is performed in a different way.

When a scheme with two transmit antennas and only one receive antenna is being used, the receive estimates are calculated from Equation 5.1 - 13:

$$\widehat{s} = \frac{1}{\sqrt{2}} h^2 \mathbf{s} + \mathbf{H}_{\nu}^{\text{H}} \widetilde{\mathbf{n}}.$$

On the other hand, when there is one transmit antenna and two receive antennas, the estimate of the received signal is obtained following the MRC formula:

$$\widehat{s} = s_1 h^2 + n_0 h_1^* + n_1 h_2^*,$$

where $h^2 = |h_1|^2 + |h_2|^2$.

Finally, when two antennas at both ends of the communication system are used, the estimation is performed as in Equation 5.1 - 15:

$$\widehat{s} = \frac{1}{\sqrt{2}} h^2 \mathbf{s} + \mathbf{H}_{\nu}^{\text{H}} \widetilde{\mathbf{n}}.$$

In this case, the channel gain is $h^2 = \|\mathbf{h}_1\|^2 + \|\mathbf{h}_2\|^2$.

Chapter 6

Adaptive Modulation and Coding

The growing demand of all types of services, not only voice and data but also multimedia services, aims for the design of increasingly more intelligent and agile communication systems, capable of providing spectrally efficient and flexible data rate access. These systems are able to adapt and adjust the transmission parameters based on the link quality, improving the spectrum efficiency of the system, and reaching, in this way, the capacity limits of the underlying wireless channel. Link adaptation techniques, often referred to as adaptive modulation and coding (AMC), are a good way for reaching the cited requirements. They are designed to track the channel variations, thus changing the modulation and coding scheme to yield a higher throughput by transmitting with high information rates under favorable channel conditions and reducing the information rate in response to channel degradation.

This chapter is focused on the implementation of such techniques. A theoretical explanation, necessary to understand the operation principles of adaptive modulation and coding, is briefly given. Also a performance analysis of the AMC scheme implemented in the simulator is furthermore presented in this chapter.

6.1 Theory on the AMC technique

6.1.1 Introduction to adaptive transmission mechanisms

Since the available radio spectrum for wireless communications is extremely scarce, there is a rapid growth in the demand of services for portable and wireless devices, and, as these services become more and more complex, the use of spectrally efficient transmission schemes supporting higher information rates is needed.

In traditional communication systems, the transmission is designed for a "worst case" channel scenario thus coping with the channel variations and still delivering an error rate below a specific limit. Adaptive transmission schemes, however, are designed to track the channel quality by adapting the channel throughput to the actual channel state. These techniques take advantage of the time-varying nature of the wireless channel to vary the transmitted power level, symbol rate, coding scheme, constellation size, or any combination of these parameters, with the purpose of improving the link average spectral efficiency, i.e. the number of information bits transmitted per second per Hz bandwidth used.

Adaptive modulation and coding (AMC) is a promising tool for increasing the spectral efficiency of time-varying wireless channels while maintaining a predictable BER [28]. In AMC, not only the modulation order but also the FEC scheme are varied by adjusting their code rate to the variations in the communication channel. For example, in periods of high fade when the channel is in a poor state, i.e. low SNR, the signal constellation size is reduced in order to improve fidelity, lowing the effective SNR to make transmission more robust. Conversely, in periods of low fade or high gain (high SNR), the signal constellation size is increased in order to allow higher data rate modulation schemes to be employed with low probability of error, thus improving the instantaneous SNR. An example of utilization of the cited AMC scheme is illustrated in Figure 6.1 - 1. It shows that as the range increases, the system steps down to a lower modulation, but as closer to the base station, higher order modulations can be used for increased throughput.

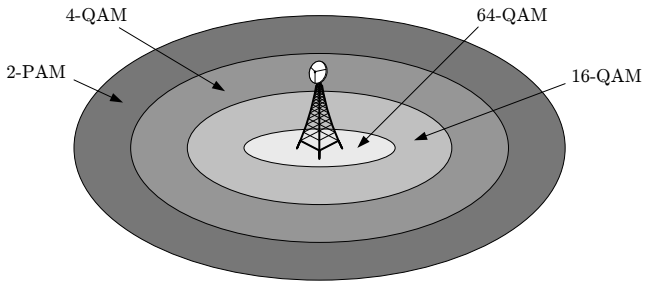

Figure 6.1 - 1: Scheme for the utilization of AMC.

6.1.2 Performance of the AMC scheme

A good performance of AMC schemes requires accurate channel estimation at the receiver and a reliable feedback path between that estimator and the transmitter on which the receiver reports channel state information (CSI) to the transmitter. In order to perform a good implementation the next steps must be followed:

Channel quality estimation

The transmitter requires an estimate of the expected channel conditions for the next transmission interval. Since this knowledge can only be gained by prediction from past channel quality estimations, the adaptive system can only operate efficiently in an environment with relatively slowly-varying channel conditions [29]. Therefore, the delay between the quality estimation and the actual transmission in relation to the maximal Doppler frequency of the channel is crucial for the system implementation since poor system performance will result if the channel estimate is obsolete at the time of transmission.

Although there are different ways to estimate the channel quality, the AMC scheme explained in this section is related with the measurement of the SNR, as it is often used in many systems as the channel quality information.

Parameter adaptation

The choice of the appropriate modulation and coding mode to be used in the next transmission is made by the transmitter, based on the prediction of the channel conditions for the next time interval. An SNR threshold such that it guarantees a BER below the target BER, BER_0, is defined by the system for each scheme whenever the SNR is above the SNR threshold.

The SNR thresholds are obtained from the BER vs. SNR characteristics of a modulation mode on an AWGN channel. As outlined in Figure 6.1 - 2, the method consists on splitting the SNR range into $N+1$ SNR regions by $N+2$ SNR thresholds, $\{\gamma\}_{\mathrm{n}=0}^{N+1}$, with $\gamma_0 = 0$ and $\gamma_{N+1} = \infty$.

Each of the N schemes is then assigned to operate within a particular SNR region. When the SNR γ falls within the SNR region $\gamma_{\mathrm{n}} \leq \gamma \leq \gamma_{\mathrm{n}+1}$, the associated channel state information is sent back to the transmitter. The transmitter then adapts its transmission rate and coding and modulation schemes by transmitting with a modulation scheme such that it guarantees a BER below BER_0. This enables the system to transmit with high spectral efficiency when the SNR is high, and to reduce the spectral efficiency as the SNR decreases.

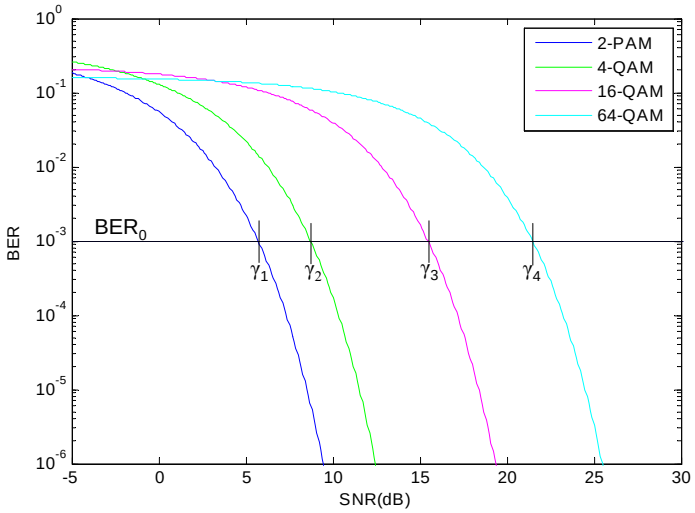

Figure 6.1 - 2: BER vs. SNR relationship and corresponding SNR thresholds for N coding and modulation schemes employed by AMC.

Feedback mechanism

Once the receiver has estimated the channel SNR, converted it into BER information for each mode candidate, and, based on a target BER, selected the mode that yields the largest throughput while remaining within the BER target bounds, it has to feed back the selected mode to the transmitter in order that the adaptation can be performed.

However, the challenge associated with adaptive modulation and coding is that the mobile channel is time-varying, and thus, the feedback of the channel information becomes a limiting factor. Therefore, the assumption of a slowly-varying as well as a reliable feedback channel is necessary in order to achieve an accurate performance of the AMC scheme. In this way, no delay or transmission error can occur in the feedback channel so that no discrepancy between the predicted and the actual SNR of the next frame appears.

Moreover, the receiver must also be informed of which demodulator and decoding parameters to employ for the next received packet.

6.2 AMC implementation

This section explains the implementation of the cited adaptive modulation and coding scheme. A few differences between this simulator version and the last one that was mentioned when implementing the MIMO system are encountered. On one hand, besides the channel coefficients, the channel

estimator also estimates the corresponding SNR. On the other hand, a new block is introduced with the aim of deciding the modulation and coding mode to be switched at the transmitter. Furthermore, as appreciated in Figure 6.2 - 1, not only the encoder and mapper in the transmit side but also the decoder and demapper in the receiver are grouped into a unique block, which implementation and function will be later discussed.

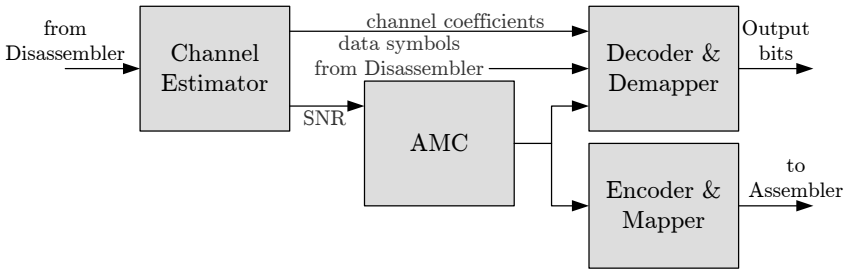

Figure 6.2 - 1: AMC mechanism in the WiMAX system.

6.2.1 SNR estimation

The calculation of the SNR is performed in the channel estimator. As well known, the SNR is obtained from dividing the signal power between the noise power. Thus, the instantaneous SNR for each frame is calculated as

$$\text{SNR} = \frac{\overline{s}}{\overline{n}},$$

where $\overline{s}$ and $\overline{n}$ are the average signal and noise power, respectively, in each frame. While the signal power is obtained from the channel coefficients, the noise power is calculated from the noise variance, σ_ν^2.

As stated in Section 2.5, the long training sequences are an interpolated version of the sequence P_{ALL}, where either P_{EVEN} or P_{ODD} use a subset of even or odd subcarriers, respectively, while keeping null the remaining subset. However, the training symbols are received with some additive noise, and thus, the previous null carriers have now a non-zero value. The noise is calculated from these carriers.

Furthermore, as it happened with the channel estimation, it has to be taken into account whether the system uses one or two transmit antennas. When only one transmit antenna is used the noise is obtained from P_{EVEN}. If the system has two transmit antennas, both P_{EVEN} and P_{ODD} are used instead.

6.2.2 The AMC block

This block deals with the task of finding the decision thresholds, deciding which of the modulation and coding schemes shown in Table 2.2 - 1 may be employed in the next frame transmission, and feeding back this information not only to the transmitter but also to the receiver.

As explained before, the SNR thresholds are calculated from the BER vs. SNR curves. The curves depicted in Figure 6.2 - 2 have been obtained from simulations performed with a perfect knowledge of the channel coefficients in an AWGN scenario. The figure shows seven curves corresponding to the seven different modulation and coding schemes allowed by the WiMAX system, defined from AMC1 to AMC7. The set of adaptation/switching thresholds is obtained by reading the SNR points corresponding to a target BER.

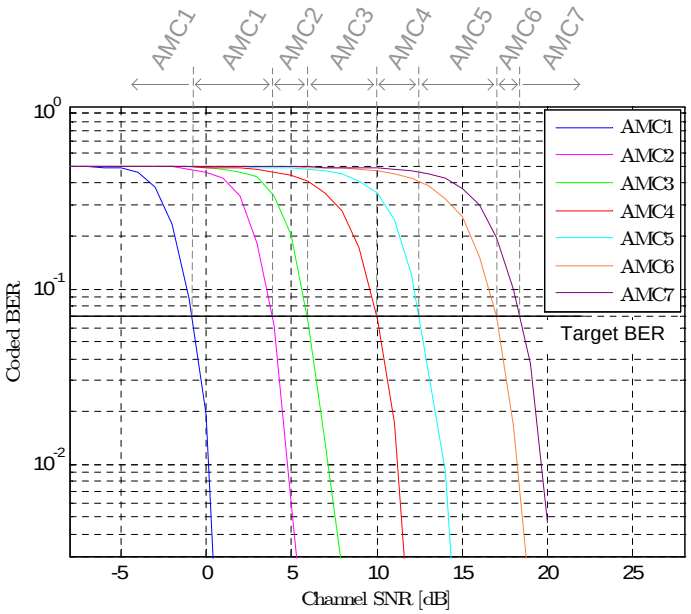

Figure 6.2 - 2: BER vs. SNR curves.

The implementation of this method is performed in a Matlab file. The obtained coded BER values for a given SNR, for each of the different AMC schemes, are programmed. According to a target BER specified by the user a selection function calculates the SNR thresholds, and the AMC scheme to use in the next frame is decided by comparing these thresholds with the estimated SNR of the channel.

6.2.3 Coding and decoding

Both transmitter and receiver have to be informed about which AMC scheme to employ in the next transmission frame. An encoder and mapper in which the parameters to be used were specified by the user were performed in the simulator without the adaptive modulation and coding mechanism. However, a bank of seven encoders and mappers, each one with a fixed AMC scheme, is now set up so that the transmitter can switch from one AMC scheme to another based on the feedback information. The same operation is performed at the receiver, where instead of only a demapper and a decoder, a bank with seven demappers and decoders is also implemented.

Chapter 7

Simulation results

In this chapter, simulation results will be presented along with the underlying assumptions. The goal is to evaluate the performance of the simulator as well as to obtain a more accurate understanding of the operation of the WiMAX system. Through numerous comparisons between simulation results obtained with different simulation parameters, some discussions about the use of these different parameters and options are given with the purpose of offering a complete view on the better manner of performance of the transmission. Thus, not only the two demapping methods but also the impact of the channel estimation are analyzed. Furthermore, the transmission gain obtained when using multiple antennas instead of only a single antenna at one or both ends of the transmission link is also examined. The different channel models and scenarios are applied in different simulations so that the fading phenomenon can be studied. To end, results when activating the AMC mechanism are offered, thus showing the mentioned increase in spectral efficiency and data throughput.

7.1 A single antenna transmission

This section shows simulation results when using a single antenna not only at the transmitter but also at the receiver. The common assumptions to most of the simulations are as follows: the simulation is carried out for downlink transmissions at a carrier frequency of 2 GHz and a 20 MHz channel bandwidth. The length of the cyclic prefix is defined by $G = 1/32$ and the frame duration is specified to be 2.5 msec. Thus, only changes performed on these assumptions will be mentioned from now on.

7.1.1 Modulation schemes and coding rates

This section gives a comparison between the different modulation schemes and coding rates used in the simulator. These results have been obtained in an AWGN channel, with a system using least-squares channel estimation and hard demapping.

The simulated performance for different modulation schemes and coding rates tested is shown in Figure 7.1 - 1 and Figure 7.1 - 2. As specified in the standard, WiMAX allows for seven different combinations of modulation order and coding rates, which are briefly summarized next.

AMC Mode	Modulation scheme	Overall coding rate
AMC1	2-PAM	1/2
AMC2	4-QAM	1/2
AMC3	4-QAM	3/4
AMC4	16-QAM	1/2
AMC5	16-QAM	3/4
AMC6	64-QAM	2/3
AMC7	64-QAM	3/4

Table 7.1 - 1: Modulation schemes and coding rates.

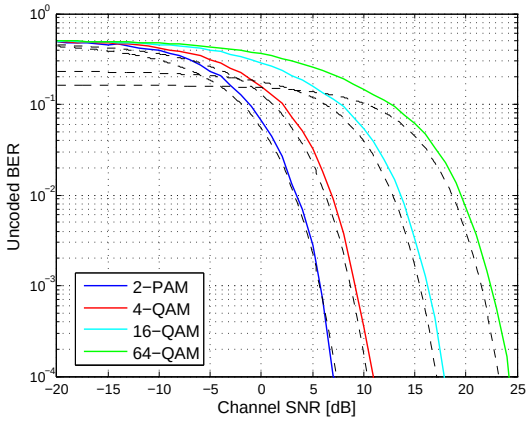

Figure 7.1 - 1: Comparison between modulation schemes in the uncoded BER.

The curves show the BER as a function of the bit energy to noise rate (E_b/N_0), which is a measure of the energy efficiency of a modulation scheme. If a higher E_b/N_0 is needed to transfer data for a given modulation scheme, it means that more energy is required for each bit transfer. Low spectral efficiency modulation schemes, such as 2-PAM and 4-QAM, require a lower

E_b/N_0, and hence, are more energy efficient and less vulnerable to bit errors. Furthermore, the BER versus the SNR can be calculated from E_b/N_0. The SNR for each modulation takes into account the number of bits per symbol, and so, the signal power corresponds to the energy per bit times the number of bits per symbol.

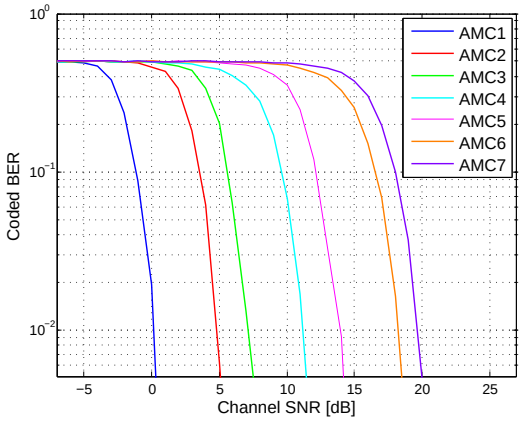

Figure 7.1 - 2: Comparison between different modulation chemes and coding rates in the coded BER.

As we can see, a comparison between the different modulation schemes is performed. The dashed black curves in Figure 7.1 - 1 represent the AWGN theoretical BER curves. They have been calculated from the probability of bit error expressions as follows [30]:

$$P_{\mathrm{bc}} = 2\left(1 - \frac{1}{\sqrt{M_{\mathrm{a}}}}\right) \mathrm{Q}\left(\sqrt{\frac{3}{M_{\mathrm{a}} - 1}\frac{\mathrm{E_b}}{\mathrm{N_0}}}\right), \tag{7.1 - 1}$$

where P_{bc} is the probability of bit error per carrier, M_{a} defines the modulation alphabet, and $\mathrm{Q}(x)$ is related to the complementary Gaussian error function by $\mathrm{Q}(x) = \frac{1}{\sqrt{2\pi}} \int_x^\infty \exp\left(\frac{-x^2}{2}\right) dx = \frac{1}{2}\mathrm{erfc}\left(\frac{x}{\sqrt{2}}\right)$, which is the probability that a Gaussian distributed variable x_0 is larger than x.

Therefore, the probability of bit error is calculated as

$$P_{\mathrm{b}} = 1 - (1 - P_{\mathrm{bc}})^2. \tag{7.1 - 2}$$

Note that the theoretical curves experiment a small shift if compared with those simulated. This shift can be calculated analytically and is a loss in the SNR of the system: $\mathrm{SNR_{loss}} = 10\log_{10}\left(\frac{200}{192}\frac{33}{32}\right) = 0.3\mathrm{dB}$. It expresses the mentioned shift, where 200/192 is the ratio of the number of non-zero

subcarriers (data and pilots) to the data subcarriers, and 33/32 represents the relationship between the data symbol with and without adding the cyclic prefix, which, in this case, is defined by $G = 1/32$.

A comparison between all different modulation schemes and coding rates is given in Figure 7.1 - 2, where the coded BER vs. SNR curves have been plotted. It can be noticed that the higher the code rate, the more the curves are shifted to the right, and as it has been discussed for the uncoded BER curves, the higher the modulation scheme, the higher the bit error rate.

7.1.2 Types of channel fading

The different channel fading and the effects of the velocity of the user are discussed in the current section. As mentioned through the thesis, three kinds of channel fading are implemented in the simulator, block fading, time-variant fading, and time-variant block fading channel. As expected, the time-variant channel experiments the worse results as a consequence of the varying channel coefficients. In order to improve the performance of this time-variant channel, a time-variant channel estimator could be implemented. The block fading channel, which has no variation of its channel coefficients through the whole process of transmission, is the one that obtains better results instead. These observations, which regard to the different fading types, are shown in Figure 7.1 - 3, where the parameters are set to be AMC3, perfect channel knowledge, hard demapping, and a user velocity of 3 km/h.

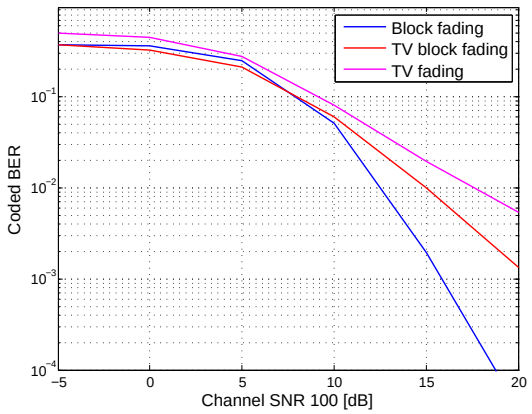

Figure 7.1 - 3: Comparison between different types of fading.

Also discussed in this section is the velocity of the user terminal, analyzed next. With this purpose, the following graphics show the performance of the

system not only for the uncoded BER curves, but also for the coded BER curves, when passing the signal through a time-variant channel, in scenario F. The parameters used in this simulations are soft demapping, perfect channel knowledge, and AMC3.

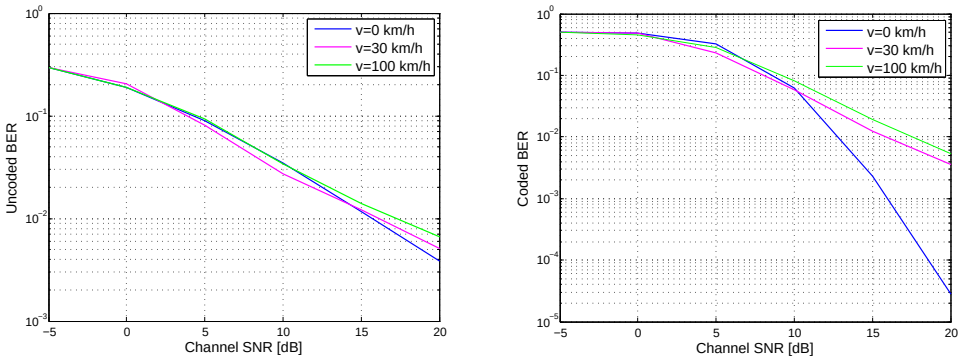

(a) (b)

Figure 7.1 - 4: BER vs. SNR curves in a time-variant channel for scenario F.

Figure 7.1 - 4 depicts results obtained for a time-variant channel. It is shown that while the velocity of the user is not an important factor when computing the uncoded BER curve, it plays an essential role in the coded BER curve, where, as expected, the lower the velocity the better the results.

7.1.3 Demapping and channel estimation

This section compares hard and soft demapping. More specifically, the max-log-MAP algorithm implemented for the soft demapping is analyzed. The first results compare the demapping and the channel estimation methods for an AWGN channel using a 4-QAM modulation format, and an overall coding rate of 1/2 (AMC2).

Figure 7.1 - 5 shows the BER performance for both hard and soft (max-log-MAP) demapping. It is a plot of the coded BER vs. SNR curves where a perfect knowledge of the channel coefficients has been assumed. The figure shows that soft demapping outperforms hard demapping in approximately 2 dB in SNR. In the same way, a comparison between channel estimation and a perfect knowledge of the channel coefficients is made. In this case, hard demapping has been used at the receiver. As expected, better results are obtained with the knowledge of the channel coefficients. However, when removing the assumption of ideal channel knowledge it is noticed that the performance curves become 1 dB more degraded in SNR. Therefore, in an

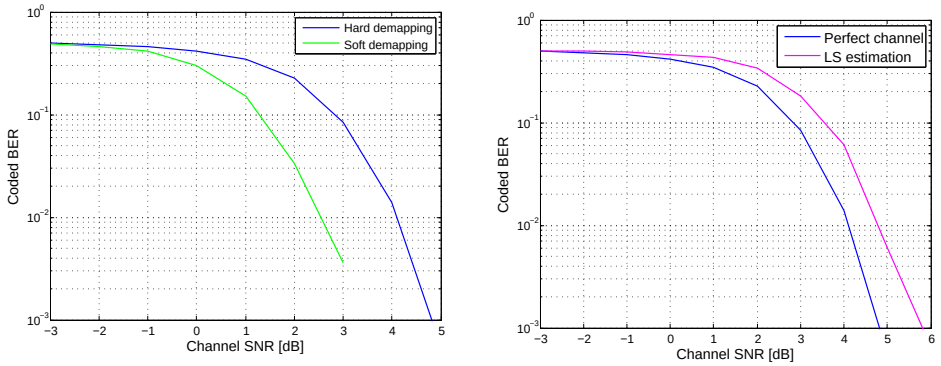

(a) Hard demapping vs. soft demapping. (b) Perfect channel knowledge vs. least-squares channel estimation.

Figure 7.1 - 5: Demapping and channel estimation in an AWGN channel.

implementation more effort should be spent on implementing a soft demapper than a better channel estimator.

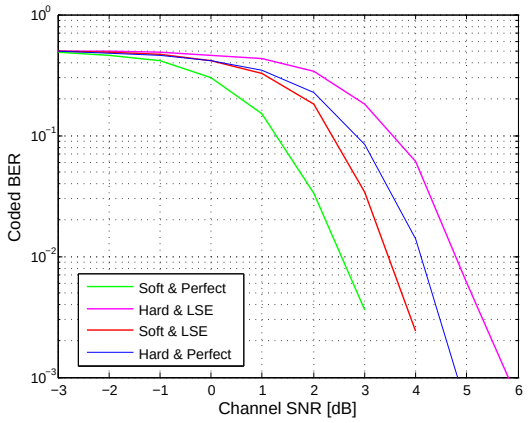

Figure 7.1 - 6: Comparison between hard and soft demapping and channel estimation in an AWGN channel.

These four possible combinations of demapping and channel estimation are plotted in Figure 7.1 - 6. As mentioned, 2 dB of gain are obtained when using soft demapping instead of hard demapping. On the other hand, there is 1 dB of loss in the SNR when channel estimation is applied. Therefore, it can be deducted that the scheme using the soft demapping algorithm and a perfect knowledge of the channel will outperform that with hard demapping and least-squares channel estimation in approximately 3 dB in SNR. In the

same way, if soft demapping is combined with LSE[1], the gain obtained with the soft demapping is damaged by the application of the least-squares channel estimation, and only 1 dB of gain in SNR is achieved.

In addition to this, both demapping and channel estimation is analyzed for the block fading channel. As in the AWGN channel, the comparison between the demapping methods is performed with a perfect knowledge of the channel, and the one for channel estimation, using hard demapping.

The following figures analyze not only both demapping methods but also the channel estimation results in scenario F. They show that the gain obtain with soft demapping increases as the SNR increases. The same occurs with the gain obtained when using perfect channel knowledge instead of least-squares channel estimation. Therefore, the receiver is able to better utilize the diversity of the frequency-selective channel.

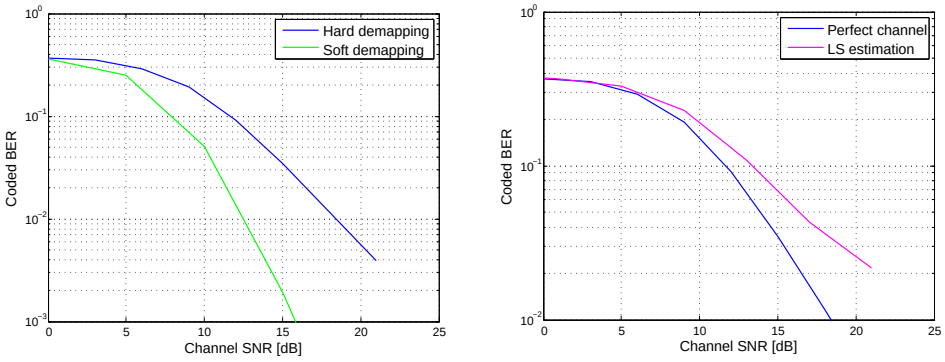

(a) Hard demapping vs. soft demapping. (b) Perfect channel knowledge vs. least-squares channel estimation.

Figure 7.1 - 7: Demapping and channel estimation in a block fading channel.

[1] Least-Squares Estimation

7.1.4 AMC and its effects in the results

This sections discusses the consequences caused in the results when applying the AMC mechanism. Several aspects, including the type of channel, the velocity of the user, or the channel estimation, are analyzed with this purpose, thus letting us notice the enhancement AMC offers.

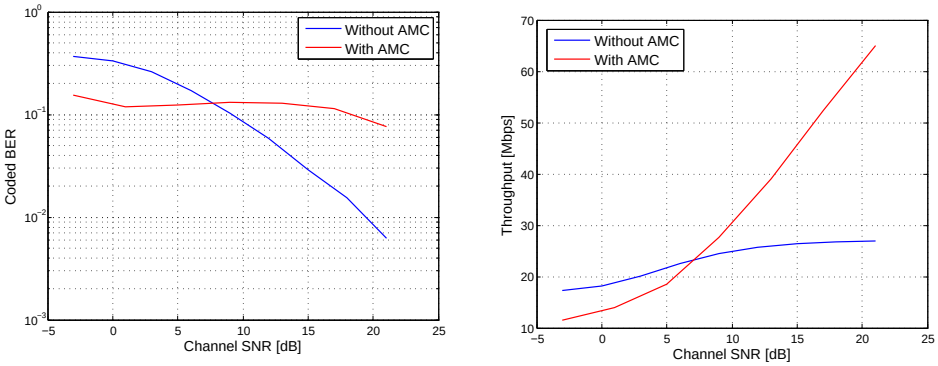

(a) Coded BER vs. SNR curves. (b) Throughput vs. SNR curves.

Figure 7.1 - 8: Comparison between results obtained with and without using the AMC scheme.

To begin with, a comparison between results with and without using the mentioned AMC scheme is performed. Figure 7.1 - 8 depicts the coded BER and the throughput curves for scenario A in a block fading channel. The setting parameters are hard demapping, perfect channel knowledge, and AMC3. The results show an enormous increase in the throughput when using the AMC mechanism from approximately 7 dB of channel SNR onwards. On the other hand, the prize for this enhancement is, as previously explained, the support of a predictable BER, which maintains small variations around a fixed value.

Furthermore, the selection of the AMC mode is made in such a way that it guarantees a BER below a given target BER. With our operating point at a target BER of 10^{-1}, we have the ranges specified in Table 7.1 - 2 for each AMC scheme. We came to these levels in the following way: at an operating BER of 10^{-1}, there is no AMC scheme that gives us our desired performance at an SNR below -1 dB. Therefore, we choose AMC1 as it is the most robust. Between -1 and 3 dB, there is only one scheme that gives us our desired performance below 10^{-1}, and that is AMC1. Between 3 and 6 dB, AMC2 gives us our desired BER. Between 6 and 9 dB the AMC scheme giving the desired BER performance at a better spectral efficiency is AMC3. Likewise,

as the channel SNR is higher, higher AMC schemes are used to give us the best spectral efficiency while providing the desired BER performance.

	Target BER=10^{-1}	**Target BER=10^{-2}**
AMC1	SNR<-1 dB	SNR<0 dB
AMC1	-1 dB<SNR<3 dB	0 dB<SNR<5 dB
AMC2	3 dB<SNR<6 dB	5 dB<SNR<7 dB
AMC3	6 dB<SNR<9 dB	7 dB<SNR<11 dB
AMC4	9 dB<SNR<12 dB	11 dB<SNR<13 dB
AMC5	12 dB<SNR<16 dB	13 dB<SNR<18 dB
AMC6	16 dB<SNR<18 dB	18 dB<SNR<19 dB
AMC7	SNR>18dB	SNR>19dB

Table 7.1 - 2: AMC scheme to SNR range.

In the same way, the chart shows the SNR ranges for a given target BER of 10^{-2}. In this case the SNR thresholds are shifted to the right (higher SNR) due to decreasing nature of the BER curves with the SNR. Therefore, as Figure 7.1 - 9 shows, if the target BER is higher, the performance of the system will be worse as worse channel quality conditions (higher target BER to guarantee a BER below it) are required. However, it can be seen that the target BER is not achieved. The channel fading is so fast (low temporal correlation and short coherence time) that the SNR varies too much during the transmission of each codeword, and therefore, more effort should be spent on optimizing the AMC mechanism.

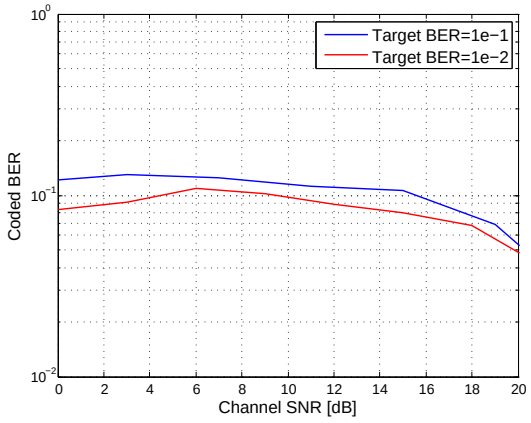

Figure 7.1 - 9: The influence of the target BER in the AMC mechanism.

Another aspect to take into account is the velocity of the user. Since the channel conditions change more rapidly when the user moves faster, the AMC mechanism needs to shift from one mode to another more often to follow the variations of the channel. On the other hand, the feedback of the channel information to the transmitter becomes a limiting factor as while it is being performed, the channel conditions change continuously. Thus it can be thought, as Figure 7.1 - 10 shows, that better results are obtained if the velocity of the user is smaller. The setting parameters for this curves are time-variant block fading channel, scenario B, soft demapping, and least-squares channel estimation.

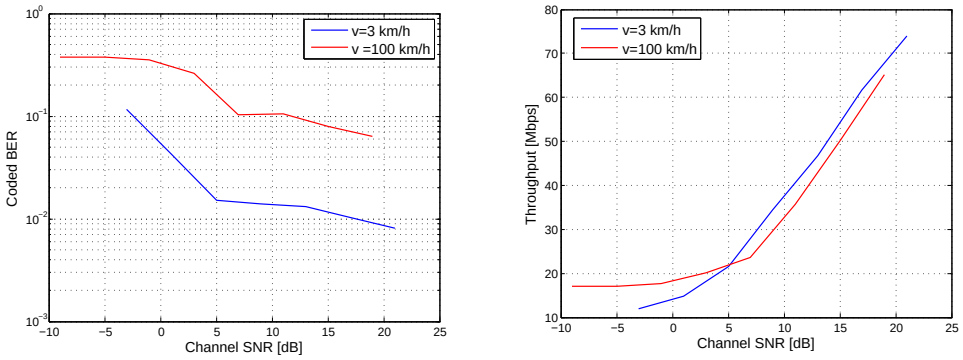

(a) Coded BER vs. SNR curves. (b) Throughput vs. SNR curves.

Figure 7.1 - 10: AMC results for a time-variant block fading channel with different user velocities.

Additionally, both demapping and channel estimation are analyzed with the performance of the AMC scheme. As expected, better results have been obtained for soft demapping and a perfect channel knowledge instead of hard demapping and channel estimation, respectively. Results for scenario C in a block fading channel using AMC3 are shown in Figure 7.1 - 11. The curves comparing hard demapping and soft demapping have been obtained with least-squares channel estimation, and those comparing channel estimation and perfect channel knowledge, with soft demapping.

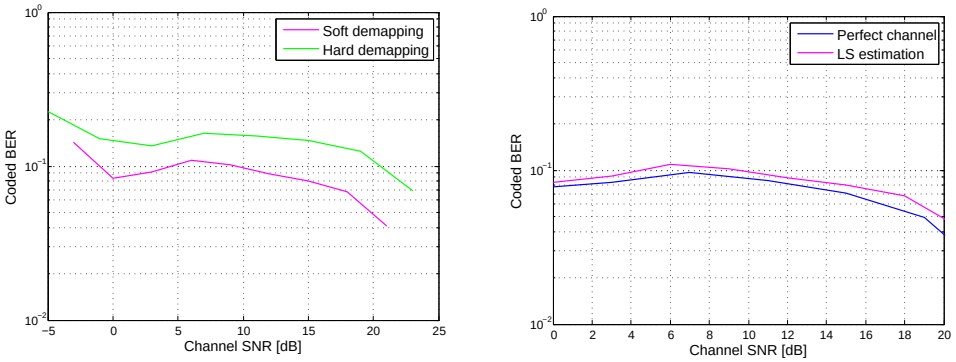

(a) Comparison between hard and soft demapping.

(b) Comparison between perfect channel knowledge and channel estimation.

Figure 7.1 - 11: Demapping and channel estimation when using the AMC scheme.

7.2 Multiple antenna transmission

Results obtained when using more than one antenna either at the transmitter or at the receiver, or at both ends of the communication link, are discussed in this section. As in the results for only one antenna, the common assumptions to all of the simulations are:

- f_c=2 GHz
- BW=20 MHz
- G=1/32
- T_{frame}=2.5 msec
- AMC=3

Furthermore, the hard demapping algorithm, a perfect knowledge of the channel coefficients, and a block fading channel model are used.

7.2.1 SISO, SIMO, MISO, and MIMO systems

As mentioned in Chapter 5, wireless channels key problem is fading. In order to combat this fading and hence, improve the capacity and the throughput of the system, multiple antennas at both ends of the communication link are used. This section analyzes the enhancement achieved with such structures, making a comparison of the performance of not only systems with multiple

transmit but also multiple receive antennas. As Figure 7.2 - 1 illustrates, the performance of the system drastically improves with a diversity system in place, in this case, using scenario C. The slope of the BER curves is an indicator of the degree of diversity that has been achieved. The degree of diversity is defined as the performance improvement in BER, in terms of power of ten, for a 10 dB higher SNR. As can be observed, the curve for the 1×1 system improves its error probability with a factor 10, i.e. power of 1 for a 10 dB rise in SNR. In this case, the degree of diversity is said to be equal to one, i.e. no diversity at all. However, when simulating with a 1×2 or a 2×1 system, which have diversity order of two, better performance is achieved. Likewise, the degree of diversity achieved with the 2×2 system is of order four. Therefore, it can be concluded that the degree of diversity is equal to $N_T N_R$, being N_T and N_R the number of transmit and receive antennas, respectively. Furthermore, it is shown that although both 1×2 and 2×1 achieve the same degree of diversity, the scheme that uses multiple antennas at the receiver offers a significant improvement of 3 dB of gain in the channel SNR. This gain is deducted from the formula of the received signal when using the MRC and the Alamouti scheme. As only one symbol is transmitted in one time interval with the MRC algorithm, the unity average transmit power is already achieved in each time interval, and the resultant signal is not multiplied by the factor $1/\sqrt{2}$ as in the Alamouti algorithm.

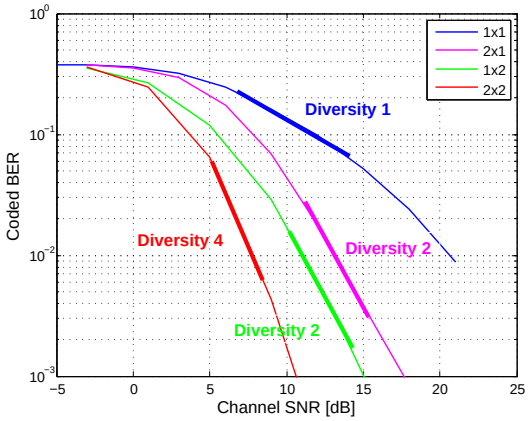

Figure 7.2 - 1: Comparison between different degrees of diversity.

The throughput of the system is analyzed next. Figure 7.2 - 2 illustrates that the higher the diversity order the more improvement in throughput is achieved.

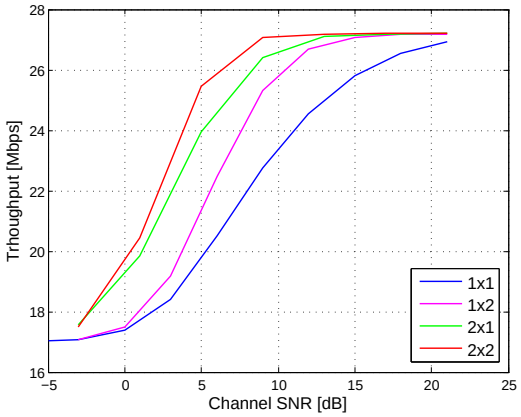

Figure 7.2 - 2: Throughput of the system using diversity schemes.

7.2.2 Channel model scenarios

This section analyzes the performance of the system when using the different I-METRA [31] scenarios implemented in the simulator. Simulation results for scenarios U, A and F, in a 2×2 MIMO system are presented. The results show that although both scenarios, A and U, represent environments experiencing flat fading, scenario A is worse than scenario U, thus showing that better performance is achieved in a non-correlated flat fading channel (scenario U) than in a correlated (scenario A). On the other hand, the best results are obtained with scenario F due to the higher frequency diversity this channel model has.

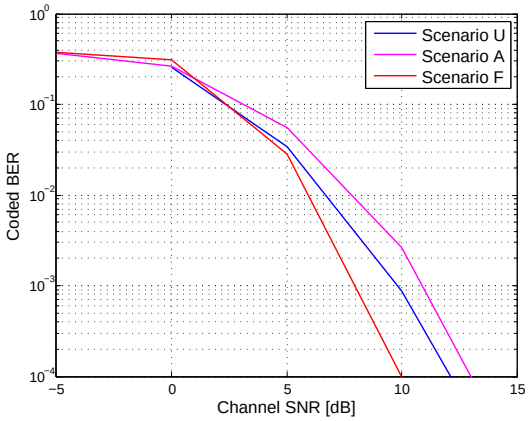

Figure 7.2 - 3: Comparison between different channel model scenarios in a MIMO system.

Chapter 8

Conclusion

The wireless communications industry is gaining momentum in both fixed and mobile applications. The continued increase in demand for all types of wireless services (voice, data, and multimedia) is fueling the need for higher capacity and data rates not only in fixed but also in mobile applications. WLANs and 3G cellular networks are experiencing several difficulties for reaching a complete mobile broadband access, bounded by factors such as bandwidth, coverage area, or infrastructure costs. In this context, WiMAX appears to fulfil these requirements, providing vehicular mobility and high service areas and data rates. Defined to provide broadband wireless access, it is increasingly gaining interest as an alternative last mile technology to DSL lines and cable modems, and a complementary technology where wireless networks are not sufficiently developed. This thesis is devoted to the study of the WiMAX system. More specifically, it examines the implementation of a WiMAX simulator, targeted to the 256-point FFT OFDM PHY layer, built with Matlab Simulink. With this purpose, the different parts of the simulator have been analyzed.

The flexible and parametrizable OFDM transmitter was explained in Chapter 2. Specifically, the length of the cyclic prefix, the coding scheme, the modulation alphabet, the channel bandwidth, and the frame duration, can be freely chosen by setting appropriate parameter values.

Chapter 3 has focused on the channel implementation. Changes in the environment due to the movement of not only objects but also receiver and transmitter introduce time-varying fading on the communication channel. The multipath channel propagation manifests itself by different echoes of possibly different transmitted symbols overlapping at the receiver, which leads to error rate degradation. The effects of ISI on the transmission error statistics are negligible as long as the delay spread is shorter than the cyclic prefix. The simulator implements three different kinds of channels, block

fading, time-variant, and time-variant block fading channels. If the block fading channel is selected for simulation, one impulse response is generated randomly for every frame transmitted. The time-variant channel model is implemented as a Jake's model and a time-variant convolution of the transmit signal with the impulse response. The time-variant block fading channel is a combination of the block fading and the time-variant channel model with time-invariant channel filtering. This model can be used as a low complexity approximation for the time-variant channel model if only slow speeds are considered.

The receiver was studied in detail in Chapter 4. Particularly, demapping algorithms and channel estimation methods were discussed. On one hand, it was shown that soft demapping outperforms hard demapping by 2 dB of gain in SNR. The information given by the demapper can contain not only the demodulated message (hard output) but also the degree of confidence in the decision (soft output). Performing the exact calculation of the bitwise metric in a soft demapper with a MAP algorithm is very tedious work. In order to reduce the complexity of the MAP algorithm for LLR calculation I replaced the mathematical logarithm function of the LLR expression with simple max or min functions, leading to the max-log-MAP approximation. On the other hand, the system BER with channel estimates from training sequences was evaluated. Results showed that simple least-squares channel estimation costs 1 dB in SNR when compared with a perfect channel knowledge. Therefore, since soft demapping gives a higher gain in the channel SNR, more efforts should be spent on implementing a soft demapper than a better channel estimation.

Another important aspect studied through the thesis is the performance gain by MIMO presented in Chapter 5. The ability to transmit and receive through multiple antennas enables us, while applying spatial diversity, to combat fading and ultimately have substantially improved reliability and increased capacity. The increased capacity, under proper coding, eventually translates into increased throughput. Specifically, the concepts of maximum ratio combining (MRC) and space-time coding (STC) were introduced. It is necessary for simple decoding of STC systems that the channel must be slowly varying (remain constant over two consecutive time steps). The simulator implements MIMO up to two transmit and/or receive antennas. Simulated results showed that the degree of diversity achieved, and hence the increase in throughput, is proportional to the number of antennas with which the communication system is equipped. Furthermore, it was found that a gain of 3 dB in the channel SNR appears in the BER curves when two antennas are used at the receiver instead of at the transmitter.

A final contribution is the performance evaluation of the AMC scheme presented in Chapter 6. AMC schemes employ multiple modulation and coding schemes (codecs) in order to instantaneously adapt spectral efficiency to the variations in the channel SNR while maintaining an acceptable BER. The implemented scheme estimates the channel SNR for each frame and compares it with a set of SNR thresholds obtained in such a way that they guarantee a BER below a given target BER. The codec associated to each threshold is fed back to the transmitter in order that the adaptation can be performed. The proposed scheme has been shown to be effective from approximately 7 dB of channel SNR onwards, where an enormous increase in the throughput of the system is achieved with the use of the AMC scheme. However, although a rising throughput is obtained with such schemes, the target BER is not achieved due to the fast fading of the channel, and more efforts should be spent on optimizing the mentioned AMC mechanism.

Appendix A

OFDM theory

OFDM can be viewed as a form of frequency division multiplexing (FDM) with the special property that each tone is orthogonal with every other tone, but it is different from FDM in several ways. On one hand, FDM requires, typically, the existence of frequency guard bands between the frequencies so that they do not interfere with each other. On the other hand, OFDM allows the spectrum of each tone to overlap, and because they are orthogonal, they do not interfere with each other. Furthermore, the overall amount of required spectrum is reduced due to the overlapping of the tones.

A.1 Multicarrier modulation

In a single carrier modulation system the data is sent serially over the channel by modulating one single carrier at a baud rate of R symbols per second, being the data symbol period $T_{\text{sym}} = 1/R$.

The basic idea of the multicarrier modulation is, nevertheless, that the available bandwidth, W, is divided into a number N_{c} of subbands, commonly called subcarriers. As shown in Figure A.1 - 1, each one of these subcarriers has a width of $\Delta f = W/N_{\text{c}}$. Instead of transmitting the data symbols in a serial way at a baud rate R, a multicarrier transmitter partitions the data stream into blocks of N_{c} data symbols and those are transmitted in parallel by modulating the N_{c} subcarriers.

The symbol duration for a multicarrier scheme is then $T_{\text{sym}} = N_{\text{c}}/R$.

One of the main advantages of using a multicarrier modulation is that inter-symbol interference can be reduced when the number of subcarriers, N_{c}, increases. In a multipath fading channel, ISI can appear due to the fact that the time dispersion is significant compared with the symbol period. If a single carrier modulation is used, a complex equalizer for compensating the

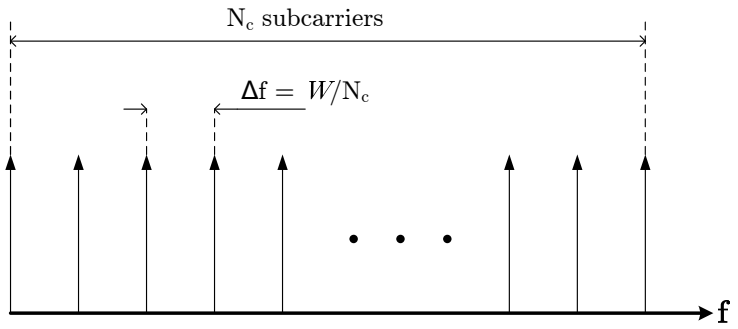

Figure A.1 - 1: Subdivision of the bandwidth, in a multicarrier transmission, into N_c subbands.

channel distortion is needed. However, the multicarrier modulation simplifies the equalization into single multiplications in the frequency domain.

A.2 Orthogonality

In order to assure a high spectral efficiency the subchannel waveforms must have overlapping transmit spectra. Nevertheless, to enable simple separation of these overlapping subchannels at the receiver they need to be orthogonal. Orthogonality is a property that allows the signals to be perfectly transmitted over a common channel and detected without interference. However, loss of orthogonality results in blurring between these information signals and degradation in communication.

Set of functions are orthogonal to each other if they match the conditions in Equation A.2 - 1. It means that if any two different functions within a set are multiplied and integrated over a symbol period, the result is zero for orthogonal functions:

$$\int_0^T S_{\mathrm{i}}(t)S_{\mathrm{j}}(t)dt = \begin{cases} C & \mathrm{i} = \mathrm{j} \\ 0 & \mathrm{i} \neq \mathrm{j}. \end{cases} \tag{A.2 - 1}$$

Furthermore, a general set of orthogonal waveforms is given by

$$\psi_{\mathrm{k}}(t) = \begin{cases} \frac{1}{\sqrt{T_{\mathrm{sym}}}} \exp(j2\pi f_{\mathrm{k}} t) & t\epsilon[0, T_{\mathrm{sym}}] \\ 0 & \text{otherwise}, \end{cases} \tag{A.2 - 2}$$

with $f_{\mathrm{k}} = f_0 + k\Delta f$, being $k = 0, 1, ..., N_{\mathrm{c}} - 1$.

In Equation A.2 - 2, f_{k} represents the subcarrier frequency, and f_0 is the lowest frequency used, corresponding to the index $k = 0$. The inter-carrier

spacing must satisfy $\Delta f = 1/T_{\text{sym}} = R/N_{\text{c}}$, where T_{sym} is the symbol period described above.

Each OFDM subcarrier has a sinc(x)[1] frequency response. This is the result of the symbol time corresponding to the inverse of the carrier spacing. The *sinc* shape has a narrow main lobe with many side lobes that decay slowly with the magnitude of the frequency difference away from the centre. Each carrier has a peak at its centre frequency and nulls evenly spaced with a frequency gap equal to the carrier spacing.

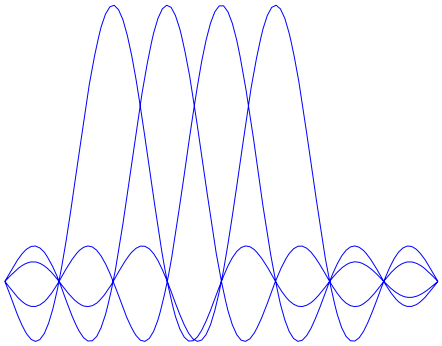

Figure A.2 - 1: Spectrum of an OFDM signal.

The orthogonal nature of the transmission is a result of the peak of each subcarrier corresponding to the nulls of all other subcarriers, as shown in Figure A.2 - 1.

A.3 Cyclic Prefix

Passing the signal through a time-dispersive channel causes ISI. In an OFDM system, a loss of the orthogonality appears due to ISI, resulting in ICI[2].

For a given system bandwidth the symbol rate for an OFDM signal is much lower than a single carrier transmission scheme. It is because the OFDM system bandwidth is broken up into N_{c} subcarriers resulting in a symbol rate that is N_{c} times lower. This low symbol rate makes OFDM naturally resistant to effects of ISI caused by multipath propagation.

The multiple signals that appear due to the multipath propagation arrive at the receiver at different times, spreading, this way, the symbol boundaries and causing energy leakage between the OFDM symbols. Furthermore, in an OFDM signal the amplitude and phase of the subcarrier must remain

[1] sinc(x)=sin(x)/x

[2] Inter-Carrier Interference

constant over a period of the symbol in order to maintain the orthogonality of the subcarriers. If they are no constant, the spectral shape will not have nulls at the correct frequencies, resulting in ICI.

In order to combat the effects of ISI on an OFDM signal, a guard period to the start of each symbol is added. This guard period, which is called the cyclic prefix (CP), is a copy of the last part of the OFDM symbol, thus extending the length of the symbol waveform. Figure A.3 - 1 shows the structure of an OFDM symbol. The CP is prepended to the transmitted symbol and removed at the receiver before the demodulation. Then, the total length of the symbol can be written as $T_{\text{sym}} = T_{\text{g}} + T_{\text{b}}$, where T_{sym} is the total length of the symbol in samples, T_{g} is the length of the guard period in samples, and T_{b} is the size of the IFFT used to generate the OFDM signal, representing the useful symbol time.

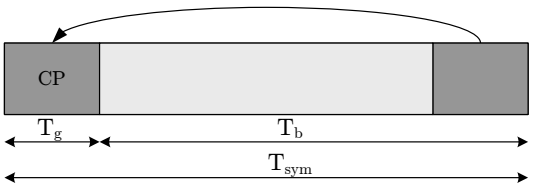

Figure A.3 - 1: Addition of the cyclic prefix to an OFDM signal.

Consequently, the benefit obtained for the addition of a cyclic prefix is twofold. First, it avoids ISI acting as a guard band between two successive symbols. Seconds, it converts the linear convolution with the channel impulse response into a cyclic convolution.

However, the length of the cyclic prefix has to be chosen carefully. On one hand, it should be, at least, as long as the significant part of the impulse response experienced by the transmitted signal, allowing some time for the transient signal to decay, and thus, avoiding ISI and ICI. One the other hand, it should be as small as possible because the transmitted energy increases with its length, causing a loss in the SNR. Equation A.3 - 1 gives the SNR loss due to the insertion of the CP. Moreover, the number of symbols per second that are transmitted per Hz of bandwidth also decreases with the CP. This decreasing is expressed by $R(1 - T_{\text{g}}/T_{\text{sym}})$.

$$SNR_{\text{loss}} = -10 \log_{10} \left(1 - \frac{T_{\text{g}}}{T_{\text{sym}}} \right) \qquad \text{(A.3 - 1)}$$

A.4 The OFDM system model

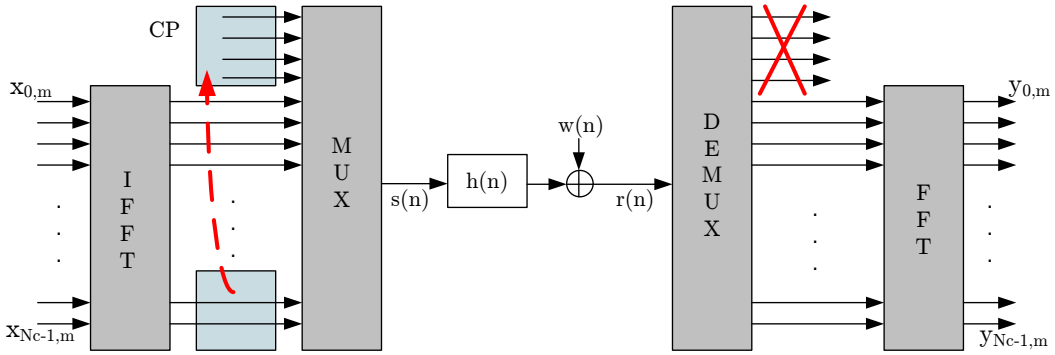

Figure A.4-1: Model of an OFDM system.

OFDM signals are typically generated digitally due to the difficulty in creating large banks of phase lock oscillators and receivers in the analog domain. Figure A.4-1 shows the block diagram of a such an OFDM system[3].

In the transmitter, the incoming data stream is grouped in blocks of N_c data symbols, which are the OFDM symbols, and can be represented by a vector x_m. Next, an IFFT is performed on each data symbol block and a cyclic prefix of length N_g is added.

The received signal is, generally, the sum of a linear convolution with the discrete channel impulse response, $h(n)$, and an additive white Gaussian noise, $w(n)$. It has to be said that it is implicitly assumed that the channel fading is slow enough to consider it constant during one symbol, and both, transmitter and receiver, are perfectly synchronized. At the receiver, the cyclic prefix is removed, and then, the data symbol $y_{k,m}$ (frequency index k, OFDM symbol m) is obtained by performing the FFT operation

Moreover, the transmitted data symbols, $x_{k,m}$, can be estimated from the received data symbols, $y_{k,m}$, using a single tap equalizer followed by a slicer. This estimated symbol is obtained by dividing each received data symbol by its corresponding channel coefficient.

[3]A more detailed analysis of the mathematical expressions of the OFDM conforming process can be found in [32] and [33].

A.5 Summary

After the explanation given about OFDM, it can be said that OFDM is a wideband modulation scheme that is specifically able to cope with the problems of the multipath reception. This is achieved by transmitting many narrowband overlapping digital signals in parallel, inside one wide band. Increasing the number of parallel transmission channels reduces the data rate that each individual carrier must convey, and that lengthens the symbol period. As a result, the delay time of reflected waves is suppressed to within one symbol time.

The basics that have been explained, as well as the OFDM system model, are derived for a time-invariant channel. When working with time-variant channels, the variations erode the orthogonality of the subcarriers and cause ICI or "FFT leakage". In those cases, a more complex system is needed to model such behaviour [32] [33].

Appendix B

Derivation of formulas

B.1 Description of the correlation matrices

The correlation matrices describing correlation properties at both ends of a communication system are explained in this appendix. These parameters can be extracted from measurement results, but they can also be derived from single-input multiple-output (SIMO) results already published in the open literature [31].

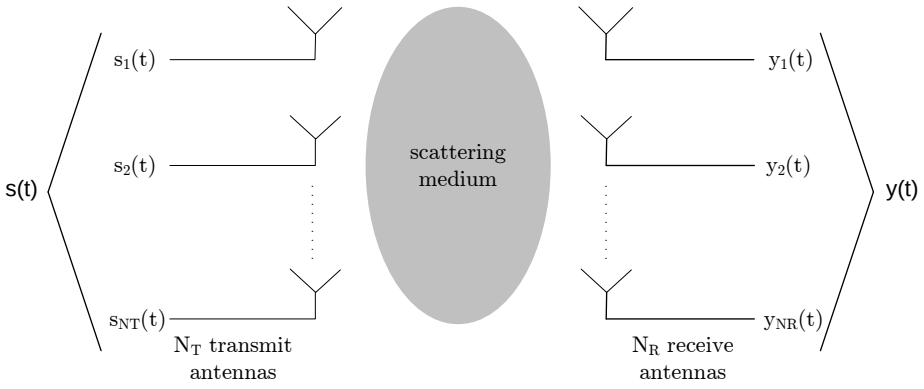

Figure B.1 - 1: A MIMO channel model in a scattering environment.

Figure B.1 - 1 shows a MIMO scenario with N_T transmit antennas and N_R receive antennas. The signals at the transmit antenna array are denoted by the vector $\mathbf{s}(t) = [s_1(t), s_2(t), ..., s_{N_T}(t)]^T$, and similarly, the signals at the receiver are $\mathbf{y}(t) = [y_1(t), y_2(t), ..., y_{N_R}(t)]^T$, where $(\cdot)^T$ denotes transposition,

and $s_m(t)$ and $y_n(t)$ are the signals at the m-th transmit antenna port and at the n-th receive antenna port, respectively.

The flat fading MIMO radio channel describing the connection between transmitter and receiver can be expressed as

$$\mathbf{H} = \begin{pmatrix} \alpha_{11} & \alpha_{12} & \cdots & \alpha_{1\mathrm{N_T}} \\ \alpha_{21} & \alpha_{22} & \cdots & \alpha_{2\mathrm{N_T}} \\ \vdots & \vdots & \ddots & \vdots \\ \alpha_{\mathrm{N_R}1} & \alpha_{\mathrm{N_R}2} & \cdots & \alpha_{\mathrm{N_R N_T}} \end{pmatrix}, \tag{B.1-1}$$

where α_{nm} is the complex transmission coefficient from antenna m at the transmitter to antenna n at the receiver, and it has been assumed to be complex Gaussian distributed with identical average power.

The relation between the vectors $\mathbf{s}(t)$ and $\mathbf{y}(t)$ can be expressed as

$$\mathbf{y}(t) = \mathbf{H}(t)\mathbf{s}(t). \tag{B.1-2}$$

Assuming that all antenna elements have the same polarization and the same radiation pattern, the spatial complex correlation coefficient at the transmitter between antennas m_1 and m_2 is given by Equation B.1-3, where the spatial correlation coefficient at the transmitter, $\rho^{\mathrm{TX}}_{m_1 m_2}$, is assumed to be independent of n. Similarly, the spatial complex correlation coefficient observed at the receive side, $\rho^{\mathrm{RX}}_{n_1 n_2}$, defined in Equation B.1-4, is assumed to be independent of m:

$$\rho^{\mathrm{TX}}_{m_1 m_2} = \langle \alpha_{nm_1}, \alpha_{nm_2} \rangle, \tag{B.1-3}$$

$$\rho^{\mathrm{RX}}_{n_1 n_2} = \langle \alpha_{n_1 m}, \alpha_{n_2 m} \rangle. \tag{B.1-4}$$

The operation $\langle a, b \rangle$[1] denotes an inner product between a and b, and is calculated as $\langle a, b \rangle = E\{ab^*\}/(\sigma_a \sigma_b)$, where σ_a is the standard deviation of the variable a, and $(\cdot)^*$ performs the conjugation operation.

The symmetrical complex correlation matrices can be defined from both, Equation B.1-3 and Equation B.1-4:

$$\mathbf{R}_{\mathrm{T}} = \begin{pmatrix} \rho^{\mathrm{TX}}_{11} & \rho^{\mathrm{TX}}_{12} & \cdots & \rho^{\mathrm{TX}}_{1\mathrm{N_T}} \\ \rho^{\mathrm{TX}*}_{21} & \rho^{\mathrm{TX}}_{22} & \cdots & \rho^{\mathrm{TX}}_{2\mathrm{N_T}} \\ \vdots & \vdots & \ddots & \vdots \\ \rho^{\mathrm{TX}*}_{\mathrm{N_T}1} & \rho^{\mathrm{TX}*}_{\mathrm{N_T}2} & \cdots & \rho^{\mathrm{TX}}_{\mathrm{N_T N_T}} \end{pmatrix}_{\mathrm{N_T} \times \mathrm{N_T}}, \tag{B.1-5}$$

[1] $\langle a, b \rangle = \langle b, a \rangle^*$

$$\mathbf{R}_{\mathrm{R}} = \begin{pmatrix} \rho_{11}^{\mathrm{RX}} & \rho_{12}^{\mathrm{RX}} & \cdots & \rho_{1\mathrm{N_R}}^{\mathrm{RX}} \\ \rho_{21}^{\mathrm{RX}*} & \rho_{22}^{\mathrm{RX}} & \cdots & \rho_{2\mathrm{N_R}}^{\mathrm{RX}} \\ \vdots & \vdots & \ddots & \vdots \\ \rho_{\mathrm{N_R}1}^{\mathrm{RX}*} & \rho_{\mathrm{N_R}2}^{\mathrm{RX}*} & \cdots & \rho_{\mathrm{N_R}\mathrm{N_R}}^{\mathrm{RX}} \end{pmatrix}_{\mathrm{N_R}\times\mathrm{N_R}} . \qquad \text{(B.1-6)}$$

Moreover, the correlation coefficient between two arbitrary transmission coefficients connecting two different sets of antennas is expressed as

$$\rho_{m_2 n_2}^{m_1 n_1} = \langle \alpha_{n_1 m_1}, \alpha_{n_2 m_2} \rangle = \rho_{m_1 m_2}^{\mathrm{TX}} \rho_{n_1 n_2}^{\mathrm{RX}}. \qquad \text{(B.1-7)}$$

Finally, it can be deducted from all this mathematical analysis that the spatial correlation matrix of the MIMO radio channel is represented by the Kronecker product of the spatial correlation matrices in both transmit and receive ends, and is given by $\mathbf{R}_{\mathrm{MIMO}} = \mathbf{R}_{\mathrm{T}} \otimes \mathbf{R}_{\mathrm{R}}$, where $\otimes$ represents the Kronecker product [31].

B.2 Estimation of the transmitted symbols when using STC

B.2.1 Alamouti with one receive antenna

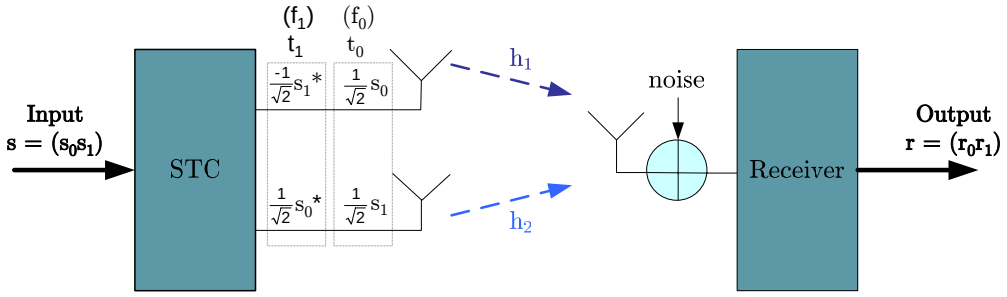

Figure B.2-1: 2×1 Alamouti scheme.

As shown in Figure B.2-1, the signal obtained at the receiver side when using the Alamouti algorithm is defined as

$$\begin{pmatrix} r_0 \\ r_1^* \end{pmatrix} = \frac{1}{\sqrt{2}} \begin{pmatrix} h_1 & h_2 \\ h_2^* & -h_1^* \end{pmatrix} \begin{pmatrix} s_0 \\ s_1 \end{pmatrix} + \begin{pmatrix} n_0 \\ n_1^* \end{pmatrix}. \qquad \text{(B.2-1)}$$

The estimated transmitted signal is then calculated from the formula $\widehat{\mathbf{s}} = \mathbf{H}_{\nu}{}^{\mathrm{H}}\mathbf{y}$, where $\mathbf{y} = [r_0, r_1^*]^{\mathrm{T}}$.

The hermitian of the virtual channel matrix is

$$\mathbf{H}_\nu{}^{\mathrm{H}} = \begin{pmatrix} h_1^* & h_2 \\ h_2^* & -h_1 \end{pmatrix}.$$

Finally, the estimated transmit signal is given by

$$\widehat{\mathbf{s}} = \mathbf{H}_\nu{}^{\mathrm{H}}\mathbf{y}$$

$$\Downarrow$$

$$\begin{pmatrix} \widehat{s_0} \\ \widehat{s_1} \end{pmatrix} = \mathbf{H}_\nu{}^{\mathrm{H}} \begin{pmatrix} r_0 \\ r_1^* \end{pmatrix} =$$

$$= \frac{1}{\sqrt{2}}\mathbf{H}_\nu{}^{\mathrm{H}}\mathbf{H}_\nu \begin{pmatrix} s_0 \\ s_1 \end{pmatrix} + \mathbf{H}_\nu{}^{\mathrm{H}} \begin{pmatrix} n_0 \\ n_1^* \end{pmatrix} =$$

$$= \frac{1}{\sqrt{2}} \begin{pmatrix} h_1^* & h_2 \\ h_2^* & -h_1 \end{pmatrix} \begin{pmatrix} h_1 & h_2 \\ h_2^* & -h_1^* \end{pmatrix} \begin{pmatrix} s_0 \\ s_1 \end{pmatrix} + \begin{pmatrix} h_1^* & h_2 \\ h_2^* & -h_1 \end{pmatrix} \begin{pmatrix} n_0 \\ n_1^* \end{pmatrix} =$$

$$= \frac{1}{\sqrt{2}} \begin{pmatrix} h_1^*h_1 + h_2h_2^* & h_1^*h_2 - h_2h_1^* \\ h_2^*h_1 - h_1h_2^* & h_2^*h_2 + h_1h_1^* \end{pmatrix} \begin{pmatrix} s_0 \\ s_1 \end{pmatrix} + \begin{pmatrix} h_1^*n_0 + h_2n_1^* \\ h_2^*n_0 - h_1n_1^* \end{pmatrix} =$$

$$= \frac{1}{\sqrt{2}} \begin{pmatrix} |h_1|^2 + |h_2|^2 & 0 \\ 0 & |h_1|^2 + |h_2|^2 \end{pmatrix} \begin{pmatrix} s_0 \\ s_1 \end{pmatrix} + \begin{pmatrix} h_1^*n_0 + h_2n_1^* \\ h_2^*n_0 - h_1n_1^* \end{pmatrix} =$$

$$= \frac{1}{\sqrt{2}}(|h_1|^2 + |h_2|^2) \begin{pmatrix} 1 & 0 \\ 0 & 1 \end{pmatrix} \begin{pmatrix} s_0 \\ s_1 \end{pmatrix} + \begin{pmatrix} h_1^*n_0 + h_2n_1^* \\ h_2^*n_0 - h_1n_1^* \end{pmatrix} =$$

$$= \frac{1}{\sqrt{2}}h^2\mathbf{I}_2\mathbf{s} + \widetilde{\mathbf{n}}. \qquad \text{(B.2 - 2)}$$

Once the corresponding operations for estimating the transmitted signal have been performed, the result is represented in Equation B.2 - 2, where:

- $h^2 = |h_1|^2 + |h_2|^2$ is the power gain of the channel,
- $\mathbf{I}_2$ is the 2×2 identity matrix,
- $\mathbf{s} = [s_0, s_1]^{\mathrm{T}}$ represents the transmitted symbols, and
- $\widetilde{\mathbf{n}} = \begin{pmatrix} h_1^*n_0 & h_2n_1^* \\ h_2^*n_0 & -h_1n_1^* \end{pmatrix}$ is some modified noise.

B.2.2 Alamouti with two receive antennas

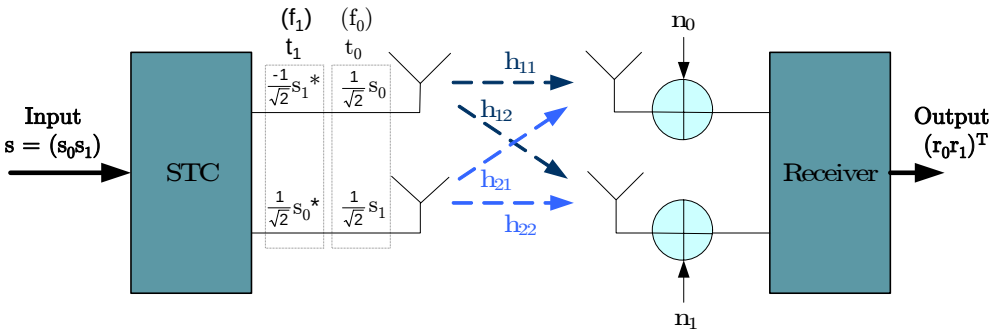

Figure B.2 - 2: 2×2 Alamouti scheme.

The received signal from a 2×2 Alamouti scheme, as depicted above, is

$$\mathbf{y} = \begin{pmatrix} r_0(1) \\ r_0(2) \\ r_1^*(1) \\ r_1^*(2) \end{pmatrix} = \frac{1}{\sqrt{2}} \begin{pmatrix} h_{11} & h_{21} \\ h_{12} & h_{22} \\ h_{21}^* & -h_{11}^* \\ h_{22}^* & -h_{12}^* \end{pmatrix} \begin{pmatrix} s_0 \\ s_1 \end{pmatrix} + \begin{pmatrix} n_0(1) \\ n_0(2) \\ n_1^*(1) \\ n_1^*(2) \end{pmatrix}. \quad \text{(B.2 - 3)}$$

The estimated transmitted signal can be calculated from $\widehat{\mathbf{s}} = \mathbf{H}_\nu^{\mathrm{H}}\mathbf{y}$, where $\mathbf{y} = [r_0(1)r_0(2)r_1^*(1)r_1^*(2)]^{\mathrm{T}}$.

The virtual channel matrix, $\mathbf{H}_\nu$, is expressed as

$$\mathbf{H}_\nu = \begin{pmatrix} h_{11} & h_{21} \\ h_{12} & h_{22} \\ h_{21}^* & -h_{11}^* \\ h_{22}^* & -h_{12}^* \end{pmatrix}.$$

Therefore, the hermitian of the virtual channel matrix is

$$\mathbf{H}_\nu^{\mathrm{H}} = \begin{pmatrix} h_{11}^* & h_{12}^* & h_{21} & h_{22} \\ h_{21}^* & h_{22}^* & -h_{11} & -h_{12} \end{pmatrix}.$$

The estimation of the transmitted symbols is performed as follows:

$$\begin{pmatrix} \widehat{s_0} \\ \widehat{s_1} \end{pmatrix} = \mathbf{H}_\nu{}^{\mathrm{H}} \begin{pmatrix} r_0(1) \\ r_0(2) \\ r_1^*(1) \\ r_1^*(2) \end{pmatrix} = \frac{1}{\sqrt{2}} \mathbf{H}_\nu{}^{\mathrm{H}} \mathbf{H}_\nu \begin{pmatrix} s_0 \\ s_1 \end{pmatrix} + \mathbf{H}_\nu{}^{\mathrm{H}} \begin{pmatrix} n_0(1) \\ n_0(2) \\ n_1^*(1) \\ n_1^*(2) \end{pmatrix} =$$

$$= \frac{1}{\sqrt{2}} \begin{pmatrix} h_{11}^* & h_{12}^* & h_{21} & h_{22} \\ h_{21}^* & h_{22}^* & -h_{11} & -h_{12} \end{pmatrix} \begin{pmatrix} h_{11} & h_{21} \\ h_{12} & h_{22} \\ h_{21}^* & -h_{11}^* \\ h_{22}^* & -h_{12}^* \end{pmatrix} \begin{pmatrix} s_0 \\ s_1 \end{pmatrix} + \widetilde{\mathbf{n}} =$$

$$= \frac{1}{\sqrt{2}}(|h_{11}|^2 + |h_{21}|^2 + |h_{12}|^2 + |h_{22}|^2) \begin{pmatrix} 1 & 0 \\ 0 & 1 \end{pmatrix} \begin{pmatrix} s_0 \\ s_1 \end{pmatrix} + \widetilde{\mathbf{n}} =$$

$$= \frac{1}{\sqrt{2}}(\|\mathbf{h}_1\|_2^2 + \|\mathbf{h}_2\|_2^2)\mathbf{I}_2 + \widetilde{\mathbf{n}} = \frac{1}{\sqrt{2}} h^2 \mathbf{I}_2 \mathbf{s} + \widetilde{\mathbf{n}}. \qquad \text{(B.2 - 4)}$$

Equation B.2 - 4 expresses the obtained result for the process of estimating the transmitted symbols. As described in the previous section:

- $\mathbf{I}_2$ is the 2×2 identity matrix,
- $\mathbf{s}$ is the transmitted signal,
- $h^2 = \|\mathbf{h}_1\|_2^2 + \|\mathbf{h}_2\|_2^2 = |h_{11}|^2 + |h_{21}|^2 + |h_{12}|^2 + |h_{22}|^2$ is the power gain of the channel, and
- $\widetilde{\mathbf{n}} = \begin{pmatrix} h_{11}^* n_0(1) + h_{12}^* n_0(2) + h_{21} n_1^*(1) + h_{22} n_1^*(2) \\ h_{21}^* n_0(1) + h_{22}^* n_0(2) - h_{11} n_1^*(1) - h_{12} n_1^*(2) \end{pmatrix}$ represents some modified noise.

Appendix C

Parameters of the simulator

C.1 Parameters description

C.1.1 OFDM symbol description

An OFDM symbol is composed by three types of subcarriers, data, pilots, and null subcarriers used for guard bands and the zero DC offset. The number of these subcarriers will determine the required size for the FFT (or IFFT) algorithm. Once the OFDM signal is converted into time domain, a copy of the last part of the useful symbol period, termed cyclic prefix (CP), is appended at the beginning of each symbol to maintain the orthogonality of the tones. From all these OFDM symbol characteristics, some parameters can be defined.

The standard [4] (see page 428) defines two types of parameters, the primitive parameters, that will be specified by users or system requirements, and the derived parameters, defined in terms of the primitive ones.

Five are the primitive parameters that characterize the OFDM symbol:

- BW: nominal channel bandwidth.
- N_{data}: number of data subcarriers.
- N_{pilot}: number of pilot subcarriers.
- n_{f}: sampling factor, used with BW and N_{used} (number of non-zero subcarriers) to determine the subcarrier spacing and the useful symbol time.
- G: ratio of CP time to useful time.

Next, derived parameters, which are dependent of the primitive parameters, are listed:

- N_{used}: number of used non-zero subcarriers.

$$N_{\text{used}} = N_{\text{data}} + N_{\text{pilot}}$$

- N_{FFT}: number of points used to perform the FFT. It is specified to be the smallest power of two, and greater than N_{used}.

$$N_{\text{FFT}} = 2^{\lceil \log_2(N_{\text{data}}) \rceil}$$

- F_{s}: sampling frequency.

$$F_{\text{s}} = \left\lfloor \frac{n_{\text{f}} BW}{8000} \right\rfloor 8000$$

- Δf: subcarrier spacing.

$$\Delta f = \frac{F_{\text{s}}}{N_{\text{FFT}}}$$

- T_{b}: useful symbol time.

$$T_{\text{b}} = \frac{1}{\Delta f}$$

- T_{g}: CP time.

$$T_{\text{g}} = G T_{\text{b}}$$

- T_{sym}: OFDM symbol time.

$$T_{\text{sym}} = T_{\text{b}} + T_{\text{g}}$$

- T_{s}: sampling time.

$$T_{\text{s}} = \frac{T_{\text{b}}}{N_{\text{FFT}}}$$

C.1.2 Transmission parameters

Besides the parameters that describe the OFDM symbol, other parameters are required in order to define parameters for the transmission, such as the frame duration, the packet size, or the total number of transmitted OFDM symbols. As in the previous section, they are classified either in primary or in secondary parameters.

The primary parameters are:

- N_{train}: number of training symbols in one frame.
- T_{frame}: frame duration.

The following parameters depend on either parameters defining the OFDM symbol or the transmission.

- N_{OFDM}: number of transmitted OFDM symbols in one frame.

$$N_{\text{OFDM}} = \frac{T_{\text{frame}}}{T_{\text{sym}}}$$

- N_{Tsym}: total number of transmitted symbols in one frame.

$$N_{\text{Tsym}} = N_{\text{OFDM}} + N_{\text{train}}$$

- $N_{\text{tx-data}}$: number of transmitted data symbols.

$$N_{\text{tx-data}} = N_{\text{data}} N_{\text{OFDM}}$$

- N_{tcb}: total number of coded bits per allocation subchannel per OFDM symbol.

$$N_{\text{tcb}} = N_{\text{tx-data}} M_{\text{a}}$$

- $N_{\text{tx-sym}}$: total number of transmitted symbols.

$$N_{\text{tx-sym}} = N_{\text{used}} N_{\text{OFDM}}$$

- S_{packet}: packet size transmitted by the source.

$$S_{\text{packet}} = N_{\text{OFDM}} R N_{\text{data}} M_{\text{a}}$$

C.1.3 Channel parameters

In order to define the channel model, several parameters need to be specified. In the simulations, the following default values were used:

- Sampling frequency of the channel simulator: $f_{\text{sam}} = 100$ MHz
- Speed of light: $c = 3 \cdot 10^8$ m/s
- Carrier frequency: $f_{\text{c}} = 2$ GHz
- Velocity of the mobile subscriber, v: variant
- Maximum doppler frequency: $f_{\text{d}} = v\frac{f_{\text{c}}}{c}$
- Number of paths of the time-variant channel model: $N_{\text{path}} = 8$. This parameter defines the number of sinusoids used for the Rosa-Zheng time variant-channel model.

C.1.4 Parameter values

Furthermore, the required values for some of these parameters are described in the standard. These values are given in Table C.1 - 1.

Parameter	**Value**
N_{data}	192
N_{pilot}	8
N_{train}	3
BW	Variable, from 1.25 to 20 MHz, being an integer multiple of 1.25, 1.5 or 1.75 MHz
n_{f}	1. For channel bandwidths multiple of 1.75 MHz, $n_{\text{f}} = 8/7$ 2. For channel bandwidths multiple of 1.5 MHz, $n_{\text{f}} = 86/75$ 3. For channel bandwidths multiple of 1.25 MHz, $n_{\text{f}} = 144/125$ 4. For channel bandwidths multiple of 2.75 MHz, $n_{\text{f}} = 316/275$ 5. For channel bandwidhts multiple of 2.0 MHz, $n_{\text{f}} = 57/50$ 6. For channel bandwidths not otherwise specified, $n_{\text{f}} = 8/7$
G	$1/4, 1/8, 1/16, 1/32$
Number of lower frequency guard subcarriers	28
Number of higher frequency guard subcarriers	27
Frequency offset indices of guard subcarriers	$-128, -127, ..., -101$ $+101, +102, ..., +127$
Frequency offset indices of pilot carriers	$-88, -63, -38, -13$ $+13, +38, +63, +88$
T_{frame}(msec)	2.5, 4, 5, 8, 10, 12.5, 20

Table C.1 - 1: Values for primary parameters.

C.2 WiMAX vs. Wi-Fi simulator

As already mentioned in Section 1.1.2, there are several differences between WiMAX and Wi-Fi systems. In this way, both simulators will differ from each other in some parameter values. The main differences between both are summarized in the following chart:

	WiMAX	**Wi-Fi**
$\mathbf{N}_{\text{data}}$	192	48
$\mathbf{N}_{\text{pilot}}$	8	4
$\mathbf{N}_{\text{FFT}}$	256	64
BW	variable (1.25 to 20 MHz)	fixed (20 MHz)
Coding	CC+RS	CC
CP	variable	fixed

Table C.2 - 1: Differences between WiMAX and Wi-Fi parameters.

Appendix D

WiMAX simulator block diagram

In order to have a general view of the WiMAX simulator described through the thesis, a complete block diagram of the Simulink model file is given in this appendix (see Figure D.0 - 1). A brief description of the different blocks is exposed with the purpose of offering a better understanding of the figure.

As mentioned in Chapter 2, data from a binary source is first encoded and mapped into QAM symbols. The block **"Coding TX"** performs these operations. It is composed of a bank of seven different sources, encoders, and mappers, each of which is optimized to work with a different data rate depending on the modulation and coding scheme being used. The encoder, as explained, consists on a concatenation of an outer Reed-Solomon encoder with an inner convolutional encoder. It is a flexible coding process due to the puncturing of the signal, allowing different coding rates. The last part of the encoder is a process of interleaving to avoid large blocks of bit errors.

Once the data from the source is mapped into QAM symbols, the OFDM symbols must be constructed. An OFDM symbol is composed by 192 data subcarriers, 8 pilot subcarriers, 1 zero DC subcarrier, and 55 guard carriers. Furthermore, preambles consisting of 3 OFDM symbols are appended at the beginning of each frame. Preambles are formed with a short training sequence, followed by a long training sequence, and the FCH[1]. Depending on the number of transmit antennas, two kinds of long training sequences are used. If only one antenna is transmitting, the long training sequence utilizes even subcarriers, therefore it is called P_{EVEN}. However, another long training sequence shall be used when transmitting space-time coded downlink bursts. Because the STC scheme achieves diversity by transmitting with two antennas, a preamble has to be transmitted from both transmit antennas simultaneously. Thus, the first antenna transmits a preamble using P_{EVEN}

[1] Frame Control Header

and the preamble transmitted from the second antenna is set according to the sequence P_{ODD}, which uses, in this case, a subset of odd subcarriers. Blocks **"Pilot"**, **"Training Ant. 0"**, and **"Training Ant. 1"** generate the pilot and both training sequences, respectively.

OFDM data symbols are obtained after rearranging the data vector from the **"Coding TX"** block in a matrix form that has 192 rows (number of data subcarriers in an OFDM symbol). Moreover, if Alamouti coding is selected in a parameter file, **"STC"** performs the Alamouti algorithm described in Section 5.1.2 to the OFDM data symbols. Otherwise, this block has no impact on the signal.

The next block, called **"Assembler"**, deals with the task of rearranging data, pilots, trainings, and zero DC subcarrier, as explained in Section 2.6. After the assembling process, the 55 guard bands are appended at the end of each frame, the signal is converted to the time domain and the cyclic prefix is added. Then, the signal is sent over the channel, which is implemented in the block **"Channel Model"**.

The receiver performs the reverse operations to get the transmitted data. The cyclic prefix is removed from each symbol and the signal is converted to the frequency domain using an FFT algorithm. As it has been told before, an OFDM symbol consists of data, pilot, trainings, a zero DC subcarrier, and some guard bands. Thus, a process to separate all these subcarriers is needed. First, the guard bands are removed, and then, a disassembling is performed to obtain pilots, data, and trainings. The trainings are utilized in the **"Channel estimator"**. The estimated channel coefficients can be used in the demapper to realize an equalization of the data symbols to compensate the frequency-selective fading of the multipath propagation channel. To end, data is decoded following the inverse steps as performed in the transmitter (deinterleaving, inserting zeros as the inverse process of puncturing, Viterbi decoding of the convolutional code, and Reed-Solomon decoding). These two last steps, demapping and decoding, are performed in the **"Decoding RX"** block. As its analogous block, it consists of a bank of seven demappers and decoders, where the appropriate modulation and coding scheme is selected by the AMC signal explained next.

Furthermore, a feedback mechanism of adaptive modulation and coding (AMC) is performed in order to allow the system to shift modulation scheme and so, maintain the connection quality and link stability, thus allowing the system to overcome time-selective fading. This AMC mechanism works by estimating the SNR of the channel, and depending on the desired conditions of the channel established by a given target BER, changing modulation and coding. These operations are performed in the **"Calculate AMC"** block.

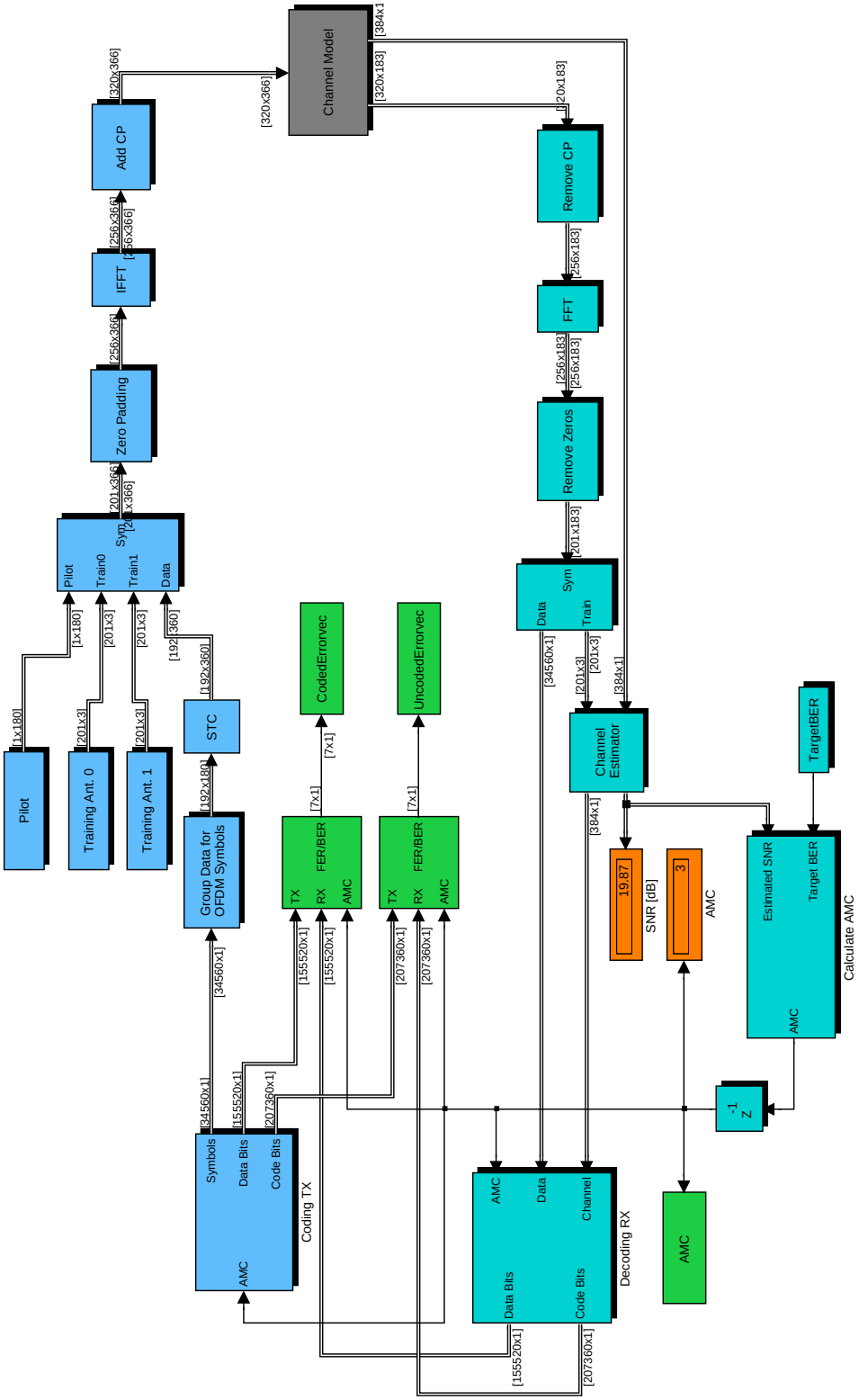

Figure D.0-1: Simulink block diagram of the WiMAX simulator.

Appendix E

Abbreviations and Symbols

E.1 List of abbreviations

3G	Third Generation
3GPP	Third Generation Partnership Project
4G	Fourth Generation
AAS	Adaptive Antenna System
AMC	Adaptive Modulation and Coding
AP	Access Point
ARQ	Automatic Retransmission Request
AWGN	Additive White Gaussian Noise
BER	Bit Error Rate
BS	Base Station
BTC	Block Turbo Coding
CC	Convolutional Coding
CIR	Channel Impulse Response
CP	Cyclic Prefix
CSI	Channel State Information
CTC	Convolutional Turbo Coding
DC	Direct Current
DFS	Dynamic Frequency Selection
DL	DownLink
DSL	Digital Subscriber Line
FCH	Frame Control Header
FDD	Frequency Division Duplexing
FDM	Frequency Division Multiplexing
FEC	Forward Error Correction

FFT	Fast Fourier Transform
GF	Galois Field
HSDPA	High Speed Downlink Packet Access
ICI	Inter-Carrier Interference
i.i.d.	Independent Identically Distributed
IEEE	Institute of Electrical and Electronics Engineers
IFFT	Inverse Fast Fourier Transform
I-METRA	Intelligent Multi-Element Transmit and Receive Antennas
IMT	International Mobile Telecommunications
IP	Internet Protocol
IQ	In-phase Quadrature-phase
ISI	Inter-Symbol Interference
LGPL	Lesser General Public License
LLR	Log-Likelihood Ratio
LoS	Line of Sight
LS	Least Squares
LSE	Least Squares Estimation
MAC	Medium Access Control
MAN	Metropolitan Area Network
MAP	Maximum A Posteriori
MEA	Multi-Element Antenna
MIMO	Multiple-Input Multiple-Output
MISO	Multiple-Input Simple-Output
MRC	Maximum Ratio Combining
MS	Mobile Station
MSS	Mobile Subscriber Station
NLoS	Non Line of Sight
OFDM	Orthogonal Frequency Division Multiplexing
OFDMA	Orthogonal Frequency Division Multiple Access
PAM	Pulse Amplitude Modulation
PDA	Personal Digital Assistant
pdf	Probability Density Function
PDP	Power Delay Profile
PRBS	Pseudo-Random Binary Sequence
QAM	Quadrature Amplitude Modulation
QoS	Quality of Service
RRC	Root-Raised Cosine
RF	Radio Frequency
RMS	Root Mean Square
RS	Reed-Solomon
SC	Single Carrier

SIMO	Single-Input Multiple-Output
SINR	Signal-to-Interference-plus-Noise Ratio
SISO	Single-Input Single-Output
SNR	Signal-to-Noise Ratio
SOHO	Small-Office Home-Office
SS	Spread Spectrum
SS	Subscriber Station
STBC	Space-Time Block Coding
STC	Space-Time Coding
TDD	Time Division Duplexing
TDM	Time Division Multiplexing
TDMA	Time Division Multiple Access
UL	UpLink
UMTS	Universal Mobile Telecommunications System
VoIP	Voice over IP
WCDMA	Wide-band Code Division Multiple Access
Wi-Fi	Wireless-Fidelity
WiMAX	Worldwide Interoperability for Microwave Access
WLAN	Wireless Local Area Network
WMAN	Wireless Metropolitan Area Network

E.2 List of symbols

$\otimes$	Continuous-time convolution
$(\cdot)^*$	Complex conjugation operation
$(\cdot)^{-1}$	Inversion operation
$(\cdot)^{\mathrm{T}}$	Transposition
$(\cdot)^{\mathrm{H}}$	Hermitian operation
$\overline{a}$	Binary inversion of the sequence a
A_{s}	Vector that represents the points in the constellation map
b_{k}	Bit on position k
B_{coh}	Coherence bandwidth
B_{d}	Doppler spread
BER_0	Target BER
BW	Nominal channel bandwidth
c	Speed of light
$c_{\mathrm{i}}(t)$	Tap coefficients
C	Amplitude of the fading component
C_{m}	Normalization factor in the modulation map
$\mathbb{C}$	Set of complex numbers
d_{E}	Euclidean distance
$E\{\}$	Mathematical expectation
$\mathrm{E_b/N_0}$	Bit energy to noise rate
f_{c}	Carrier frequency
f_{d}	Doppler frequency
f_{M}	Maximum Doppler shift
f_{N}	Nyquist frequency
$f_{\mathrm{Ray}}(a)$	Rayleigh fading distribution
$f_{\mathrm{Rice}}(a)$	Rice fading distribution
f_{sam}	Sampling frequency of the channel simulator
F_{s}	Sampling frequency of the OFDM symbol
G	Ratio of the CP time to the useful symbol time
$\mathbf{G}$	Channel gain matrix
$\mathbf{h}$	Vector of channel coefficients
$\hat{h}$	Channel coefficients estimates
$h(t)$	Channel impulse response
$h(t,\tau)$	Channel time-varying impulse response
$h_{\mathrm{b}}(t,\tau)$	Baseband equivalent impulse response of the channel
$\mathbf{H}$	Channel matrix
$H_{\mathrm{rc}}(f)$	Raised cosine filter frequency response
$H_{\mathrm{rrc}}(f)$	Root-raised cosine filter frequency response

$H_{\mathrm{R}}(f)$	Frequency response of the receive filter
$H_{\mathrm{T}}(f)$	Frequency response of the transmit filter
$\mathbf{H}_{\nu}$	Virtual channel matrix
I	Vector for the interleaving matrix
I_0	Modified Bessel function of first kind and order zero
$\mathbf{I}_2$	2×2 identity matrix
k	Number of uncoded bits that enter the RS encoder
K	Rice distribution factor
l	Length of the binary sequences of a Galois field GF(2^l)
L	Number of multipath components
$\mathrm{N_T}$	Number of transmit antennas
M_{a}	Number of transmitted bits per symbol (modulation alphabet)
n	Number of coded bytes at the output of the RS encoder
$\overline{n}$	Average noise power
$\mathbf{n}$	Noise vector
$\widetilde{\mathbf{n}}$	Modified noise vector
n_{f}	Sampling factor, used in the definition of the OFDM symbol
$\mathrm{N_R}$	Number of receive antennas
N_{c}	Number of subbands the OFDM signal is divided in
N_{columns}	Number of columns in the interleaving matrix
N_{cpc}	Number of transmitted bits per symbol
N_{data}	Number of used data subcarriers
N_{FFT}	Number of points used when performing the FFT algorithm
N_{OFDM}	Number of transmitted OFDM symbols in one frame
N_{path}	Number of paths of the time-variant channel model
N_{rows}	Number of rows in the interleaving matrix
N_{RS}	Number of blocks used in the RS encoder
N_{tcb}	Total number of coded bits
N_{train}	Number of training symbols per frame
$N_{\mathrm{tx\text{-}data}}$	Number of transmitted data symbols
$N_{\mathrm{tx\text{-}sym}}$	Total number of transmitted OFDM symbols
N_{Tsym}	Total number of transmitted symbols in one frame
N_{used}	Number of used non-zero subcarriers
$\mathcal{N}_{\mathcal{C}}(0,1)$	Set of complex numbers, with zero mean and unit variance
p_{s}	Vector containing the pilot subcarriers
$p(y\|s)$	Conditional probability, probability of y given s
P_{b}	Probability of bit error
P_{bc}	Probability of bit error per carrier
P_{ALL}	Frequency domain sequence from which are derived all full bandwidth preambles

P_{EVEN}	Frequency domain sequence for long training symbols constructed with even subcarriers of P_{ALL}
P_{ODD}	Frequency domain sequence for long training symbols constructed with odd subcarriers of P_{ALL}
P_{SHORT}	Frequency domain sequence for short training symbols
$Q(x)$	Complementary Gaussian error function
r	Vector of received symbols
R	Overall rate
$Re\{\}$	Operation to extract the real part
$\mathbf{R}_{\mathrm{MIMO}}$	Spatial correlation matrix of the MIMO channel
$\mathbf{R}_{\mathrm{R}}$	Transmit correlation matrix
R_{sym}	Symbol rate
$\mathbf{R}_{\mathrm{T}}$	Receive correlation matrix
$\overline{s}$	Average signal power
$\mathbf{s}$	Vector containing the transmitted symbols
$\widehat{s}$	Transmit symbol estimates
S_{packet}	Packet size, in bits, that is transmitted by the source
$\mathbf{S}$	Symbol block matrix
t	Number of bytes a RS encoder can correct
T_{b}	Useful symbol time
T_{coh}	Coherence time
T_{g}	CP symbol time
T_{frame}	Frame duration
T_{m}	Multipath spread
T_{s}	Sampling time of the OFDM symbol
T_{sym}	OFDM symbol time
v	Vehicle speed
w_{k}	Output of the PRBS generator
W	Signal bandwidth
$\mathbf{y}$	Vector containing the received symbol
α	Roll-off factor
α_{nm}	Complex transmission coefficient from antenna m to antenna n
β_{i}	Weight factor
γ_{n}	SNR threshold
$\delta(t)$	Dirac delta function
Δf	Subcarrier spacing
ϵ	Property operator
φ	Angle of arrival of the received signal component
ϕ	Phase delay of a multipath signal
ρ^2	Power of the received non-fading signal
$\rho_{\mathrm{ij}}^{\mathrm{TX}}$	Spatial correlation coefficient at the transmitter

$\rho_{\mathrm{ij}}^{\mathrm{RX}}$	Spatial correlation coefficient at the receiver
σ_{x}	Standard deviation of x
σ_{τ}	RMS delay spread
σ_{v}^{2}	Noise variance
θ	Phase alteration experienced by the multipath fading signal
τ	Channel multipath delay

Bibliography

[1] S. Sampei: "*Applications of Digital Wireless Technologies to Global Wireless Communications*," Prentice Hall, 1997.

[2] Intel White Paper, Wi-Fi and WiMAX Solutions: "*Understanding Wi-Fi and WiMAX as Metro-Access Solutions*," Intel Corporation, 2004.
http://www.intel.com/netcomms/technologies/wimax/304471.pdf

[3] J. Pino Lacosta: "*WiMAX: una alternativa d'accés a les xarxes*," Master Thesis, Universitat Oberta de Catalunya, Enginyeria Informàtica, June 2004.

[4] LAN/MAN Standards Committee: "*802.16 IEEE Standard for Local and Metropolitan Area Networks. Part 16: Air Interface for Fixed Broadband Wireless Access Systems*," IEEE Standards, October 2004.

[5] C. Eklund, R. B. Marks, K. L. Stanwood, and S. Wang: "*IEEE Standard 802.16: A Technical Overview of the WirelessMAN Air Interface for Broadband Wireless Access*," IEEE Communications Magazine, pp. 98-107, June 2002.
http://www.wirelessman.org/tutorial

[6] WiMAX Forum: "*Mobile WiMAX. Part I: A Technical Overview and Performance Evaluation*," August 2006.
http://www.intel.com/netcomms/technologies/wimax

[7] T. Cooklev: "*Wireless Communication Standards. A Study of IEEE* 802.11^{TM}, 802.15^{TM}, *and* 802.16^{TM}," Standards Information Networks IEEE Press, 2004.

[8] P. Stavroulakis: "*Third generation mobile telecommunication systems: UMTS and IMT-2000*," Springer, 2001.

[9] A. M. Michelson, and A. H. Levesque: "*Error Control Techniques for Digital Communications*," Wiley-Interscience Publications, 1985.

[10] S. B. Wicker: "*Error Control Systems for Digital Communication and Storage*," School of Electrical and Computer Engineering, Georgia Institute of Technology, Prentice Hall, 1995.

[11] E. P. Lawrey: "*Adaptive Techniques for Multiuser OFDM*," Ph. D. Thesis, School of Engineering, James Cook Univeristy, December 2001.
http://www.skydsp.com/publications

[12] K. V. Ramasami: "*A Primer on Root Raised Cosine Filter Design*," December 2004.
http://www.ittc.ku.edu/ rvc/documents/rcdes.pdf

[13] T. S. Rappaport: "*Wireless Communications: principles and practice*," Prentice Hall, 1996.

[14] R. J. McEliece, and W. E. Stark: "*Channels with block interference*," IEEE Transactions on Information Theory, vol. 46, no. 2, pp. 325-343, March 2000.

[15] W. C. Jakes: "*Microwave Mobile Communications*," IEEE Press, 1994.

[16] L. Staphorst: "*Viterbi decoded linear block codes for narrowband and wideband wireless communication over mobile fading channels*," Master Thesis, Department of Electrical, Electronic and Computer Engineering, University of Pretoria, July 2005.
http://upetd.up.ac.za/thesis/available/etd-08082005-120839/

[17] C. Mehlführer, F. Kaltenberger, M. Rupp, and G. Humer: "*A Scalable Rapid Prototyping System for Real-Time MIMO OFDM Transmissions*," Institute of Communications and RF Engineering, Vienna University of Technology, and ARC Seibersdorf Research GmbH, Tech Gate Vienna, Proceedings on the second IEE/EURASIP on DSP enabled Radio, September 2005.
http://publik.tuwien.ac.at/files/pub-et_10207.pdf

[18] Ki Seol Kim et al.: "*General Log-Likelihood Ratio Expression and its Implementation Algorithm for Gray-Coded QAM Signals*," ETRI Journal, vol. 28, no. 3, pp. 291-300, June 2006.
http://etrij.etri.re.kr/Cyber/servlet/BrowseAbstract?paperid=RP0508-0161

[19] "*The Matlab help: Communications Blockset*,"
http://www.mathworks.com

[20] I. E. Telatar: "*Capacity of Multi-Antenna Gaussian Channels*," European Transactions on Telecommunications, 1999, Technical Memorandum, Bell Laboratories, Lucent Technologies, vol. 10, no. 6, pp. 585-595, October 1998.

[21] G. J. Foschini, and M. J. Gans: "*On Limits of Wireless Communication in a Fading Environment when Using Multiple Antennas*," Wireless Personal Communications, vol. 6, no. 3, pp. 311-335, 1998.

[22] S. Yang, and F. Kaltenberger: "*MIMO Algorithms for Wireless LAN*," Proceedings Wireless Congress, Munich, Germany, October 2005.

[23] D. Pérez Palomar: "*A Unified Framework for Communications through MIMO Channels*," Ph. D. Thesis, Departament de Teoria del Senyal i Comunicacions, Universitat Politècnica de Catalunya, May 2003.
http://www.ist-imetra.org/thesis/Palomar_phd_thesis.pdf

[24] G. Gritsch, G. Kolar, H. Weinrichter, and M. Rupp: "*Two Adaptive Space-Time Block Coded MIMO Systems Exploiting Partial Channel Knowledge at the Transmitter*," Institute for Communications and Radio Frequency Engineering, Vienna University of Technolgoy, 5th International ITG Conference on Source and Channel Coding (SCC04), Erlangen, Germany, January 2004.
http://publik.tuwien.ac.at/files/pub-et_8504.pdf

[25] S. M. Alamouti: "*A Simple Transmit Diversity Technique for Wireless Communications*," IEEE Journal on Selected Areas in Communications, vol. 16, no. 8, pp. 1451-1458, October 1008.

[26] A. van Zelst, R. van Nee, and G. A. Awater: "*Space division multiplexing (SDM) for OFDM systems*," IEEE 51st Vehicular Technology Conference (VTC) Proceedings, vol. 2, pp. 1070-1074, Tokyo, Spring 2000.

[27] V. Tarokh, N. Seshadri, and A. R. Calderbank: "*Space-time codes for high data rate wireless communication: performance criterion and code construction*," IEEE Transactions on Information Theory, vol. 44, no. 2, pp. 744-765, 1998.

[28] A. J. Goldsmith, and S. G. Chua: "*Adaptive Coded Modulation for Fading Channels*," IEEE Transactions on Communications, vol. 46, no. 5, pp. 595-602, May 1998.
http://wsl.stanford.edu/ ee359/adapt_cod.pdf

[29] T. Keller, and L. Hanzo: "*Adaptive Multicarrier Modulation: A Convenient Framework for Time-Frequency Processing in Wireless Communications*," IEEE Transaction on Communications, vol. 88, no. 5, pp. 611-640, May 2000.
http://eprints.ecs.soton.ac.uk/4099

[30] L. W. Couch: "*Digital and Analog Communication Systems*," 6th edition, Prentice Hall, 2001.

[31] L. Schumacher, J. P. Kermoal, K. I. Pedersen, P. E. Mogensen, and F. Frederiksen: "*A Stochastic MIMO Radio Channel Model with Experimental Validation*," IEEE Journal on Selected Areas in Communications, vol. 20, no. 6, pp. 1211-1226, August 2002.

[32] M. Engels: "*Wireless OFDM systems. How to make them work?*,", Kluwer Academic, 2002.

[33] R. S. Bahai, and B. R .Saltzberg: "*Multi-carrier digital communications: theory and applications of OFDM*," New York Springer, 2004.